Quaternary Science Reviews 272 (2021) 107242

Contents lists available at ScienceDirect

Quaternary Science Reviews

journal homepage: www.elsevier.com/locate/quascirev

Invited paper

A latest Pleistocene and Holocene composite tephrostratigraphic framework for northeastern North America

Britta J.L. Jensen [a, *], Lauren J. Davies [a, 1], Connor Nolan [b], Sean Pyne-O'Donnell [c], Alistair J. Monteath [a, d], Vera Ponomareva [e], Maxim Portnyagin [f], Robert Booth [g], Marcus Bursik [h], Eliza Cook [i], Gill Plunkett [c], James W. Vallance [j], Yan Luo [a], Les C. Cwynar [k], Paul Hughes [d], D. Graham Pearson [a]

[a] Department of Earth and Atmospheric Sciences, University of Alberta, Edmonton, AB, T6G 2E3, Canada
[b] Stanford Woods Institute for the Environment, Stanford University, Stanford, CA, 94305, USA
[c] Archaeology & Palaeoecology, School of Natural and Built Environment, Queen's University Belfast, Belfast, BT7 1NN, UK
[d] Department of Geography and Environment, University of Southampton, Southampton, SO17 1BJ, UK
[e] Institute of Volcanology and Seismology, Piip Boulevard 9, Petropavlovsk-Kamchatsky, 683006, Russia
[f] GEOMAR Helmholtz Center for Ocean Research Kiel, Wischhofstrasse 1-3, Kiel, D-24148, Germany
[g] Earth and Environmental Sciences, Lehigh University, Bethlehem, PA, 18015, USA
[h] Department of Geology, University at Buffalo, North Campus, Buffalo, NY, 14260, USA
[i] Physics of Ice, Climate and Earth, Niels Bohr Institute, Tagensvej 16, Copenhagen, 2200, Denmark
[j] U.S. Geological Survey, Cascades Volcano Observatory, 1300 SE Cardinal Court, Vancouver, WA, 98683, USA
[k] Department of Biology, University of New Brunswick, Fredericton, New Brunswick, E3B 5A3, Canada

ARTICLE INFO

Article history:
Received 21 June 2021
Received in revised form
3 October 2021
Accepted 10 October 2021

Handling Editor: Giovanni Zanchetta

Keywords:
Cryptotephra
Tephrochronology
Volcanic ash
North America
Greenland
Kamchatka
Peat
Bayesian
Radiocarbon
Holocene

ABSTRACT

Lakes and bogs in northeastern North America preserve tephra deposits sourced from multiple volcanic systems in the Northern Hemisphere. However, most studies of these deposits focus on specific Holocene intervals and the latest Pleistocene, providing snapshots rather than a full picture. We combine new data with previous work, supplemented by a broad review of the characteristics and ages of potential source regions and volcanoes, to develop the first composite tephrostratigraphic framework covering the last ~14,000 years for this region. We report new cryptotephra records from three ombrotrophic peat bogs—Irwin Smith (Michigan), Bloomingdale (New York), and Sidney Bog (Maine)—as well as new analyses and age models from previously reported sites, Nordan's Pond Bog (Newfoundland) and Thin-Ice Pond (Nova Scotia). A new tephra (Iliinsky) from the NGRIP and GRIP ice cores is also presented as it can be correlated to new data from these terrestrial records and helps validate radiocarbon age models. We identify 21 new tephra in addition to the 15 already known, several of which cover the entire region – the White River Ash east, Newberry Pumice, Ruppert (NDN-230), and Mazama. For the first time we find Mount St. Helens Yn (ca. 3660 cal yr BP) and a set P tephra (~3000–2550 cal yr BP), and confirm the presence of Jala Pumice from Volcan Ceboruco, Mexico, and KS_1 from Ksudach volcano, Kamchatka. We describe new "ultra-distal" tephra, including the early Holocene KS_2 eruption, and propose correlations to volcanoes Iliinsky and Shiveluch of Kamchatka, and Ushishir of the Kurile Islands. Not all of these tephra represent large eruptions, with several plausible correlations to sub-Plinian events. Using Bayesian age-modeling, we present new age estimates for the newly described tephra, for tephra with previously poor age control, and for several proximal correlatives. Overall, we demonstrate northeastern North America's importance for providing transcontinental linkages between paleoenvironmental records and providing insights into ash distribution from different styles and sizes of eruptions.

1. Introduction

The use of tephra to date and correlate depositional sequences—commonly referred to as tephrochronology or

* Corresponding author.
E-mail address: bjjensen@ualberta.ca (B.J.L. Jensen).
[1] Current address Department of Geography, University of Cambridge, Cambridge, UK.

https://doi.org/10.1016/j.quascirev.2021.107242

tephrostratigraphy—has a long history in North America, with important developmental research and discoveries being published as early as the 1960s (e.g., Powers and Wilcox, 1964; Stuiver et al., 1964; Wilcox, 1965; Theisen et al., 1968; Westgate and Dreimanis, 1967; Smith and Westgate, 1968). However, the application of tephrochronology has largely been limited to the west, where tephra are visible, abundant, and relatively proximal to their volcanic sources (e.g., Westgate, 1977; Porter, 1978; Riehle, 1985; Sarna-Wojcicki et al., 1987; Mullineaux, 1996; Preece et al., 1999; Lakeman et al., 2008; Kuehn et al., 2009; Jensen et al., 2013; Foit and Mehringer, 2016). In contrast, in northwestern Europe, with few proximal sources and visible deposits, the application of tephrochronology was limited until ground-breaking work by Persson (1966), followed by Dugmore (1989a, 1989b) and Pilcher and Hall (1992). These studies recognized the widespread presence of cryptotephra (tephra deposits not visible to the naked eye) across Scandinavia, Scotland and Ireland, and stimulated a flurry of research that has resulted in the establishment of a mature and complex tephrostratigraphic framework that reaches across northern Europe, the north Atlantic, and Greenland (e.g., Dugmore et al., 1995; Pilcher et al., 1995; Turney et al., 2004; Wastegård and Davies, 2009; Davies et al., 2012, 2014; Lawson et al., 2012; Bourne et al., 2015; Lowe et al., 2015; Plunkett and Pilcher, 2018).

In light of this research, it seemed plausible that areas of North America outside of the region draped by visible tephra falls had excellent potential to expand the geographical reach of tephrochronology. However, cryptotephra have not been widely examined in North America, despite Zoltai (1989) clearly illustrating their potential in his study of tephra in central Alberta peat bogs. The first truly systematic cryptotephra studies began almost 20 years later from peat bogs in SW and SE Alaska (Payne and Blackford, 2008; Payne et al., 2008). It was not until Pyne-O'Donnell et al. (2012) that the first record of cryptotephra outside the limits of visible tephra deposition in North America was reported, from Nordan's Pond Bog in Newfoundland. Being so far from western sources and in the opposite direction of prevailing winds from Iceland, expectations were low. However, the resulting record was a surprise—there were multiple tephra, none from Iceland, all from sources to the west, and some from as far as 6000 km away, much further than previously reported in cryptotephra studies outside of Greenland and Antarctica. Since this pioneering work, several additional publications have reported cryptotephra in the north-central to north-eastern portions of North America (Jensen et al., 2014; Mackay et al., 2016; Pyne-O'Donnell et al., 2016; Spano et al., 2017, Rabett et al., 2019) (Table 1). However, with the exception of Nordan's Pond Bog (Pyne-O'Donnell et al., 2012), these published studies are limited to the mid-to late Holocene (Mackay et al., 2016), the latest Pleistocene and early Holocene (Pyne-O'Donnell et al., 2016), or target specific tephra (Jensen et al., 2014; Spano et al., 2017, Rabett et al., 2019; Monteath et al., 2019) (Table 1).

Tephra identified in this region thus far include established marker horizons such as Mount St. Helens We (Washington; ~1482 CE), White River Ash, eastern lobe (WRAe, Alaska; 853 ± 1 CE), Newberry Pumice (Oregon; 1350–1275 cal yr BP), Aniakchak CFE II (Alaska; 3290–3510 cal yr BP), and Mazama (Oregon; 7682–7584 cal yr BP) (Egan et al., 2015; Davies et al., 2016; Mackay et al., 2016; Toohey and Sigl, 2017). Several of these tephra are distributed among continents and/or present in the Greenland ice cores, including WRAe, Aniakchak CFE II, Mazama, and Glacier Peak G (Zdanowicz et al., 1999; Pearce et al., 2004; Coulter et al., 2012; Jensen et al., 2014; Pyne-O'Donnell and Jensen, 2020). This region also seems well-placed to receive tephra from far afield sources such as Kamchatka, Mexico and, potentially, Japan (e.g., KS_1, Jala Pumice, FFB12-162) (Mackay et al., 2016). The abundance and diversity of tephra already identified in these few studies indicates that eastern North America is a key location for building a more developed tephrostratigraphic framework that would benefit studies both within and well beyond this region.

Here we take a major step in developing a composite framework for this region. We expand the network of sites examined for cryptotephra that covers a timespan similar to the original study at Nordan's Pond Bog. Focusing on regionally distributed ombrotrophic peat bogs located in Michigan, New York and Maine, we develop three independent tephrostratigraphies that cover the past ~7000 to 8000 years. We re-examine portions of Nordan's Pond Bog, in particular NDN-230 (Pyne-O'Donnell et al., 2012), present new data from Thin-Ice Pond, Nova Scotia (e.g., Pyne-O'Donnell et al., 2016), and describe a new tephra located in Greenland ice cores that integrates into this new framework. Age models are developed for all the new cores and updated for Nordan's Pond Bog and Thin-Ice Pond. We also present new geochemical data and update age constraints for several (potential) correlative deposits that are proximal to their volcanic source.

The result is the first composite tephrostratigraphic framework of the past ~14,000 years from the north central to eastern portion of the USA and Canada that will facilitate both regional and transcontinental correlations. New and updated ages for the cryptotephra will provide additional chronologic data points for the region and help refine age-depth models for these and future paleoenvironmental records. Finally, these tephrostratigraphies also inform broader issues of tephra distribution and implications for eruption frequency and shifting synoptic climate patterns.

2. Site localities

Atmospherically fed bogs (i.e., ombrotrophic peatlands) are sought-after sources of paleo-drought records and vegetation change in more humid regions of central and eastern North America because they are particularly sensitive to moisture changes (e.g., Booth, 2010; Booth et al., 2012a; Clifford and Booth, 2013). These peatlands preserve paleoenvironmental proxies such as pollen, plant macrofossils, and testate amoebae, and are well suited to tracking atmospherically transported pollutants, dust and tephra (e.g., Aaby, 1976; Barber et al., 1994; Nichols et al., 2006; Amesbury et al., 2012; Booth et al., 2012b; Mackay et al., 2016). Tephra are generally easy to find and define in ombrotrophic bogs because of the absence or low quantities of minerogenic sediment, minimal reworking and limited vertical movement (e.g., Payne et al., 2005; Payne and Gehrels, 2010). Therefore, ombrotrophic bogs have been the main target in developing the tephrostratigraphic framework presented here.

In this study we examined cryptotephra in four new bog sites, re-examined two previously studied sites and compared them with a tephra layer found in two Greenland ice cores (Fig. 1; Table 1). The bogs we examined were initially cored to illuminate drought and vegetation changes across the region (e.g., Booth et al., 2012a; Clifford and Booth, 2013; LeBoeuf, 2014; Charman et al., 2015; Mackay et al., 2021) (Fig. 1). Irwin Smith Bog (ISB) is in eastern Michigan, Bloomingdale Bog (BB) is in the north-central Adirondack Mountains in New York, and Sidney Bog (SB) is in south-central Maine (Fig. 1). The two cores from Sidney Bog collectively contain the most continuous sequence without hiatuses or major accumulation changes over the past ~8000 years. We revisited the core from Nordan's Pond Bog (NDN; Newfoundland), which was originally examined in 5 cm intervals, to recount several sections at

Table 1
Location information all sites reporting cryptotephra in the study region. If blank the data are missing from the publication.

Site	State/Province	Lat	Long	Approximate maximum age (cal yr BP)	Composite depth (cm)	[a]Cryptotephra interval (analyses and counts)	Reference
Long Bog (LB)	Wisconsin	46.001	−89.717	12,250	468	200–468 cm (~6500 −12,250 cal yr BP)	This study
Irwin Smith Bog (ISB)	Michigan	45.032	−83.618	6600	177	Full record	This study
Bloomingdale Bog (BB)	New York	44.383	−74.138	7700	190	Full record	This study
Sidney Bog (SB) core 1	Maine	44.390	−69.790	7000	404	Full record	This study
Sidney Bog (SB) core 2	Maine	44.390	−69.790	10,850	750	Full record	This study, Charman et al. (2015)
Thin-Ice Pond (TI)	Nova Scotia	43.908	−65.857	14,900	658	215–658 cm (~4000 −14,900 cal yr BP)	This study, Pyne-O'Donnell et al. (2016)
Nordan's Pond Bog (NDN)	Newfoundland	49.164	−53.600	9550	780	Full record	This study, Pyne-O'Donnell et al. (2012)
Veinot Lake (VL)	Nova Scotia	44.736	−64.538	14,000	930	840–848 cm; 13,500–13,800	Pyne-O'Donnell et al. (2016)
Crocker Pond (CP)	Maine	44.308	−70.824	14,500	1450	1368–1374; ~12,900–13,400	Pyne-O'Donnell et al. (2016)
Petite Bog (PB)	Maine	45.140	−63.940	13,450	865	150–160 cm; ~1070–1240 cal yr BP	Jensen et al. (2014)
Jeffrey's Bog (JRB)	Newfoundland	48.208	−58.818	3500	395	0–130 cm; < ~1200 cal yr BP	Mackay et al. (2016)
Framboise Bog (FBB)	Nova Scotia	45.719	−60.552	10,200	450	0–160 cm; < ~3000 cal yr BP	Mackay et al. (2016)
Villagedale Bog (VDB)	Nova Scotia	43.518	−65.526	6000	455	0–180 cm; < ~2100 cal yr BP	Mackay et al. (2016)
Saco Heath (SCH)	Maine	43.551	−70.034	7000	515	0–210 cm; < ~2500 cal yr BP	Mackay et al. (2016)
Pound Cove Bog (PCB)	Newfoundland	49.268	−53.591	8000	580	30–80 cm; ~500–1500 cal yr BP	Monteath et al., 2019
Baby Pond Bog (BPB)	Newfoundland	47.268	−53.541	uncertain (<10 ka)	490	50–100 cm	Monteath et al., (2019)
Keweenaw Bay, Lake Superior (KB)	Michigan	47.130	−87.820	–	~800	360–530 cm	Spano et al. (2017)
Isle Royale, Lake Superior (IR)	Michigan	47.970	−88.470	–	~675	268–328 cm	Spano et al. (2017)
Balsam Creek kettle lake (BCK)	Ontario	46.476	−79.150	10,500	363	275–330 cm	Rabett et al. (2019)

[a] some records were counted over longer intervals or the full record (e.g., Balsam Creek kettle lake), but only targeted peaks were extracted and analysed.

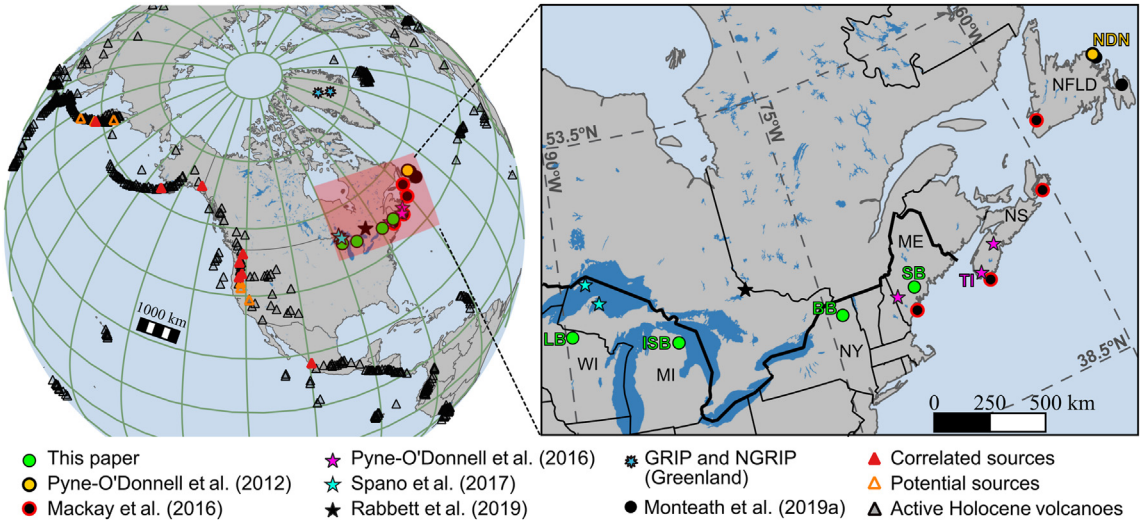

Fig. 1. Location of sites discussed in this study, details on all new and previously reported locations are provided in Table 1. Long Bog (LB) in Wisconsin (WI), Irwin Smith Bog (ISB) in Michigan (MI), Bloomingdale Bog (BB) in New York (NY), and Sidney Bog (SB) in Maine (ME) are first described here. Thin-Ice Pond (TI) in southern-most Nova Scotia (NS), and Nordan's Pond Bog (NDN) in northern Newfoundland (NFLD), have new data presented here although they were first discussed by Pyne-O'Donnell et al. (2012, 2016).

a 1 cm resolution to clearly locate key isochrons and resample NDN-230. We examined two additional sites, including Long Bog (LB), Wisconsin, and the previously reported Thin-Ice Pond (TI) in Nova Scotia (Pyne-O'Donnell et al., 2016), to delineate the record between the Mazama (~7600 cal yr BP) and Glacier Peak tephra (~13,700–13,400 cal yr BP). Finally, we report a tephra from Greenland's GRIP and NGRIP ice cores that likely correlates with a newly described tephra from Sidney Bog. Detailed summaries of these locations, and those that have previously reported cryptotephra in this region, are noted in Fig. 1 and Table 1.

3. Methods

3.1. Tephra processing

To produce shard concentration profiles for the bogs, loss-on-ignition residue from 1 to 3 cm^3 of peat was dissolved in dilute HCl, passed through a 20 μm sieve and mounted on slides with glycerol. Slides were examined for glass shards (reported as shards/cm^3) using light microscopy with plane-polarized light. Sidney Bog core 2 (SB–C2) was initially screened at 5 cm intervals, with targeted 1 cm counts in certain intervals, in particular around and

below White River Ash. Targeted recounts on Nordan's Pond Bog were also conducted at 1 cm resolution. For Thin-Ice Pond the post-glacial Holocene lake gyttja between 515 and 215 cm depth was contiguously examined for the presence of cryptotephra glass shards at 5 cm resolution. Samples were sieved between 80 μm and 25 μm, followed by heavy liquid flotation (Turney, 1998) to extract glass shards. Sections of core with high shard concentrations were then more closely examined at 1 cm resolution. Shard concentration profiles are available in Tables S11-S16.

Glass from shard peaks for geochemical analyses were extracted from the peat or lake sediments by floatation, using sodium polytungstate (SPT) or lithium heteropolytungstate (LST) at 2.45 g/cm^3 and, as appropriate, acid digestion (detailed methods outlined in Dugmore et al., 1992, Turney, 1998, Blockley et al., 2005; Roland et al., 2015, Monteath et al., 2019). Both methods were applied to separate splits of a few samples (e.g., WRAe, Newberry and Mazama) to ensure the glass geochemistry was not affected by acid-digestion. Extracts were mounted by pipette into acrylic pucks placed on double-sided tape. After drying, holes with samples were filled with epoxy (Struers SpeciFix-40 or 20), polished and carbon-coated for electron-microprobe analysis. Tephra from NGRIP and GRIP ice cores were located through contiguous ice core sampling scanning for cryptotephras at 15–20 cm intervals. Samples were mounted on glass slides with epoxy for both optical assessment and geochemical analyses (e.g., Cook et al., 2018a).

3.2. Tephra analyses

Glass shards were analysed for major and minor element geochemistry at three different institutes using electron microprobes with five wavelength dispersive spectrometers (WDS-EMPA). All cryptotephra (except TI-323, NGRIP and GRIP tephra) and several reference samples, were analysed at the University of Alberta on a JEOL 8900R Superprobe or CAMECA SX100 using an accelerating voltage of 15 KeV, 6 nA current and 10 μm beam. For samples too small for the larger beam size, a 5 μm beam was used with the time-dependent intensity correction methodology integrated into the Probe for Windows software (e.g., Donovan et al., 2015; Jensen et al., 2019; Foo et al., 2020). This provides a means to correct for Na-loss and potential related increases in Si and Al due to the more focused beam. Two secondary standards—a Lipari obsidian (ID 3506) and Old Crow tephra (UA 1099)—were analysed at the start, end, and during each analytical run (e.g., Jensen et al., 2008; Kuehn et al., 2011) to track calibration, drift, and any other potential analytical complications. We have found that it is important, especially when using non-standard analytical methods, to use an additional natural glass standard that is more similar to the tephra being analysed (e.g., secondarily hydrated Old Crow tephra collected 1500 km from source). This standard is more sensitive to the electron beam than the young and less hydrated Lipari obsidian standard, and more closely tracks the behavior of cryptotephra under analysis. NGRIP, GRIP, Thin-Ice Pond, and selected Sidney core 2 tephra were analysed at the Tephra Analytical Unit, School of Geosciences, University of Edinburgh, on a CAMECA SX100 microprobe with a 15 keV accelerating voltage and focused 3 or 5 μm beam diameter (see Hayward, 2012 for details). Secondary standards varied between analytical runs but always included the Lipari obsidian, paired with either U.S. Geological Survey (USGS) basaltic glass BCR-2G or Old Crow standards. Thin-Ice Pond tephra TI-323 and several reference Kamchatkan samples were analysed at the GEOMAR Institute in Kiel on a JEOL JXA 8200 using a 15 kV accelerating voltage, 6 nA current and 5 μm beam (detailed analytical methodology is outlined in Portnyagin et al., 2020). Standards included Smithsonian rhyolitic glass VG-568 and basaltic glass VG-A-99 (Jarosewich et al., 1980). All glass major and minor element geochemical data presented here are normalized to 100% on a water and volatile-free basis; these data and all secondary standard data are available in Tables S1, S3-S9.

Trace element geochemistry was acquired for several cryptotephra samples and their potential proximal equivalents. Mono Craters reference tephra and an Irwin Smith Bog cryptotephra were analysed at the Arctic Resources Geochemistry Laboratory, University of Alberta, using a Resolution ArF 193 nm excimer laser (Applied Spectra, USA) system, with a Laurin-technic S155 2-vol ablation cell, connected via nylon tubing to a sector-field ICPMS Thermo Element XR (Thermo Fisher Scientific Inc., Bremen, Germany). The mass spectrometer was operated in low mass resolution mode (M/ΔM = ca. 300). Mono tephra samples were analysed with a 23 μm spot size, 5 Hz frequency, and 3 J/cm^2 fluence. ISB-1 was measured using a 10 μm spot size, 5 Hz frequency, and 5 J/cm^2 fluence (see Table S2 for full analytical conditions). Calibration was performed using NIST SRM 612 in conjunction with internal standardization using ^{29}Si. The mass content of Si was determined from WDS-EPMA. All data were reduced offline using Iolite v3 (Paton et al., 2011; https://iolite-software.com/) and included careful screening of time-resolved counts to help screen out inclusions and other problematic data points. The results of the secondary standards (e.g., ATHO-G) agree with the reference values within relative uncertainties of typically 5–10% or better at the 95% confidence level. TI-323, TI-317 and KS_2 trace elements were measured at the Institute of Geosciences (Christian Albrecht University, Kiel) using a 193 nm excimer Coherent laser with a custom built two-volume ablation cell (ETH Zurich, Fricker et al., 2011) coupled with a quadrupole-based ICP-MS (Agilent 7500cs). Data were collected over a number of years and the evolution of the methods is summarized in Portnyagin et al. (2020). For samples analysed here, ablation was performed using either a 16, 24, or 50 μm diameter laser spot with a 5 Hz frequency and fluence between 7.5 and 10 J/cm^2. Rhyolite reference glass ATHO-G was used for calibration. Concentrations were calculated using CaO as the internal standard, with the reference value measured by WDS-EPMA. Ti and Si concentrations (analysed as unknown) were compared to the WDS-EPMA data for the same glass shards. Data points were rejected when the values disagreed by 20% indicating likely entrapment of significant amounts of crystal phases (e.g., pyroxene, magnetite and plagioclase) during analysis. None of the trace element data from either lab was corrected for potential fractionation at smaller beam sizes (generally not observed), or for lower concentrations (−3 to −5%) observed on standards when correcting to ^{29}Si (e.g., Tomlinson et al., 2010). All trace element data, standards and analytical conditions are noted in Table S2.

The number of final analyses required to define a unit as a primary tephra deposit was based on criteria including the size and shape of the glass shard concentration peaks, morphology of the glass, the presence or absence of multiple populations within a sample and the repetition of a population(s) over multiple depths, and its relationship (e.g., radiocarbon age, stratigraphy) to other samples and potential correlatives. Also considered was the total number of individual analyses per sample, including discards related to mixed mineral-glass analyses, unsuccessful analyses (e.g., shards too small), and/or poor totals, as well as the presence/absence of detrital and re-worked glass (i.e., how many glass shards can be found in a typical random sample). Detrital glass is often visibly weathered with altered geochemistry (e.g., Table S3). Given these considerations, it was determined that for most samples a minimum of six or seven individual shard major-element analyses was required to define a geochemical population that likely represents a primary deposit. If a successfully characterized primary tephra was not confidently correlated to a known tephra, they were

named after their location (e.g., Bloomingdale Bog = BB; Sidney Bog = SB), and numbered from youngest to oldest (e.g., Irwin Smith Bog = ISB-1, ISB-2, etc.). Tephra from Thin-Ice Pond and Nordan's Pond Bog follow the naming conventions of the original studies and are named by their depth in core (e.g., TI-317, NDN-230) (Table 1). All primary tephra in this study have been accessioned within the University of Alberta tephra database, their numbers (UA 3###) are noted in Table S1. All point-by-point glass shard data, including detrital glass, populations with fewer than six analyses, secondary standard data, and some reference tephra are available in supplementary data (Tables S1-S9).

3.3. Radiocarbon dating and modelling

Radiocarbon dates, some of which were previously reported (e.g., Daley et al., 2009; Clifford and Booth, 2013; Charman et al., 2015), constrain the ages of the bog and lake sediments (Table S10). In total 20–28 radiocarbon dates per peat core, and seven for the Thin-ice Pond core, were used to develop the initial age-depth models. Typically, *Sphagnum* stems were selected for dating; Thin-Ice Pond dated material is noted in Table S10.

Age-depth models assume that deeper sediments in a core are older, allow sedimentation rate to vary with time, have matching uncertainty at adjacent levels, and have variable uncertainty at undated levels (i.e., levels with a known date should have smaller uncertainty ranges than levels far from any chronological marker). Bchron is a simple and flexible R package developed for age-depth modeling that satisfies these criteria (Parnell et al., 2011; Parnell, 2014). Using this package, we generated three different age-depth models for each site, all dates calibrated using IntCal20 (Reimer et al., 2020): age model 1 is based only on the radiocarbon dates; age model 2 was generated by incorporating the ages of the WRAe, Mazama and Glacier Peak G (when present) into age model 1; and age model 3 incorporated all confidently correlated tephra with relatively well-constrained ages (e.g., layer T, Mount St. Helens set W, Jala Pumice, Newberry Pumice, Mount St. Helens Yn) into age model 2. The tephra ages were input into the age-depth models as chronological control points using their calendar year ages with a normal distribution. The goal in providing three different age-depth models is to offer the best age estimate for tephra of unknown origin, or of known origin but with poorly constrained age, while allowing a critical examination of distal and cross-core correlations. When a tephra appears in multiple records, we plotted the probability densities of the estimated ages from all sites to examine cross-core correlations and calculated a final age. The final age was calculated by combining the predicted age distributions from each of the cores in which the tephra were present and defining one sigma and two sigma quantiles for that combined distribution (Fig. 2; Table 2).

In reviewing potential correlatives, we compiled all published radiocarbon ages for the proximal tephra deposits: North and South Mono, Newberry Pumice, East Lake tephra, Chaos Crags, Jala pumice, KS_1, Us-Kr, and Iliinsky. These original radiocarbon dates were recalibrated using IntCal20 (Reimer et al., 2020) and modelled using the Tau_Boundary Function, within an OxcCal v.4.4 Sequence model (Blockley et al., 2008; Bronk Ramsey 2009a, 2009b). This function is well suited to modelling tephra ages as it assesses how radiocarbon dates would logically cluster around a boundary or event – in this case the tephra deposition (representing a relatively instantaneous event). It assumes that the ages above and below the boundary would be exponentially distributed, with most of the ages clustering around the boundary. This function allows for a statistical assessment of the radiocarbon dates and will flag dates that fall significantly outside the expected distribution of ages, which provides an independent means of interrogating the dates. This modelling has been applied to the reassessment of several established tephra ages in North America (e.g., Davies et al., 2016; Jensen et al., 2019).

All new ages, previously published ages, and newly recalculated ages for proximal deposits are reported in Table 2. All individual radiocarbon dates (except those from Charman et al., 2015 for Sidney Bog core 2), age-depth models, and recalculated ages are available in supplementary data Tables S10-S17.

4. Results and discussion

4.1. Shard counts and peaks

Over 40 distinct peaks in glass shards were identified in Irwin Smith, Bloomingdale and Sidney Bogs (Fig. 3). Additional complexity and multiple populations were identified in the short interval re-sampled in Nordan's Pond Bog, and three new shard peaks were located in Thin-Ice Pond. Irwin Smith Bog presented a challenge as there was a large background signal of detrital glass grains in the core. Detrital glass is sometimes observable during counting as visibly weathered grains (Fig. 4F) that are often geochemically altered with high K_2O and low Na_2O and forming no discrete populations (e.g., Tables S3-S5). Irwin Smith Bog is much closer to midwestern aeolian deposits that contain a glass component and is more commonly affected by wind-blown dust; we suspect that this is the main source of this detrital glass. As a result, we were unable to extract and analyze primary glass shards from several peaks with high detrital glass content (e.g., 12–18 cm, 90 cm, 130 cm; Tables S3 and S11). This challenge also played a role in our inability to collect useable data from Long Bog, Wisconsin, which was targeted to examine the poorly represented time between ~13,500 cal yr BP and 8000 cal yr BP. Two complications for this record include its existence as a fen (i.e., groundwater and surface-water influenced) during this time period, and detrital glass that dominated the signal, masking small shard peaks that may have contained primary material and leaving us with few unambiguous analyses. Because of these results, Long Bog will not be discussed further. We present this as a cautionary tale for those hoping to carry out cryptotephra studies in, and adjacent to, the Midwest, and any other North American locale affected by loess deposition, past (e.g., last glacial, deglacial) or present (e.g., interior Yukon and Alaska).

Background levels of glass in Bloomingdale and Sidney Bogs were lower and shard peaks were better defined. Volcanic glass was successfully extracted and analysed for the majority of these peaks. In a few cases, we were unable to extract glass or obtain enough analyses from a sample to include in the final results (e.g., Tables 2, S1), although all analyses are available in Tables S3-S7. A hiatus was identified around the time of the White River Ash deposition in both Irwin Smith and Bloomingdale Bog cores (e.g., Booth et al., 2012a; LeBoeuf, 2014), but Sidney Bog was uninterrupted. The composite record from both Sidney Bog cores represents an exceptional record of tephra deposition on the east coast of North America and a rare example of two fully counted and characterized cores from a single site.

Nordan's Pond Bog was resampled around the original sample NDN-230, which was linked to Augustine G, but newer proximal data show that this correlation is incorrect (Pyne O'Donnell et al., 2012; Blockley et al., 2015). We resampled and recounted this core section at 1 cm resolution and identified multiple peaks, highlighting how the initial 5-cm 'range-finding' masked some of the inherent complexity of this record. Additionally, the samples are spread across a core break and show some potential issues with tephra reworking at the core bottom and top. A similar problem was encountered in Irwin Smith Bog where three major tephra

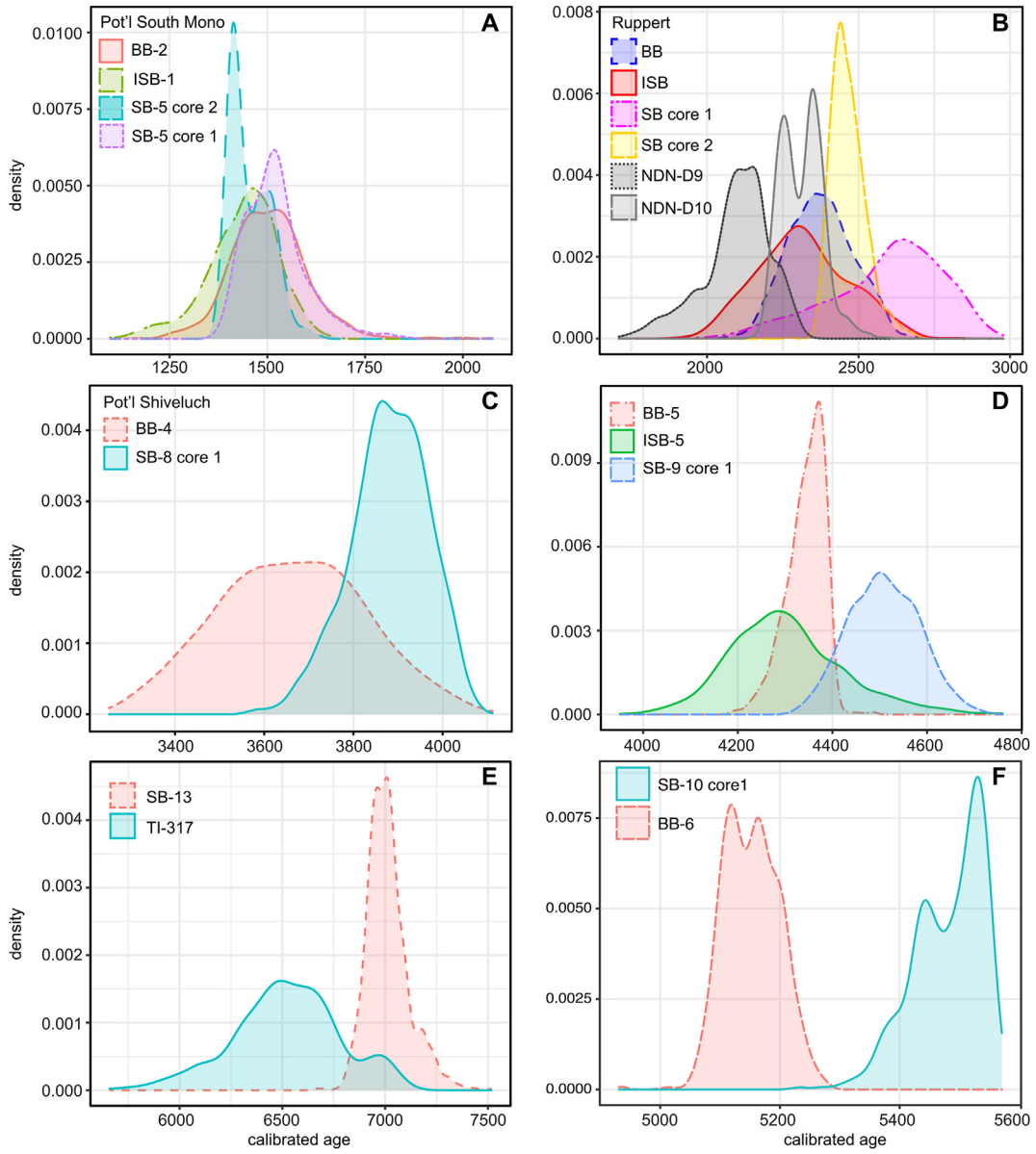

Fig. 2. Probability density functions illustrating the calibrated age distribution of selected tephra. Plots on panels A to E depict modelled age ranges of tephra correlated across different cores. All ages of correlated tephras overlap within two-sigma confidence interval, most within one-sigma confidence interval, supporting their geochemical correlations. Note that in (B) NDN-230 straddles a core boundary and Ruppert is present in both D9 and D10. The age distributions from the other sites suggest that D9's age estimate may be too young. Therefore, the age from D9 was not included in calculating final age estimate for Ruppert tephra. (F) BB-6 and SB-10 were initially correlated but are now considered two tephra partly based on their disparate ages.

units were found reworked in the top of the second drive (ISB-2, 3, 4; Supplementary data Table S1, S3, S11). Sidney Bog core 2 (originally counted in 5 cm sections) had seven intervals resampled and recounted at 1 cm resolution to define peaks better and help link the two cores. Unfortunately, core 2 sampled a section of peat that experienced extensive downward movement of WRAe (similar to what was documented in Saco Bog; Mackay et al., 2016). This downward movement of WRAe made it challenging to identify the tephra closely preceding this unit that had been noted in the other cores (e.g., Newberry Pumice) as shard peaks were ambiguous and many that were sampled were dominated by WRAe. However, eight additional tephra horizons were successfully analysed, including one unique deposit.

In Thin-Ice Pond, we identified a closely spaced cluster of three cryptotephra layers in the early mid-Holocene lake gyttja within a narrow stratigraphic interval of ~35 cm (350–315 cm; Table S16). This section, which was initially sampled and counted at 5 cm intervals, was reprocessed and reanalyzed at 1 cm resolution. No other shard peaks were found between these three new tephra and the previously reported late Pleistocene Glacier Peak B and G tephra and Mount St. Helens J tephra (Pyne-O'Donnell et al., 2016). The three new tephra layers were successfully extracted and geochemically analysed. Additionally, a tephra identified from the mid-Holocene interval in the NGRIP and GRIP ice cores was compared to similar-aged tephra here. All shard counts are reported with the age models in Tables S11-16.

Of the >40 glass peaks found at the sites; 30 distinct tephra horizons were sufficiently characterized to categorize as primary deposits. Previous studies describe 15 different tephra in eastern North America, and only six of these 15 were not documented again

Table 2
Summary of all cryptotephra reported in the study region.

Tephra	Locations found	Modelled age, this study, (site, age model), cal yr BP	Age of correlative or potential correlative, [median], cal yr BP unless otherwise noted	Source for confidently correlated tephra	Probable or speculative source(s) and/or tephra	Key references
SB-1	SB core 1	230 to modern (3)	–	–	Cascades (Lassen Peak, AD 1915?)	This study
SB-2	SB core 1	230 to modern (3)	–	–	–	This study
Layer T	SB core 2, FBB	310 to modern (2)	AD 1799–1800, tree-ring[a]*	Mount St. Helens, WA	–	This study; Yamaguchi et al. (1990)*; Mackay et al. (2016); Foo et al. (2020)
Villagedale	VDB, SCH	–	AD 1500–1750 (VDB); AD 1572–1762 (SCH)*	–	Layer T?	This study, Mackay et al. (2016)*
BB-1	BB	505–205 (3)	–	–	AA-AP	This study
MSH set W(e)	SB core 1 & 2, JRB, NDN	620–385 (SB-C1, 2); 525–265 (SB-C2, 2); 770–420 (NDN, 2)	all set W AD 1479 to <1510, tree-ring[a]*	Mount St. Helens, WA	–	This study, Yamaguchi and Hoblitt (1995)*; Pyne-O'Donnell et al. (2012); Mackay et al. (2016)
SB-3	SB core 1	600–430 (3)	**650–520 [585]**	–	Mono-Inyo Craters (Inyo?)	This study; Sieh and Bursik (1986)
SB-4	SB core 1	1075–1015 (2)	975–1511*; **1060–1025, 1005–955 [995]**	–	Fish Lake II; Chaos Crags, Lassen Peak	This study; Clynne et al. (2008); Foit and Mehringer (2016)*
Jala pumice	SB core 1, VDB	1075–1015 (2)	1061–820*; **1040–680 [875]**[a]	Volcan Ceboruco, Mexico	–	This study; Sieron and Siebe (2008); Mackay et al. (2016)*
White River Ash, east	ISB, BB, SB core 1& 2, NDN, PB, JRB, FBB, VDB, SCH, PCB, BPB	1145–840 (ISB,1); 1030–690 (BB,1); 1195–1045 (SBC1); 1210–1020 (SBC2,1); 1505–900 (NDN,1)	AD 852–854 (1098–1096 cal yr BP), ice core[a]*	Mount Churchill, Wrangell volcanic field, Alaska	–	This study, Pyne-O'Donnell et al. (2012); Jensen et al. (2014); Mackay et al. (2016); Toohey and Sigl (2017)*, Monteath et al. (2019)
Newberry Pumice	ISB, BB, SB core 1, NDN	1520–1180 (ISB,2); 1370–1150 (BB,2); 1330–1140 (SBC1,2); 1670–1190 (NDN,2)	1569–1345*; **1385–1245 [1315]**[a]	Newberry Volcanic Field, OR	–	This study, MacLeod et al. (1995); Kuehn and Foit, (2000, 2006); Pyne-O'Donnell et al. (2012)*
ISB-1, BB-2, SB-5	ISB, BB, SB core 1 & 2	1670–1305 (3, all sites)	**1350–1300 [1330]**	–	Mono-Inyo Craters (South Mono?)	This study; Bursik et al. (2014)
BB-3	BB	2030–1565 (3)	**1970–1955, 1945–1830 [1890]**	–	Us-Kr, Ushishir, Kuriles	This study, Razzhigaeva et al. (2012); MacInnes et al. (2016)
KS1	BB, VDB	2085–1610 (3)	2005–1771*, 1705–1590 [1652]**, **1790–1690 [1730]**	Ksudach, Kamchatka	–	This study, Mackay et al. (2016)*, Ponomareva et al. (2017)**
Ruppert tephra	ISB, BB, SB core 1 & 2, NDN	2800–2130 (3, all sites)	2321–2109*; ~2700–2300**	–	AA-AP	This study, Pyne-O'Donnell et al. (2012)*, Monteath et al. (2017)**
NDN230-2	NDN	2470–1830 (3)	–	–	–	This study
MSH set P	ISB, SB core 1	2600–2080 (3)	2750–2470 and 2760–2590*; ~3000–2550**; 2710–2350 (upper set P)***	Mount St. Helens, WA	Upper set P (i.e., Pu/Py)	This study, Foit et al. (2004)*; Pallister et al. (2017)**; Jensen et al. (2019)***.
SB-6	SB core 2	2965–2590 (3)	3013–2794*	–	Shiveluch, (SHb/SH2800?)	This study, Ponomareva et al. (2017)*
SB-7	SB core 1	2950–2230 (3)	3212–2764*	–	Fish Lake III (Medicine Lake, CA?)	This study; Foit and Mehringer (2016)*
FBB12-162	FBB	–	3604–2643	–	Japan (Tarumai tephra Ta-c2?)	Mackay et al. (2016)
Aniakchak CFE II	NDN	-	3622 ± 6 a b2k (3572 cal yr BP)*; 3545–3425**	Aniakchak, Alaska Peninsula, Alaska	–	Vinther et al. (2006); Adolphi and Muscheler (2016)*, Davies et al., in review** (see notes below)
MSH Yn	SB core 1 & 2	3920–3530 (SBC1,2); 3810–3570 (SBC2,2)	3805–3535*[a]	Mount St. Helens, WA	–	This study, Jensen et al. (2019)*
BB-4, SB-8	BB, SB core 1	4025–3395 (3, all sites)	3898–3533	–	Shiveluch (SH#27/#28?)	This study, Ponomareva et al. (2017)
ISB-5, BB-5, SB-9	ISB, BB, SB core 1	4620–4150 (3, all sites)	–	–	–	This study
BB-6	BB	5210–5080 (3)	–	–	Glacier Peak?	
SB-10	SB core 1	5550–5335 (3)	–	–	Glacier Peak?	
BB-7	BB	5940–5745 (3)	6074–5896 (5978)*	–	NDN 430, AA-AP?	This study, Pyne-O'Donnell et al. (2012)*
SB-11, NGRIP 950.25, GRIP 883.30	SB core 1 & 2, NGRIP, GRIP	6070–5780 (3); 5853 ± 15 a b2k* (5803 cal yr BP)	5655–5620, **5610–5580 [5600]**	–	Iliinsky, Kamchatka	This study, Vinther et al. (2006); Adolphi and Muscheler (2016)*
SB-12	SB core 1	6710–6150	6464–6244*	–	NDN455, AA-AP?	This study, Pyne-O'Donnell et al. (2012)*
SB-13, TI-317	SB core 1, TI	7215–6065 (3, all sites)	–	–	AA-AP, Cascades (Rainier?)	This study

(*continued on next page*)

Table 2 (*continued*)

Tephra	Locations found	Modelled age, this study, (site, age model), cal yr BP	Age of correlative or potential correlative, [median], cal yr BP unless otherwise noted	Source for confidently correlated tephra	Probable or speculative source(s) and/or tephra	Key references
East Lake	BB, NDN	7280–6835 (3)	**6809–6587*; 7430–6555 [7130]**[a]	Newberry Volcanic Field, OR	–	This study, MacLeod et al. (1995); Kuehn and Foit, (2000, 2006); Pyne-O'Donnell et al. (2012)*
KS2	TI	7185–6970 (1)	6877–6693 [6786][a]*	Ksudach, Kamchatka	–	This study, Ponomareva et al. (2017)*
Mazama	BB, SB core 2, TI, KB, IR, BCK	7630–7335 (TI,1); 7465–6600 (BB,1); 7805–7055 (NDN,1); 7820–7595 (SBC2,1)	7682–7584[a]*	Crater Lake, OR	–	This study, Pyne-O'Donnell et al. (2012); Egan et al. (2015)*; Spano et al. (2017), Rabett et al. (2019)
BCK-325	BCK	–	8710–7865	–	Mount Mazama?	Rabett et al. (2019)
Glacier Peak B (minor G)	TI, VL, CP	–	13,710–13,410	Glacier Peak, WA	–	Pyne-O'Donnell et al. (2016)
MSH set J	TI, VL, CP	–	uncertain, <100 to >200 years after GP G	Mount St. Helens, WA	–	Kuehn et al. (2009); Schachtman et al. (2015); Pyne-O'Donnell et al. (2016)

^{14}C and GICCO5 ages for Aniakchak CFE II are difficult to reconcile so both estimates are presented (Pearce et al., 2017; Davies et al., in review.).
All ages are presented at two sigma and rounded to the nearest 5 years.
Bolded ages are newly calculated ages from published 14C dates on proximal deposits (Table S17).
[a] - indicates ages used in age models.

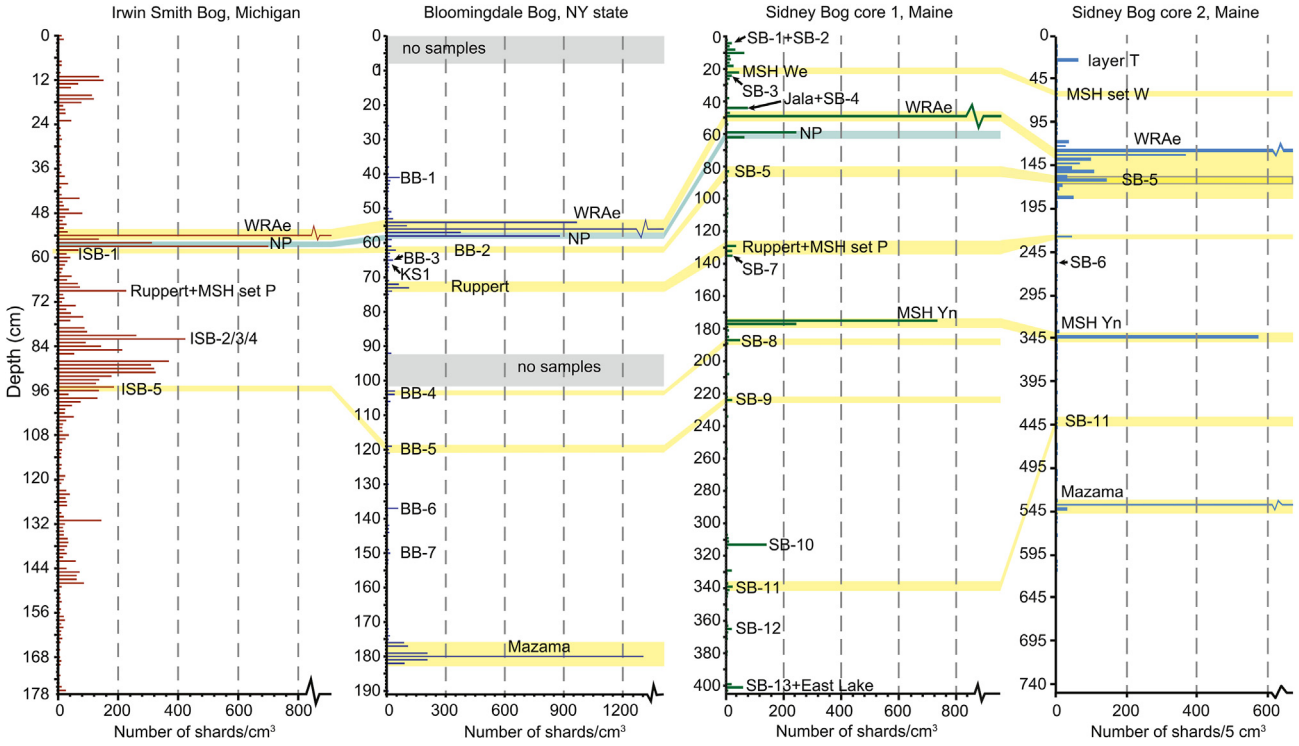

Fig. 3. Glass shard counts for the four new cores described in this study. Correlations across the sites based on geochemistry and corresponding ages are highlighted yellow. Newberry Pumice (NP) is highlighted green to differentiate it from overlying WRAe and the underlying potential South Mono correlative. Counts for WRAe were off the scales presented here for all cores. Shard/cm^3 for each site are available in Tables S11-S16.

at the new sites. Collectively, this has led to the identification of 36 unique tephra deposits in this region (Table 2). Results and discussion of the geochemical analyses are summarized below by allocating the tephra to three categories: confidently correlated tephra, tephra with probable correlations, and newly described tephra that are not confidently correlated to any published data.

4.2. Confidently correlated tephra

Out of the 30 distinct tephra characterized here, twelve have been confidently correlated to previously described units, with all but one linked to their volcanic source (Tables 2 and 3). Confidently correlated tephra have well defined geochemistry and compatible ages; nine have been described in the region previously and three are reported here for the first time.

In general, records from sites examined here were surprisingly

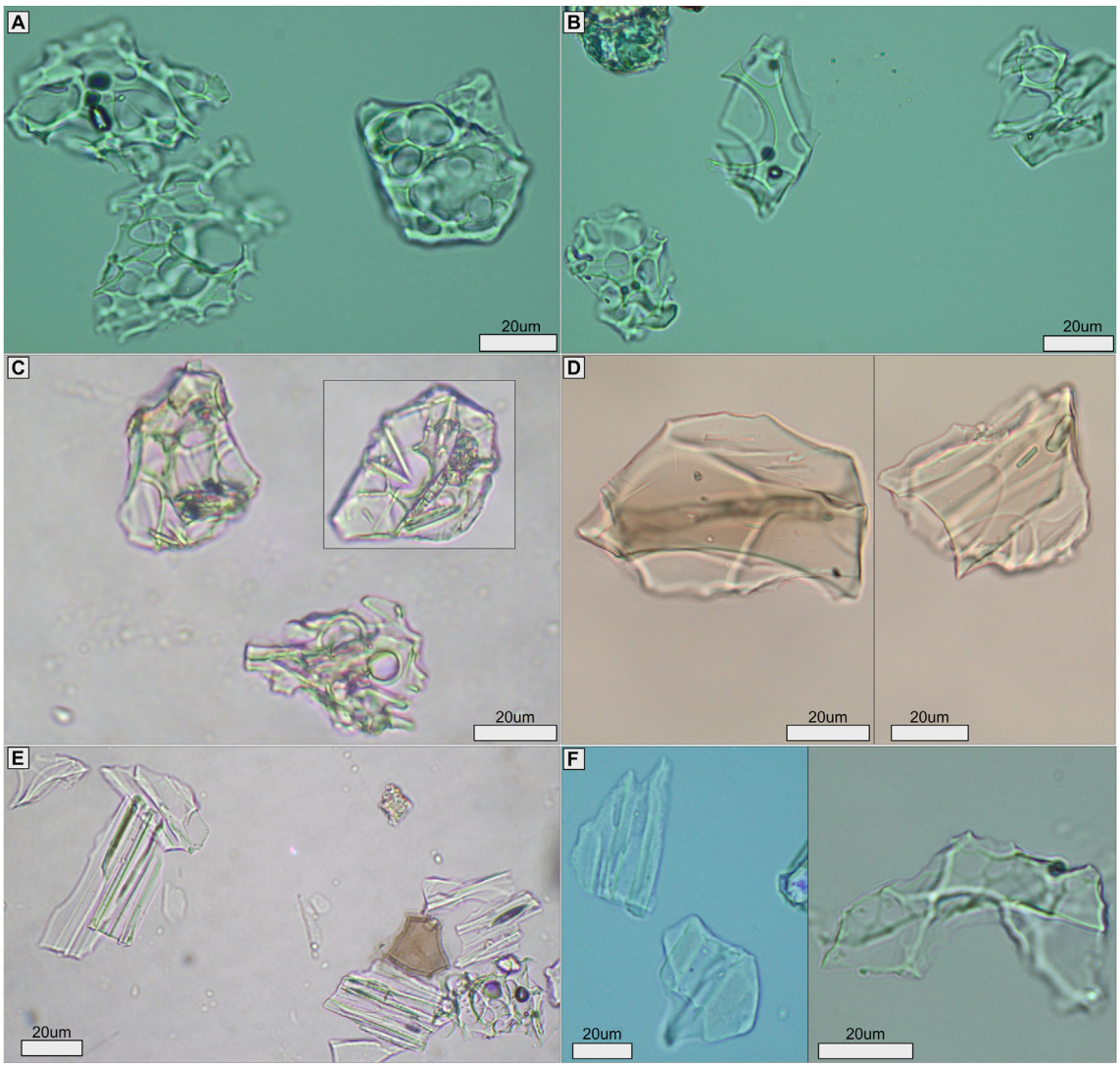

Fig. 4. Selected plane-light images of glass shards. (A) WRAe is composed almost entirely of highly inflated pumice; (B) MSH Yn is also predominately inflated pumice with a few blockier shards; (C) KS_2 is very distinct with pumice and blocky shards that are rich in microlites; (D) TI-317 tends to have blocky and platy shards with microlites and the occasional brown shard; (E) Mazama's distinct morphology is largely composed of platy glass with fluted, bubble-walled and tricuspate shards; (F) Examples of weathered glass, the image on the left is ragged and pitted but also has a haziness that is typical for altered glass, the image on the right is ragged and pitted but not hazy. Some primary shards can exhibit pitting due to the acidic bog environment, but this generally does not alter the geochemical composition. The haziness often implies that the glass is chemically altered.

consistent with those previously published ones – only three Holocene tephra reported in other eastern North American studies were not identified in this study (FBB12-162, Mackay et al., 2016; Aniakchak CFE II, Pyne-O'Donnell et al., 2012; BK-325, Rabett et al., 2019, Tables 1 and 2). We also discuss the possibility that Villagedale tephra from Mackay et al. (2016) may, in fact, be layer T from Mount St. Helens. Additionally, of the confidently correlated tephra, only Mount St. Helens set P, Mount St. Helens Yn, and KS_2 have not previously been described at other sites in the region. As Mackay et al. (2016) observe, Aniakchak CFE II was absent at all sites, suggesting it is unlikely to be present south of Newfoundland (Pyne-O'Donnell et al., 2012). This may be related to the very strongly northward directed plume for this eruption (e.g., Begét et al., 1992). FBB12-162 was a minor tephra with few analyses at the one site it was located (Mackay et al., 2016), and our inability to relocate this tephra suggests it is sparsely distributed in the region. The Balsam Creek tephra, BK-325 (Tables 1 and 2), also remains enigmatic; it was not re-located at the three localities here that contained the correct time interval. BK-325 is estimated to be ~600 years older than Mazama with very similar geochemistry. Rabett et al. (2019) argue that the character of the sediments between BK-325 and Mazama make it unlikely that it is reworked Mazama, and that the age difference is too great to be from the pre-cursor eruption known as Llao Rock (e.g., Bacon et al., 2014; Foit and Mehringer, 2016). More sites will be necessary to unambiguously determine if this is a truly unique deposit.

None of the new sites presented here has records that extended far enough into the Pleistocene to capture Glacier Peak G and B and Mount St. Helens J, which are present in Thin-Ice Pond, Crocker Pond, and Veinot Lake (Pyne-O'Donnell et al., 2016, Tables 1 and 2).

4.2.1. Mount St. Helens

Perhaps unsurprisingly, Mount St. Helens (MSH), the most active Cascade volcano during Holocene time, is the most common single source of tephra in eastern North America, with a total of five MSH tephra identified in this and past studies. The distal tephra

Table 3
Glass geochemical averages and standard deviations of confidently correlated tephra. Data are normalized to 100%.

Tephra	SiO_2	TiO_2	Al_2O_3	FeOt	MnO	MgO	CaO	Na_2O	K_2O	P_2O_5	F	Cl	SO_3	H_2Odiff	n
Layer T	70.18	0.50	15.66	2.94	0.07	0.82	2.90	4.94	1.90	–	–	0.12	–	1.65	22
	0.70	0.05	0.25	0.22	0.02	0.11	0.19	0.24	0.09	–	–	0.02	–	1.05	
MSH set W(e)	76.65	0.24	13.19	1.36	0.03	0.22	1.22	4.35	2.62	–	–	0.13	–	4.08	30
	1.23	0.05	0.77	0.15	0.02	0.06	0.30	0.32	0.16	–	–	0.05	–	4.16	
Jala pumice	71.24	0.30	15.91	1.92	0.11	0.36	1.30	5.31	3.43	–	–	0.13	–	2.83	17
	0.50	0.05	0.22	0.16	0.03	0.06	0.12	0.21	0.12	–	–	0.03	–	2.56	
WRAe	73.57	0.22	14.73	1.50	0.05	0.40	1.92	4.14	3.16	0.02	–	0.34	–	3.91	73
	0.68	0.04	0.54	0.11	0.03	0.06	0.13	0.39	0.09	0.03	–	0.04	–	2.37	
Newberry Pumice	73.34	0.23	14.55	1.93	0.07	0.16	0.86	4.71	4.02	0.00	–	0.14	–	3.50	75
	0.47	0.04	0.46	0.06	0.03	0.02	0.04	0.33	0.14	0.01	–	0.03	–	1.93	
KS1	73.59	0.37	14.29	2.40	0.11	0.44	1.99	5.23	1.42	–	–	0.20	–	3.37	7
	0.84	0.06	0.26	0.29	0.04	0.08	0.16	0.32	0.06	–	–	0.07	–	4.37	
Ruppert tephra	74.26	0.30	13.97	2.00	0.10	0.46	2.27	4.45	1.99	–	–	0.25	–	2.27	142
	0.56	0.04	0.20	0.13	0.03	0.06	0.13	0.36	0.13	–	–	0.04	–	1.63	
MSH set P	74.96	0.30	14.07	1.63	0.05	0.40	1.86	4.21	2.41	–	–	0.15	–	3.68	15
	0.73	0.03	0.33	0.27	0.03	0.07	0.27	0.25	0.19	–	–	0.10	–	5.41	
MSH Yn	75.70	0.15	14.31	1.18	0.05	0.33	1.77	4.26	2.13	0.07	–	0.13	–	4.74	45
	0.48	0.03	0.54	0.05	0.02	0.03	0.05	0.24	0.08	0.01	–	0.04	–	2.32	
East Lake	73.97	0.23	14.11	1.73	0.04	0.22	0.94	4.39	4.28	–	–	0.12	–	5.59	7
	0.20	0.04	0.11	0.08	0.03	0.03	0.05	0.20	0.09	–	–	0.02	–	1.30	
KS2	68.02	0.61	14.95	4.74	0.19	1.14	3.76	5.21	1.15	0.11	0.04	0.03	0.16	1.10	48
	2.96	0.15	0.54	1.23	0.05	0.59	1.06	0.54	0.17	0.05	0.04	0.03	0.02	1.55	
Mazama	72.91	0.42	14.51	1.91	0.05	0.46	1.56	5.17	2.76	0.07	–	0.19	–	2.01	106
	0.81	0.04	0.43	0.18	0.02	0.06	0.25	0.43	0.13	0.02	–	0.02	–	2.12	

FeOt = total Fe as FeO, H_2Odiff is water by difference (i.e., 100-original total), n = number of analyses.

from this volcano are geochemically similar, having predominantly rhyolitic glass geochemistry with SiO_2 values between ~74 and 77 wt%, relatively lower K_2O (~2.3–2 wt%) and measurable Cl (~0.2–0.15 wt%), that are, nonetheless, subtly different from one another (e.g., Foit et al., 2004; Mackay et al., 2016; Jensen et al., 2019; Foo et al., 2020). The youngest MSH unit present is layer T, the first major eruption of the 19th century Goat Rocks period (1799–1800 CE; Yamaguchi et al., 1990) and one of the few rhyodacites from MSH (Mullineaux, 1996; Foo et al., 2020). Mackay et al. (2016) first describe layer T at Framboise Bog, and here it is located at 26–27 cm in core 2 of Sidney Bog (Fig. 3; Table S14). The geochemistry and shard morphology are consistent with previously reported distal and proximal layer T samples (Fig. 5; Table 3; Mackay et al., 2016; Foo et al., 2020), and its age (modern to 1650 CE; age model 2) also overlaps with that of layer T (Table S14).

Re-examining data presented in Mackay et al. (2016), we found that the "Villagedale" tephra from Villagedale and Saco Bogs displays distinct similarities in geochemistry to layer T (Fig. 6). The ages of Villagedale tephra as presented in Mackay et al. (2016) are slightly too old (1517–1750 CE, 1572–1762 CE) and the number of shards analysed is too small to assess this, but it seems possible that the two tephra may be equivalent. Villagedale tephra exhibits characteristics similar to MSH tephra, but the presumed age of this tephra places it during the eruptions of set X, the Worm lava flows, and a dome growth period when the largest eruptions were basaltic-andesitic in composition or lithic-rich co-ignimbrite ashes (e.g., Mullineaux, 1996; Pallister et al., 2017). Tephra associated with these particular events would not likely have the geochemistry or shard morphology presented by Villagedale tephra.

The next youngest MSH unit is from "set W" (for details on what comprises a "set" see Mullineaux, 1996). Careful examination of the MSH set W tephra in Jeffrey and Nordan's Pond Bogs in Newfoundland suggested that both were likely MSH We (Pyne-O'Donnell et al., 2012; Mackay et al., 2016). This is the second of the two large Plinian events, the first being Wn, that mark the onset of set W (e.g., Mullineaux, 1996). At Sidney Bog we also find set W tephra at 20–21 cm in core 1 and 55–60 cm in core 2, but unlike the unit in Newfoundland, it is unclear if it belongs to any one tephra from set W. The tephra in Sidney Bog contains a higher percentage of >77 wt% SiO_2 shards, which are less abundant in both Wn and We than in the less voluminous tephra falls that bracket We (Wa, Wb, Wd; Fig. 7; Table 3; Jensen, unpublished data). The correlation to set W is consistent with the sample interval and age of the Sidney tephra (age model 2; core 1: 1328–1557 CE; core 2: 1424–1700 CE), as all of set W was emplaced over a relatively short period of time, from ~1479 CE for Wn, to Wd, deposited sometime prior to 1510 CE (Yamaguchi and Hoblitt, 1995). With the samples in sites further to the north clearly correlating to MSH We, and the Sidney Bog sample showing geochemical characteristics more encompassing of the set rather than a single event, it seems possible that sites further south (and closer to MSH) may see a signal from a few set W tephra rather than just We.

The two other MSH tephra present in the bogs are reported for the first time in this region. The younger of the two was located within the same interval as another known tephra (Ruppert tephra; described in more detail below) in both Irwin Smith (68–69 cm; 2649–2046 cal yr BP) and Sidney Bog (core 1, 127–129 cm; 2887–2119 cal yr BP). This cryptotephra exhibits classic MSH geochemistry and correlates with MSH set P, which was emplaced ~3000–2350 cal yr BP (Pallister et al., 2017; Jensen et al., 2019). Visible tephra from this set have been reported distally in parts of southern British Columbia (e.g., Westgate, 1977; Foit et al., 2004), although it is unclear if they represent one or more of the multiple eruptions that comprise this set (Pm, Ps, Pu, Py). The MSH set P tephra reported in Westgate (1977) from Otter Creek bog, British Columbia, was reanalyzed by Jensen et al. (2019) with some proximal set P deposits and most likely represents an 'upper' set P tephra (Pu or Py; 2710–2350 cal yr BP). Both the recalculated age and these new geochemical data compare well with this cryptotephra (Fig. 5; Table 3; Jensen et al., 2019).

The other newly reported MSH tephra is present in both Sidney Bog cores (core 1, 175–176 cm; core 2, 343 cm, Supplementary Tables S13, S14). This prominent peak in shards correlates to MSH Yn, part of set Y, which marks the Holocene reawakening of MSH after a ~6000-year dormant period. MSH Yn is the largest Holocene Plinian eruption from MSH and is widely distributed across western

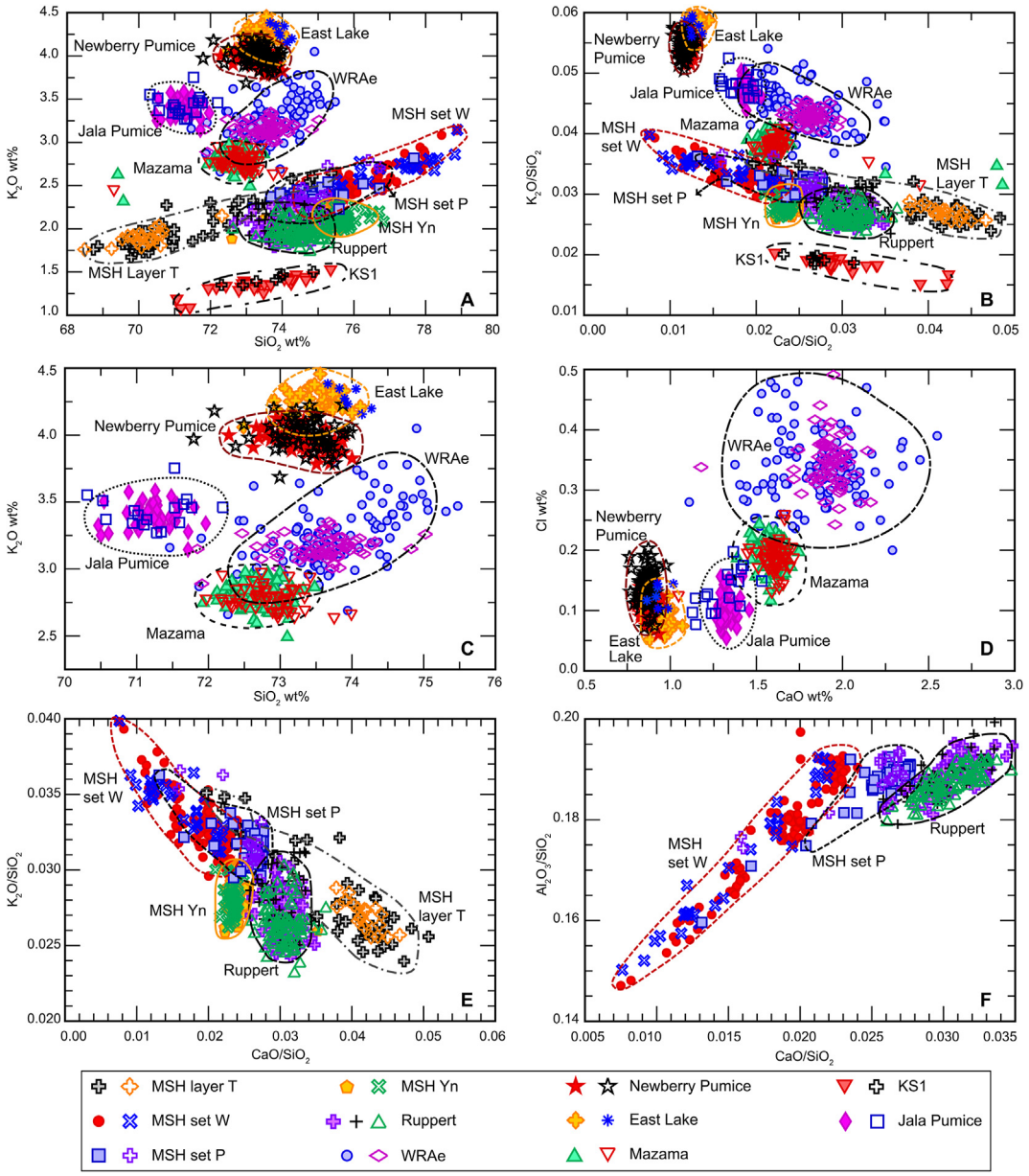

Fig. 5. Major-element geochemistry of confidently correlated cryptotephra (open symbols) plotted with reference data of proximal samples (closed symbols), with the reference data further defined by dashed outlines. KS_2 is excluded for ease of viewing (see Fig. 8). (A,B) Many of these tephra overlap geochemically, but do occupy distinct fields with certain oxide-oxide plots. (C,D) A close up on more potassic tephra shows their distinctive fields, in particular for Newberry Pumice and East Lake, which are similar but can be differentiated. (E, F) The Mount St. Helens tephra overlap but can generally be distinguished with K_2O, CaO and SiO_2. Ruppert is most similar to Mount St. Helens tephra but can be clearly distinguished in (F). Samples of Ruppert from Nordan's Pond Bog are the crosses, while all other Ruppert cryptotephra samples are the open triangles. Some plots are presented as ratios to minimize differences between analyses run in different laboratories over several years.

Canada and USA as a visible deposit. The newest revised age of the MSH Yn (3805–3535 cal yr BP; Jensen et al., 2019) overlaps very closely with the ages of the shard peaks (core 1, 3933–3547 cal yr BP; core 2, 3805–3577 cal yr BP). While there had previously been some uncertainty about the geochemistry, ages, and distribution of distal visible tephra from set Y in western Canada, a new dataset shows that the oldest (Yb) and major Plinian (Yn, Ye) set Y units can be clearly separated, both in time and geochemical space (Jensen et al., 2019). Comparison with these geochemical data shows that the cryptotephra in Sidney Bog correlates well to MSH Yn (Fig. 7; Table 3), consistent with age constraints, and glass morphology dominated by highly inflated pumice (Fig. 4).

A MSH set J tephra (ca. 13.5 ka) is also present in lake sediments in Nova Scotia and Maine (Pyne-O'Donnell et al., 2016, Table 1, 2, S16). No other records of this age range were examined in this study, so it is unclear what the regional distribution of this tephra is. Proximal glass geochemistry for set J is poorly defined so this cryptotephra is not correlated to any one tephra comprising it. Set J has at least two distally distributed tephra, which could explain discrepancies between age estimates of MSH J tephra relative to Glacier Peak G (as visible deposits, MSH J and GP-G are often found together at distal sites) and complicates any cryptotephra correlation (Table 2; Kuehn et al., 2009; Schachtman et al., 2015).

4.2.2. Other North American-sourced tephra

Of the remaining eight confidently correlated tephra, five are

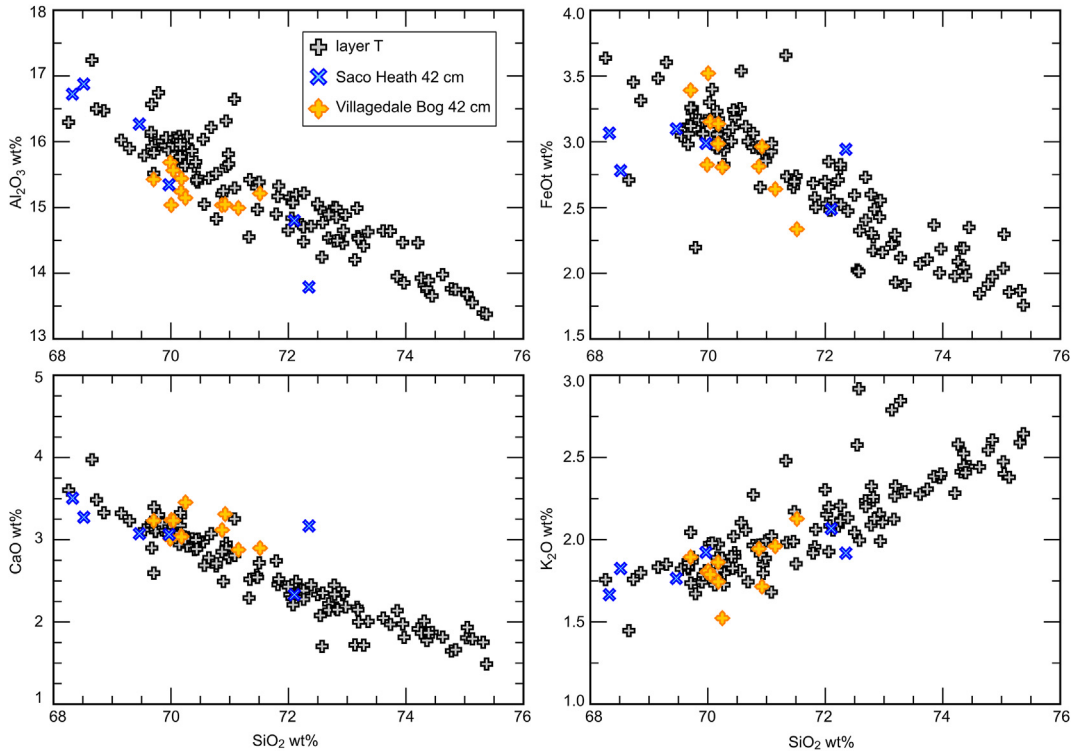

Fig. 6. Reference MSH layer T data in comparison to "Villagedale" tephra of Mackay et al. (2016). The "Villagedale" tephra samples plots well with an expanded layer T data set (Foo et al., 2020) although they display a much more limited geochemical range.

from North American sources, and all five have been previously described in northeastern North America – Newberry Pumice, East Lake tephra, Mazama, White River Ash east and Jala Pumice.

Newberry Pumice and East Lake tephra are geochemically similar but easily differentiated from other tephra presented in this study (Fig. 5; Table 3). They were first identified in Nordan's Pond Bog by Pyne-O'Donnell et al. (2012). Both were erupted from the Newberry Volcanic Field—the Newberry Pumice deposited by a Plinian eruption marking the start of the "Big Obsidian eruptive period", and the older East Lake tephra, a widespread tephra deposit overlying Mazama (e.g., MacLeod et al., 1995). Newberry Pumice is one of the most widespread tephra in our study region, and closely underlies the White River Ash east (WRAe) in all the bogs. Because of a slowdown or hiatus in growth of Irwin Smith and Bloomingdale Bogs, the two are intermingled and peaks separated only by 2–3 cm. In Sidney Bog core 1 and Nordan's Pond Bog the tephra are more clearly separated, reflecting their age difference more accurately. Newberry Pumice yields one of the largest shard concentrations after WRAe, Mazama and MSH Yn. East Lake tephra was identified only in Sidney Bog (core 1), intermixed with SB-13 (discussed later), but is also present in Nordan's Pond Bog (Pyne-O'Donnell et al., 2012).

Proximal ages for Newberry Pumice and East Lake tephra had not been examined in any detail for some time; therefore, we compiled the existing radiocarbon dates for these tephra and derived updated Bayesian ages. The new modelled ages on the proximal deposits are somewhat younger than previous estimates, and in the case of Newberry Pumice, also more constrained (Table 2; S16). These new ages are now in better agreement with our estimated ages of the correlative tephra in the different bogs, supporting the geochemical correlations (Table 2, S11-S15; Fig. 5).

The Mazama tephra is the product of the largest Holocene eruption in North America, a VEI 7 event with an estimated erupted volume of ~176 km^3 (Buckland et al., 2020). Mazama is identified in all cores included in this study that preserve the timeframe of its deposition (~7680–7580 cal yr BP; Sidney Bog core 2, Bloomingdale, Thin-Ice Pond). It is also widely reported in the region, first documented in Nordan's Pond Bog (Pyne-O'Donnell et al., 2012), as well as in cores from Lake Superior and near North Bay, Ontario (Spano et al., 2017; Rabett et al., 2019) (Table 1). It is one of several tephra in this study that have been reported in Greenland ice cores and may extend into Europe (Zdanowicz et al., 1999; Plunkett and Pilcher, 2018). Like the WRAe, discussed below, Mazama is a seminal regional marker horizon, commonly yielding one of the highest glass shard concentrations. Its high shard count, age, elongated or fluted shard morphology and distinct geochemistry make Mazama relatively easy to identify in these sequences (Figs. 4 and 5; Tables 2 and 3). At Thin-Ice Pond, Mazama shards (maximum concentration of ~5150 shards/cm^3) were measured for grain size, with an average long axis of ~44 μm ($\sigma = 16$, $n = 125$ shards measured).

The remaining two North American tephra discussed here are from sources other than the Cascade Range. The most ubiquitous of these is the eastern lobe of the White River Ash (WRAe), from Mount Churchill, Alaska. To date, every site that has been sampled from the correct time interval (ca. 1100 cal yr BP) contains this tephra, which now has a Greenland ice-core age of 853 ± 1 CE (Toohey and Sigl, 2017). Commonly the peak with the highest glass-shard concentration derives from the White River Ash. It is a distinct tephra both geochemically (Fig. 5; Table 3) and morphologically, heavily dominated by highly inflated pumice (Fig. 4).

WRAe was deposited around the time of a hiatus (including bog burning) in Irwin Smith and Bloomingdale Bogs, or during a slowdown in peat accumulation rate per Sidney Bog. The hiatus brings a number of units closely together (WRAe, Newberry Pumice and inter-core correlated ISB-1 and BB-2) complicating the

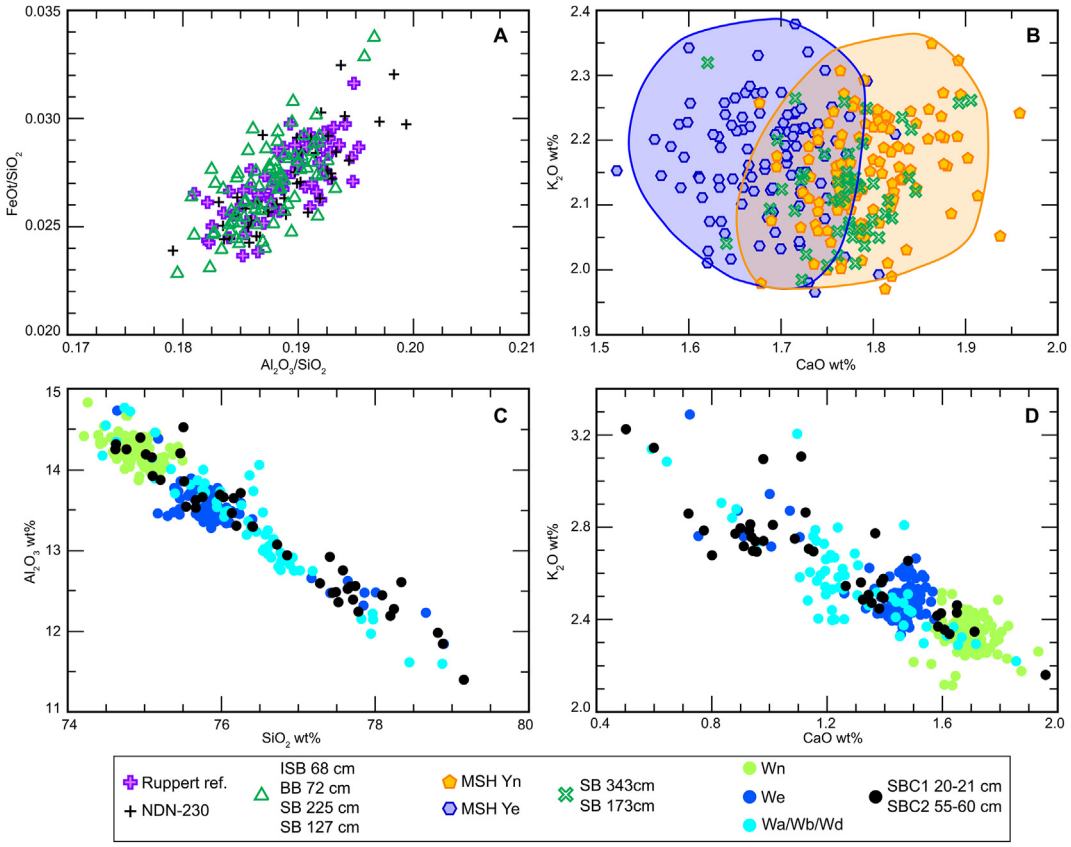

Fig. 7. Bivariate plots showing the subtle similarities and differences among several cryptotephra and their visible correlative units. (A) Ruppert reference analyses from Ruppert Lake (Monteath et al., 2017) are plotted with new data from NDN-230 and the three new bogs. (B) MSH Yn and Ye are very similar but can be distinguished by K_2O and CaO, with the cryptotephra showing a clear affinity to Yn. (C,D) The cryptotephra from Sidney Bog that correlates to MSH set W does not show any particular affinity to a specific event from the set.

stratigraphy. At Sidney Bog in core 2, we observe substantial downward movement of WRAe, possibly related to vegetation changes due to drying (as observed at Saco Bog by Mackay et al., 2016). In addition, there is a distinct shard peak with WRAe geochemistry 5 cm above the main peak at Irwin Smith. This peak is too old to correlate with the Lena tephra (~300–400 cal yr BP; Payne et al., 2008; Davies et al., 2019), the only Churchill eruption post-dating WRAe. This is likely caused by reworking of WRAe due to bog burning after its initial deposition, documented in Booth et al. (2012a), illustrating potential complexities that can arise even in a depositional environment as benign and simple as an ombrotrophic bog. A similar process was documented in central Alberta bogs after the deposition of Mazama (e.g., Zoltai, 1989; Zoltai and Vitt, 1990; Beierle and Smith, 1998). Although concentrations are not entirely comparable, it highlights that high concentration cryptotephra (e.g., >2000 shard/cm^3) can be reworked after deposition given the right circumstances.

The second North American tephra not from the Cascades is the Jala Pumice, from Volcan Ceboruco, Mexico. This tephra was first identified in Villagedale Bog, NS, by Mackay et al. (2016). We identified it in Sidney Bog (core 1), intermixed with another tephra that is tentatively correlated to Fish Lake II - Chaos Crags (discussed in section 4.3.2 below). Geochemically the Jala tephra is distinctive on SiO_2 and K_2O plots, which differentiate it from the other tephra presented here (Fig. 5; Table 3). The age of Jala tephra in Sidney Bog is 1075–1015 cal yr BP. Our result is consistent with a proximal age of Sieron and Siebe (2008) that we recalibrated and modelled to 1040–680 cal yr BP. The greater error in the new age is partially because the Tau_Boundary model considers the lack of limiting overlying ages on proximal deposits, increasing the probability that it may be younger. However, the ages of correlative cryptotephra in Sidney and Villagedale Bogs suggest that the eruption likely occurred in the older end of the proximal two sigma age range provided here (Table 2; Table S17).

4.2.3. *Ksudach, Kamchatka*

The source volcano of the final two confidently correlated tephra is Ksudach, in Kamchatka. Ksudach is a volcanic complex of the Eastern Volcanic Front in the southern portion of the Kamchatka Peninsula. The complex comprises five nested calderas, three of which are Holocene (calderas III, IV and V; e.g., Volynets et al., 1999). The two tephra deposits of interest are KS_2 (caldera IV; 6877–6693 cal yr BP) and KS_1 (caldera V; 1705–1590 cal yr BP) (Table 2; Ponomareva et al., 2017). KS_2 comprises 8.9–10.5 km^3 of ejecta and blanketed the peninsula northward, forming a key marker layer in Kamchatka (e.g., Braitseva et al., 1997; Plunkett et al., 2015). It has also been located 'ultra' distally in the Arctic, in lake sediments from Svalbard (van der Bilt et al., 2017). KS_1 is the product of the second largest Holocene eruption in Kamchatka, comprising 20–25 km^3 of ejecta and ~17 km^3 of tephra fall (Andrews et al., 2007), and is one of the most widespread markers in the region (e.g., Braitseva et al., 1996, 1997).

KS_1 was first identified in North America by Mackay et al. (2016) in Villagedale Bog and is also present in Bloomingdale Bog. This tephra is a distinctive rhyolite with relative proportions of SiO_2, Na_2O, and K_2O that distinguish it from known Cascades or Alaskan

sources (Fig. 5; Table 3). The age estimates for KS_1 from Villagedale and Bloomingdale Bogs closely agree, but only the age from Bloomingdale overlaps with most recent published proximal age estimate for KS_1 of 1705–1590 cal yr BP (Table 2; Ponomareva et al., 2017). Our newly modelled proximal age for KS_1 is 1790–1690 cal yr BP (Table 2, details available in Table S17), about 100 years older than that presented by Ponomareva et al. (2017) and overlapping with both bog age estimates. We therefore suggest our bog ages accurately reflect the true eruption age of KS_1.

We identify KS_2 for the first time in North America in Thin-Ice Pond (TI-323). It is accompanied within a relatively narrow stratigraphic interval (~35 cm) by two other cryptotephra; it lies above Mazama (TI-346) and below an uncorrelated cryptotephra that is also present in Sidney Bog (TI-317/SB-13, discussed in section 4.4.5 below).

The age estimate of KS_2 from Thin-Ice Pond produced using only radiocarbon dates (7170–6940 cal yr BP) deviates from the recent proximal age of KS_2 (6877–6693 cal yr BP; Ponomareva et al., 2017). However, we regard our model age as problematic because Thin-Ice Pond radiocarbon dates have an age-reversal in the core right at TI-323, and the age model shows variations in sedimentation rates throughout this interval (Tables S10, S16). Nonetheless, independent ages of KS_2 from several lakes in Kamchatka suggest that the age inferred in Ponomareva et al. (2017) is too young; for example, 7350–7180 and 7300–7160 cal yr BP from Plunkett et al. (2015), and ~7200 cal yr BP from Pendea et al. (2017).

Geochemically TI-323 exhibits unique low-K consistent with a Kamchatkan source (Fig. 8; Tables 3 and 4). TI-323 glass has a broad compositional range (~60–72 wt% SiO_2) encompassing andesite to rhyolite, though predominantly dacitic. The K_2O concentration (~0.7–1.4 wt%) is characteristic of the low-K tephra from Ksudach (e.g., Kyle et al., 2011) and in this case matches closely the reported major element geochemistry of KS_2 (Plunkett et al., 2015; Ponomareva et al., 2017; Portnyagin et al., 2020). Trace element analyses support the correlation (Fig. 8, Table 4). TI-323 exhibits the unfractionated near-flat REE normalized pattern of Kamchatka source glasses (e.g., Kyle et al., 2011; Ponomareva et al., 2013) that is indistinguishable from KS_2 tephra samples collected in Kamchatka (Fig. 8, Tables 4, S2).

KS_2 has a distinctive blocky glass morphology that is often vesicular and microlitic (Fig. 4)—the latter being a particularly distinct feature for both the proximal and distal deposits. Although most volcanic glass is often a pale green under glycerol, this tephra has a notably darker greenish hue. Grain-size measurements results in an average shard size of ~40 μm ($\sigma = 9$, $n = 100$).

4.2.4. Ruppert tephra

Pyne-O'Donnell et al. (2012) first identified Ruppert tephra in Nordan's Pond Bog, Newfoundland, although this tephra was originally named NDN-230. They suggested NDN-230 could correlate to "tephra G" from Augustine volcano, Alaska, because of geochemical similarities to Augustine tephra and the proximal age estimate of ~2200 cal yr BP (Waitt and Begét, 2009). This overlaps with the age of Ruppert tephra at 2800–2130 cal yr BP (Table 2). However, a more comprehensive dataset of Augustine glass geochemistry in Blockley et al. (2015) shows NDN-230 is not tephra G, although it may originate at that volcano. More recently, Monteath et al. (2017) describe a cryptotephra in the southern Brooks Range of Alaska. They named it Ruppert tephra after the lake in which it was found but inferred no regional source. Monteath et al. (2017) did suggest that the Ruppert tephra may correlate to NDN-230 and here we confirm that correlation, with concurrent geochemical analyses of samples from both cores (Figs. 5 and 7; Tables 2 and 3).

The Ruppert tephra is not particularly prominent in terms of shard counts, but it is present in all three new bogs analysed in this study. The glass concentrations in Alaska are low relative to the Aniakchak CFE II peak in Ruppert Lake and Woody Bottom Pond in the southern Brooks Range, but these two tephra were also the only ones clearly defined at those sites (Monteath et al., 2017). Cascade Lake in the northern Brooks Range also preserves Aniakchak CFE II and Ruppert, although concentrations here are approximately the same (Davies et al., in review). Plunkett and Pilcher (2018) also suggest that a small glass peak in Garry Bog (GB4-147), Ireland, correlates to Ruppert. Despite its modest concentrations at most sites, this is one of the most widespread units present and potentially another transcontinental marker horizon.

Ruppert tephra is rhyolitic (Figs. 5 and 7; Table 3) with relatively low K_2O, and higher Cl. Its chemistry is similar to tephra from Mount St. Helens, especially set P, with which it is intermixed at two sites (Fig. 5; Table S1). However, its geographic distribution from north-central Alaska to the east coast excludes more southerly sources (e.g., Cascades), leaving Alaska, Kamchatka, the Kuriles and Japan as the most likely sources. Examination of existing datasets from Japan (e.g., McLean et al., 2018), Kamchatka (e.g., Portnyagin et al., 2020) and the Kuriles (e.g., Nakagawa et al., 2008; Razzhigaeva et al., 2016) do not reveal any tephra with similar geochemical compositions to Ruppert. Alaska appears to be the most likely source as Ruppert tephra falls within the geochemical variability of Alaskan tephra, although there are no visible tephra of its composition from numerous records in and around the Kenai Peninsula and Cook Inlet (e.g., Riehle, 1985; Lemke, 2000; Payne and Blackford, 2008; Zander et al., 2013, 2018; Fortin et al., 2019; Bolton et al., 2020). However, the plume could have been deposited in the ocean or followed a more northerly direction, similar to Aniakchak CFE II, which is also not a visible bed in the proximal records to the east of the arc.

4.3. Probable tephra correlations

Our study strongly suggests correlations of the following cryptotephra to previously described tephra and/or source volcanoes. Nonetheless, the correlations are not certain because of one or more unresolved factors, and we acknowledge that they may change in the light of additional data.

4.3.1. SB-3 (600–430 cal yr BP) and ISB-1/BB-2/SB-5 (1660–1300 cal yr BP, mean 1480)—Mono-Inyo Craters

SB-3 and the inter-core correlated ISB-1/BB-2/SB-5 both likely derive from Mono-Inyo Craters, California, a volcanic field situated in an extensional tectonic environment that runs from the northwestern corner of Long Valley caldera to Mono Lake (e.g., Bursik and Sieh, 1989). Mono-Inyo Craters was active when these two cryptotephra were deposited.

SB-3 coincides in time with notable eruptions from both North Mono and Inyo Craters. The North Mono eruption is dated to 650–520 cal yr BP, a recalibrated and modelled age based on three radiocarbon dates originally presented by Sieh and Bursik (1986) (Table 2, S17). Shortly after (~1–10 years) the North Mono eruption, Inyo Craters had several eruptions that ended around 1350 CE (~600 cal yr BP) (Millar et al., 2006; Nawotniak and Bursik, 2010; Bevilacqua et al., 2018). The inter-core correlated cryptotephra of ISB-1/BB-2/SB-5 has a combined age estimate of 1670–1300 cal yr BP. This age overlaps the interval of the Plinian eruption of South Mono (1350–1300 cal yr BP) at the end of the penultimate period of activity at Mono Craters, which includes eruptions at or near

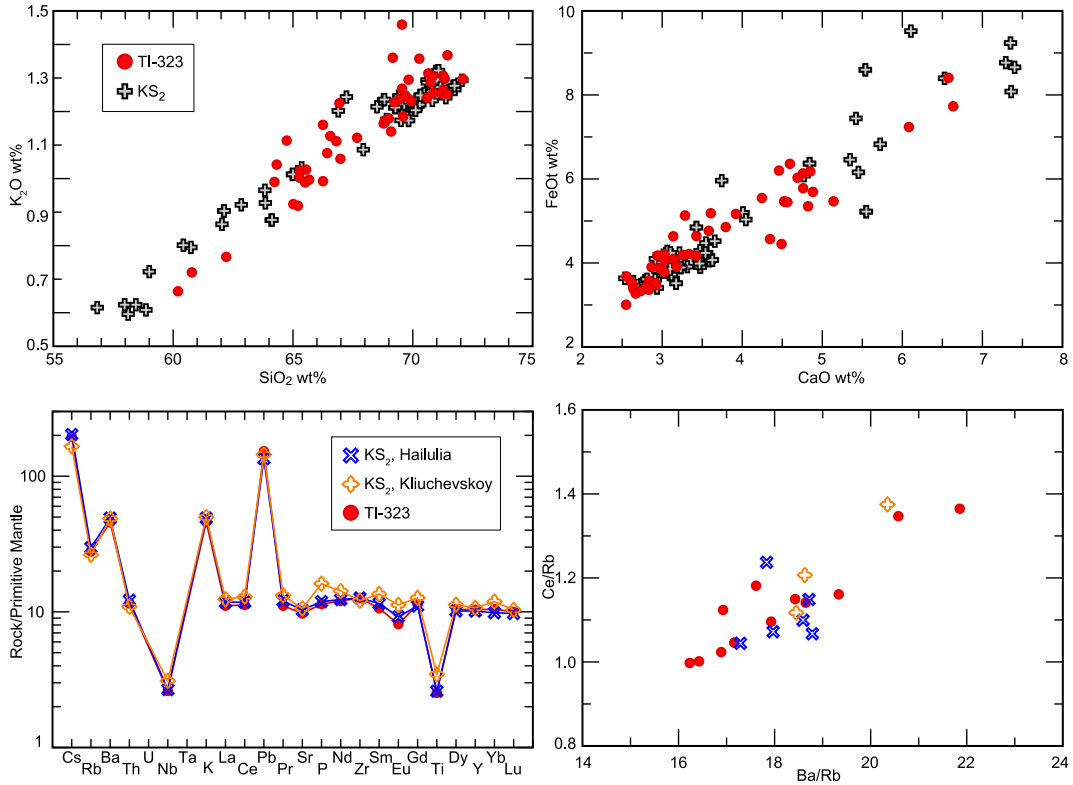

Fig. 8. The top two panels compare major-element geochemistry of KS_2 (Plunkett et al., 2015; Ponomareva et al., 2017; Portnyagin et al., 2020) and TI-323, the KS_2 correlative in Thin-Ice Pond. Major element geochemistry is largely indistinguishable and, somewhat surprisingly considering the winnowing of heavier mafic shards that can happen over distance, contains some shards comprising the lower SiO_2 portion of the tephra. The lower two panels compare average trace element geochemistry that is also largely indistinguishable despite some scatter that exists in the TI-323 data due to the analyses of small shards with the smaller laser spot, particularly in lower concentrations elements. Ta was measured but is excluded in this diagram due to its concentrations near detection limits (see Table S2 for individual analyses).

Northwest Coulee of Mono Craters (1628–1520 cal yr BP) and Wilson Butte of Inyo Craters (1611–1710 cal yr BP) (e.g., Wood, 1977; Sieh and Bursik, 1986; Bursik and Sieh, 2013; Bursik et al., 2014).

The major element geochemical characteristics of both cryptotephra share some similarities (e.g., high K_2O and low CaO wt%), with SB-3 exhibiting a greater SiO_2 range. Overall, they are distinguishable from one another but generally plot on trend (Fig. 9; Table 5). Trace-element data collected from ISB-1 show a unique trace-element profile with extremely low Ba and Sr, atypical of subduction related (arc) rhyolites (Fig. 9; Table 4).

New proximal major-element geochemistry was collected from North Mono (UA 3323–3325) and South Mono tephra (UA 3322), as well as a deposit directly underlying the main South Mono tephra deposit near its source vent (UA 2789). These data were compared with limited published data from Inyo Craters (Bursik, 2014), distal Mono and Inyo tephra (Osborn, 1989), and the two cryptotephra (Fig. 9; Table 4, S2, S8). Previous research has suggested that the high SiO_2 tephra and domes from Mono Craters have a more homogeneous major-element geochemistry and pronounced Sr and Ba anomalies compared to Inyo Craters (e.g., Wood, 1977; Sampson and Cameron, 1987; Higgins and Meilleur 2007; Bursik, 2014). Data from our proximal samples are consistent with these reports and show that tephra unit UA 2789, initially thought to represent a basal fall deposit of the South Mono eruption, is more likely the Wilson Butte tephra that commonly underlies the South Mono tephra near its source vents (see Fig. 13 in Bursik et al., 2014, sample number 095011). Although the Wilson Butte dome has long been noted to be of Mono affinity (Sampson and Cameron, 1987; Kelleher and Cameron, 1990), some of the proximal Wilson Butte pyroclastic products are now known to be of Inyo affinity (Bursik, 2014, and references therein).

The major-element geochemistry of the older cryptotephra (ISB-1/BB-2/SB-5), a much more homogeneous high-SiO_2 rhyolite, shows a clear affinity to Mono Craters (Fig. 9). The correlation between the older cryptotephra and the South Mono eruption (UA 3322) is strongly re-enforced by the trace element geochemistry (Fig. 9; Table 4, S2). Both ISB-1 and the South Mono tephra show the distinct trace element profile with anomalously low concentrations of Sr and Ba, as has been reported before, most significantly by Wood (1977) for his equivalent “Tephra 2”. While the small laser diameter (10 μm) and very low concentrations cause more scatter in the data, ISB-1 clearly shows the same trace element characteristics as the proximal Mono crater ejecta (Fig. 9). While it seems most likely that this older cryptotephra unit correlates to the South Mono eruption (as the larger and more widespread event), we must note that there are no glass geochemical data for unequivocal deposits from the Wilson Butte and Northwest Coulee eruptions.

Proximal North Mono tephra (650–520 cal yr BP) is largely indistinguishable by trace and major element geochemistry from the older South Mono tephra. This homogeneity has been observed in Mono Craters tephra deposited through the late Pleistocene, with those only being distinguished by their Fe–Ti oxides (e.g., Marcaida et al., 2014). The homogeneity also excludes North Mono as the source for SB-3. However, the glass chemistry of SB-3 does plot closely to the more heterogenous composition of UA 2789 (the potential Wilson Butte correlative), and the limited data published for Inyo Craters (Fig. 9), suggesting that SB-3 is from Inyo Craters. Nonetheless, the uncertain origin of UA 2789, the limited geochemical data for tephra from the younger Inyo eruptions, and

Table 4
Glass trace element geochemistry for cryptotephra and reference material from proximal units. All data and analytical conditions are available in Table S2.

Sample	Laser (μm)	Rb	Sr	Y	Zr	Nb	Cs	Ba	La	Ce	Pr	Nd	Sm	Eu	Gd	Tb	Dy	Ho	Er	Tm	Yb	Lu	Hf	Ta	Pb	Th	U
TI-317	16	83	282	28.4	366	21.7	4.0	693	38.0	81.2	10.0	38.2	7.9	1.8	6.4	0.9	4.9	1.0	2.8	0.4	2.6	0.4	8.9	1.4	16.7	10.2	3.6
		15.9	50	8.7	101	4.7	0.7	151	8.8	18.2	3.4	10.7	2.9	0.5	2.6	0.4	2.5	0.3	1.0	0.3	1.0	0.2	1.7	0.3	3.6	3.5	1.0
TI-323	16	18	205	47.0	142	1.9	1.5	320	7.6	20.0	3.1	16.3	4.7	1.4	6.7	1.1	7.7	1.6	4.7	0.7	5.2	0.7	3.9	0.2	10.9	1.0	0.4
(KS2)		5.3	46	8.7	34	1.0	0.5	74	2.3	4.6	0.7	5.2	1.9	0.9	1.5	0.5	2.2	0.5	1.2	0.3	1.3	0.3	1.9	0.2	3.8	0.7	0.3
KS2 ref	50	19	218	46.1	142	1.9	1.6	343	8.1	20.9	3.3	16.7	5.1	1.5	6.6	1.1	7.5	1.6	4.9	0.7	4.9	0.7	4.0	0.1	9.6	1.0	0.4
(Hailulia)		5.3	47	9.3	39	0.5	0.5	90	1.8	5.7	0.8	3.7	0.9	0.3	1.2	0.1	1.3	0.3	1.0	0.2	1.3	0.2	1.5	0.0	1.3	0.3	0.2
KS2 ref	23	18	209	45.4	132	2.1	1.5	344	8.3	22.0	3.5	18.1	5.7	1.7	6.9	1.2	7.8	1.7	5.1	0.8	5.2	0.8	3.7	0.1	10.3	1.0	0.4
(Kliuchevskoy)		8.3	84	19.6	60	0.9	0.7	145	3.0	7.8	1.2	6.7	2.8	0.6	1.6	0.3	3.5	0.6	2.1	0.3	3.0	0.3	2.1	0.1	3.2	0.4	0.1
ISB-1	10	190	5.6	23.2	93	20.6	5.6	25.0	19.7	43.5	5.4	17.8	4.3	0.2	3.7	0.7	3.5	0.7	2.3	0.4	2.2	0.4	4.4	1.6	26.6	16.5	5.6
(South Mono)		18	2.2	3.3	13	2.1	1.5	6.0	2.3	4.5	0.9	2.9	2.0	0.3	1.0	0.2	1.1	0.3	0.8	0.3	1.1	0.2	1.5	0.5	4.7	2.8	0.7
UA 3322	23	181	5.8	23.0	97	20.9	5.4	21.8	21.4	46.5	5.4	19.8	4.4	0.1	3.5	0.6	3.8	0.8	2.4	0.3	2.6	0.4	4.2	1.7	27.3	19.2	6.3
(South Mono)		4	0.5	0.8	2	0.6	0.2	1.3	0.6	1.0	0.2	1.3	0.6	0.1	0.4	0.1	0.4	0.1	0.3	0.1	0.5	0.1	0.3	0.1	1.0	0.5	0.2
UA 3323	23	180	5.7	23.4	99	20.8	5.5	22.9	22.3	47.8	5.4	19.5	4.2	0.1	3.5	0.6	3.9	0.8	2.4	0.4	2.6	0.4	4.1	1.8	27.7	19.1	6.2
(North Mono)		3	0.5	0.9	2	0.9	0.2	1.4	0.6	1.4	0.3	1.2	0.5	0.1	0.6	0.1	0.3	0.1	0.3	0.1	0.3	0.0	0.3	0.1	1.0	0.4	0.2
UA 3324	23	184	5.5	22.9	92	20.8	5.4	21.3	20.2	44.3	5.2	19.2	4.2	0.1	3.9	0.6	3.9	0.8	2.4	0.4	2.5	0.4	4.1	1.7	27.8	18.8	6.4
(North Mono)		3	0.3	0.6	2	0.5	0.1	1.0	0.6	1.1	0.2	1.0	0.4	0.0	0.5	0.1	0.4	0.1	0.3	0.1	0.3	0.1	0.3	0.1	0.8	0.4	0.1
UA 3325	23	179	5.9	23.6	97	20.5	5.4	23.3	22.6	47.0	5.4	19.1	4.3	0.1	3.8	0.6	3.9	0.9	2.5	0.3	2.7	0.4	4.3	1.7	27.8	18.9	6.1
(North Mono)		4	0.9	1.0	2	0.7	0.2	1.4	0.7	1.3	0.3	1.2	0.4	0.0	0.5	0.1	0.6	0.1	0.2	0.1	0.4	0.1	0.3	0.1	1.1	0.7	0.2
UA 3286	23	96	112	12.7	67	4.7	4.31	879	18.7	37.0	4.0	15.0	2.5	0.4	1.8	0.3	1.9	0.4	1.3	0.2	1.5	0.2	2.3	0.4	13.1	6.5	2.6
							7142857																				
(Opala 1.4 ka)		2	18	0.9	2	0.3	0.2	29	0.5	0.7	0.3	0.7	0.5	0.1	0.3	0.1	0.2	0.1	0.2	0.1	0.2	0.0	0.3	0.1	0.7	0.2	0.1

the lack of trace element geochemistry for these samples means further work is required to confirm these potential correlations.

To test another potential correlation, we collected major and trace element data on samples comprising part of the large eruption of Opala volcano at ~1400 cal yr BP (Andrews et al., 2018), similar in timing to ISB-1/BB-2/SB-5 and identified as a cryptotephra in Cascade Lake, Alaska (Davies et al., in review). Opala 1.4 ka is also a high-silica rhyolite with high K_2O and low CaO and FeOt. Both the trace element data, which shows a more typical arc profile, and the major element data lead us to discount this potential correlation (Fig. 9).

4.3.2. SB-4 (1075–1015 cal yr BP)— Fish Lake II, Chaos Crags, Lassen Volcanic Center

SB-4 is a minor tephra constituent in the same interval as Jala Pumice in Sidney Bog core 1. It is a high-SiO_2 rhyolite with relatively low FeO, CaO and Al_2O_3 (Fig. 10). Although only 6–7 shards make up this population, the age of the event and its geochemistry suggest it is a primary tephra fall event. Unfortunately, SB-4 is partially obscured because of overlap with the Jala Pumice, lower resolution counting intervals (2–3 cm), and the relatively large volume of peat (between 42 and 44 cm) used to extract sufficient glass for analyses.

SB-4 chemistry mirrors major-element geochemical data collected from Fish Lake II tephra, which has a broad age range of 1511–975 cal yr BP (recalibrated from Foit and Mehringer, 2016) (Tables 2 and 5; Fig, 8). Fish Lake, in southern Oregon, has a record of six visible tephra (Fish Lake I-VI) that Foit and Mehringer (2016) correlate to their sources in the Cascades and northern California. Fish Lake II tephra was correlated to the most recent eruption of Chaos Crags, part of the Lassen Volcanic Center, northern California, using reference material from that eruption. We do not have proximal material from that event to analyze, and no point-by-point glass geochemical data are available in the published literature for comparison. However, numerous radiocarbon ages reported by Clynne et al. (2008) from a series of pyroclastic flows associated with the eruption agree very closely with the age of SB-4 (Table 2, S17). Further analyses of Chaos Crags reference material would be required to confirm this correlation.

4.3.3. SB-7 (2950–2230 cal yr BP)— Fish Lake III, Medicine Lake, CA (?)

Sidney Bog's SB-7 is a relatively high alkaline rhyolite that is distinct from any other tephra described here. This tephra appears to correlate to the Fish Lake III tephra, with a published age-range of 3212–2764 cal yr BP (recalibrated with IntCal, 2020, Tables 2 and 5; Fig. 10). The best age estimate for SB-7 (2950–2230 cal yr BP) overlaps with this published age, but only on the younger end of the age range. However, this is not unexpected because Fish Lake age results (e.g., Fish Lake II) are consistently somewhat older than their correlatives (Foit and Mehringer, 2016).

Fish Lake III has been correlated to Medicine Lake volcano, California, but this secondary correlation is uncertain (Foit and Mehringer, 2016). Medicine Lake volcano is a large composite volcano surrounded by numerous voluminous lava flows that lies in the rear-arc of the Cascades. It comprises the largest volume of erupted material in the arc, with the possible exception of the Newberry volcanic field, another rear-arc center (e.g., Donnelly-Nolan et al., 2016). Foit and Mehringer (2016) correlated Fish Lake III to Medicine Lake based on a sample provided by Andrei Sarna-Wojcicki of the "youngest airfall pumice" from the north flank of Glass Mountain. However, this pumice must then be associated with the youngest period of rhyolitic activity from the Medicine Lake complex that occurred between ~1200 and 900 cal yr BP (Donnelly-Nolan et al., 2016), significantly younger than SB-7 and Fish Lake III. There is documented activity from Medicine Lake

around the time of the deposition of Fish Lake III tephra, but it is limited to the extrusion of basaltic and basaltic-andesitic lava flows (Donnelly-Nolan et al., 2016). Therefore, while we are fairly confident of the correlation to the Fish Lake III tephra based on the distinct major element geochemistry and age agreement, the correlation to Medicine Lake volcano is less certain.

4.3.4. BB-3 (2030–1565 cal yr BP)— Us-Kr, Ushishir, Kuriles

BB-3 is a unique tephra in Bloomingdale Bog distinguished by its notably low K_2O (~1.2 wt%), and relatively high CaO and FeOt for a high-SiO_2 rhyolite (~77.5 wt%) (Table 5; Fig. 11). This distinctive geochemistry, along with its estimated age, suggests a correlation to the central Kuriles, specifically the Us-Kr tephra (e.g., Nakagawa et al., 2008). Us-Kr has been linked to the latest caldera forming eruption of Ushishir volcano on Yankich Island, one of two main islands that comprise the Ushishir Islands (e.g., Razzhigaeva et al., 2012; Bondarenko and Rashidov, 2018). There is little published literature that clarifies how the Us-Kr tephra was correlated to Ushishir, as sites where the tephra are described are on other islands to the north (Razzhigaeva et al., 2012; MacInnes et al., 2016; Bondarenko and Rashidov, 2018). The attribution seems to come from an unpublished report by Nakagawa et al. (2008) that originates from a research cruise led by the Kuril Biocomplexity Project. They documented ~20 cm thick occurrences of the tephra on Ryponkich Island, just north of Yankich Island, and argued that these deposits originated from the caldera on Yankich Island based on ages, geochemistry, and tephra dispersal.

The glass geochemistry of Us-Kr reported by Nakagawa et al. (2008) is very similar to BB-3 (Fig. 11). The oxide data match very well, although BB-3 has on average, slightly lower SiO_2. However, BB-3 also has slightly higher Na_2O, which together with the slight deviation to lower SiO_2 values, suggests this offset might be caused by some Na-loss in the Japanese dataset. This hypothesis needs to be confirmed by re-analyses of the samples.

Radiocarbon dates reported by Razzhigaeva et al. (2012) and MacInnes et al. (2016) were used to recalculate a calibrated age for Us-Kr. The two radiocarbon ages reported by Nakagawa et al. (2008) were excluded since it was not clear whether they were from above or below the deposit (Table S17). The recalculated age has a bimodal distribution of 1970–1955 and 1945–1830 cal yr BP, with a median of 1890 cal yr BP, which agrees well with the modelled age of BB-3 of 2030–1565 cal yr BP (Table 2).

4.3.5. SB-6 (2965–2590 cal yr BP) and BB-4/SB-8 (4025–3395 cal yr BP)—Shiveluch

Shiveluch volcano is one of the most active, studied and geochemically characterized volcanoes in Kamchatka (e.g., Ponomareva et al., 2007, 2015, 2017). Rhyolitic glass compositions from Shiveluch tephra tend to be very similar to one another, consistently medium K_2O between ~2.5 and 3 wt%, with SiO_2 ranging between ~73 and 77 wt% (Fig. 11, Table 5; e.g., Ponomareva et al., 2017; Portnyagin et al., 2020). SB-6 and the inter-core correlated BB-4/SB-8 have geochemistry typical of Shiveluch, plotting well within the field of Holocene Shiveluch rhyolitic tephra. No geochemically similar tephra are known from other sources, except a vague similarity to tephra from Redoubt (e.g., Bolton et al., 2020). Overall, it is likely that these tephra correlate to Shiveluch, but not entirely clear what specific event(s) they represent.

Shiveluch erupted several times within the timeframes of SB-6 and BB-4/SB-4. Possible Shiveluch tephra matches fit three criteria—similar geochemistry (Fig. 11), overlapping timeframes (Table 2), and widespread regional distributions (e.g., Ponomareva et al., 2017). The strongest correlation is SB-6 to SHb (also referred to as SH2800). The Shb tephra is widespread, especially to the southeast (Kyle et al., 2011; Ponomareva et al., 2017). It dates at 3013–2794 cal yr BP and has a broader geochemical range than some other rhyolitic Shiveluch eruptions. Our SB-6 sample exhibits the same geochemical trend and is similar in age (2965–2590 cal yr BP) to SHb.

The identity of the BB-4/SB-8 cryptotephra (4025–3395 cal yr BP) is less certain, but Shiveluch tephras SH#27 (3898–3533 cal yr BP) and SH#32a (4240–3990 cal yr BP), with similar age and chemistry, are candidates. SB#27 likely represents a large eruption but with distribution to the north-northeast from Shiveluch into a poorly studied area, it is not as well documented. SH#32a is a prominent unit in the northeast portion of a region mapped by Ponomareva et al. (2017). The age of SH#27 agrees better with that of our cryptotephra than that of SH#32a. Nonetheless, the limited available geochemistry of both SH#27 and SH#32 are consistent with that of our cryptotephra (Fig. 11).

Shiveluch tephra are rarely identified outside of Kamchatka, perhaps because source eruptions are VEI 5 or less; nonetheless, two of our cryptotephra appear to come from that volcano. Other Shiveluch tephra identified beyond Kamchatka include SH#12 (1374–1295 cal yr BP) reported from Japan (Chen et al., 2019), and a potential "ultra-distal" Shiveluch correlation from Ireland (SLU14-60) to SH#34 (SHdv; 4700 cal yr BP; Ponomareva et al., 2017; Plunkett and Pilcher, 2018). These are intriguing potential correlations since until now transcontinental correlations have been limited to tephra from eruptions that are either caldera-forming or have estimated VEI greater than 5. Unfortunately, eruption characteristics have not been calculated for events related to SHb, SH#27 or SH#32a, but it appears that their source eruptions are not as voluminous or as explosive as eruptions that have generated other 'ultra-distal' tephra (e.g., Ponomareva et al., 2015, 2017). This example, like that of Mono-Inyo Craters, suggests that factors other than eruption magnitude and intensity can influence distribution of far-traveled tephra (e.g., Crocitti et al., 2018).

4.3.6. SB-11 (5960–5670 cal yr BP, mean 5890) and Greenland (5853 ± 15 a b2k = 5903 ± 15 cal yr BP)—Iliinsky

Tephra SB-11 from Sidney Bog has rhyolitic glass, with ~73–76 wt% SiO_2, plus lower K_2O and higher CaO than other tephra with similar SiO_2. This geochemistry matches that of a new tephra discovered in both NGRIP (NGRIP 950.25 m) and GRIP (GRIP 883.30 m) ice cores from Greenland (Fig. 11, Table 2, 5, S1). The ice core age, 5853 ± 15 a b2k (5903 ± 15 cal yr BP), derived from Adolphi and Muscheler (2016) corrected GICC05 timescale (Vinther et al., 2006), also matches our calibrated age for SB-11. Furthermore, the major-element geochemistry of both SB-11 and Greenland samples correlates well with a similarly aged tephra sourced from Iliinsky volcano in Kamchatka (Fig. 11; Tables S1, S8)

Iliinsky is a relatively small (1578 m) conical volcano located in the southernmost part of the Kamchatka Peninsula. It sits at the rim of the ~8.4 ka Kurile Lake caldera in a depression that may be the collapse crater of an older volcanic edifice (Ponomareva et al., 2004). Iliinsky deposits are compositionally related to and overlie the KO ignimbrite that erupted from the 8.4-ka caldera. Iliinsky products are low-to medium-K basalts, andesites and dacites; its most recent eruption took place in 1901.

A prominent bed of yellow pumice bombs and lapilli, informally called "upper coconuts", originated from one of the strongest Iliinsky eruptions. Initially attributed to the neighboring Zheltovsky volcano and coded ZLT (Braitseva et al., 1997), it is now known as the IL tephra (Zaretskaya et al., 2007). Ash-fall from this eruption blew northeast and a large proportion of it fell into the ocean, limiting estimates of its volume. The IL tephra bed contains charcoal and overlies a thick, well-developed, organic-rich paleosol (Ponomareva et al., 2001). Radiocarbon dates associated with the IL

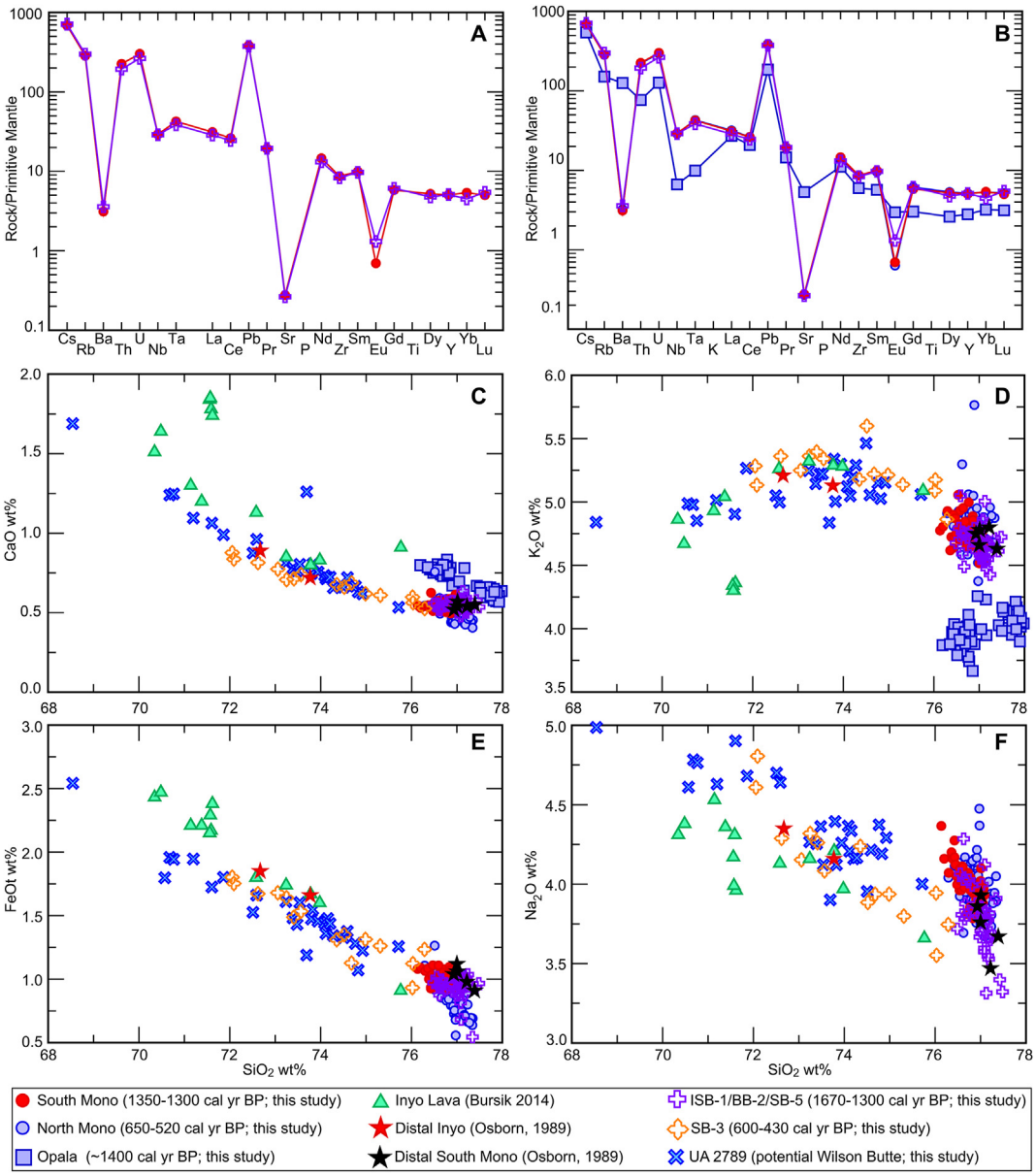

Fig. 9. Glass geochemistry of new and previously reported Mono-Inyo Craters compared with potential correlative cryptotephra. (A) Trace element geochemistry of ISB-1 shows the same characteristic trace element pattern as proximal South Mono tephra. (B) North Mono shows the same pattern including the Ba and Sr anomalies, which are also one of the main differentiating features from Opala 1.4 ka. (C,D) Opala 1.4 ka is also clearly differentiated from the cryptotephra with K_2O and CaO. (C,D,E,F) Major element geochemistry of the cryptotephra in comparison to data from proximal samples collected here, distal tephra from the Toiyabe Range, Nevada (Osborn, 1989), and Inyo lavas (Sampson and Cameron, 1987; Bursik, 2014). The published Inyo data and UA 2789 (potential Wilson Butte sample) are most similar to SB-3.

tephra range from 4570 ± 70 to 5840 ± 150 ^{14}C yr (Zaretskaya et al., 2007), likely reflecting the heterogeneous nature of organic matter in a long-lived paleosol. These dates resulted in a roughly estimated eruption age of 4800 ^{14}C yr. We recalibrated and modelled Zelenin et al. (2020) radiocarbon dates on proximal deposits to obtain a new age for the IL tephra (Table 2; S17). The resulting age has a bimodal two-sigma distribution of 5655–5620 and 5610–5580 cal yr BP, with a median age of 5600 cal yr BP—about two hundred years younger than SB-11 and the Greenland ice core tephra (whose ages agree well; Table 2). The geochemistry of the Iliinsky IL tephra matches well to that of cryptotephra from Greenland and Maine, but the age mismatch requires further investigation before the correlation can be verified. However, if this correlation holds, it continues a trend seen in this study and others (e.g., Cook et al., 2018b), whereby proximal Kamchatkan dates tend to be younger than the estimated ages of the cryptotephra.

4.4. Unknown tephra

The geochemical data and ages of these cryptotephra do not permit correlations to any one event or volcano. Nonetheless, careful comparison of the characteristics of these unknowns to the published literature does reveal, in some cases, potential relationships to specific volcanic regions that will require further exploration.

4.4.1. SB-1 and SB-2 (230 cal yr BP to modern)

SB-1 and SB-2 tephra were located in the top 2–3 cm in Sidney Bog core 1. Both share similar geochemical characteristics—they are high Si rhyolites (>76.5 wt%), with relatively low FeOt and CaO

Table 5
Glass geochemical averages and standard deviations of tephra with potential correlations. Data are normalized to 100%.

Tephra	Potential correlation	SiO_2	TiO_2	Al_2O_3	FeOt	MnO	MgO	CaO	Na_2O	K_2O	P_2O_5	Cl	H_2Odiff	n
SB-3	Mono-Inyo Craters (Inyo?)	74.15	0.14	14.06	1.42	0.06	0.08	0.69	4.10	5.24	–	0.08	3.11	15
		1.41	0.06	0.62	0.26	0.02	0.04	0.10	0.33	0.17	–	0.01	1.10	
SB-4	Fish Lake II; Chaos Crags, Lassen Peak	78.31	0.16	12.17	0.71	0.04	0.12	0.69	3.48	4.21	–	0.12	4.77	7
		1.16	0.03	0.57	0.13	0.03	0.03	0.08	0.29	0.38	–	0.03	2.75	
ISB-1, BB-2, SB-5	Mono-Inyo Craters (South Mono?)	77.02	0.07	12.86	0.93	0.04	0.03	0.54	3.76	4.67	0.00	0.09	4.96	40
		0.29	0.03	0.13	0.10	0.03	0.02	0.04	0.21	0.13	0.00	0.02	1.12	
BB-3	Us-Kr, Ushishir, Kuriles	77.41	0.20	12.90	1.43	0.12	0.35	2.16	4.00	1.20	–	0.21	7.29	7
		0.24	0.05	0.35	0.11	0.02	0.04	0.10	0.27	0.06	–	0.04	6.90	
SB-6	Shiveluch, (SHb/SH2800?)	74.30	0.27	14.15	1.40	0.05	0.39	1.53	4.91	2.86	–	0.16	4.58	9
		0.44	0.02	0.21	0.10	0.01	0.04	0.16	0.24	0.05	–	0.07	1.88	
SB-7	Fish Lake III (Medicine Lake?)	74.55	0.29	13.92	1.64	0.04	0.29	1.26	3.67	4.28	–	0.08	4.09	8
		0.38	0.05	0.13	0.10	0.03	0.05	0.10	0.14	0.13	–	0.02	1.04	
BB-4, SB-8	Shiveluch (SH#27/#28?)	75.67	0.27	13.62	1.14	0.03	0.29	1.16	4.75	2.95	–	0.16	4.06	19
		0.53	0.04	0.33	0.07	0.02	0.04	0.18	0.26	0.11	–	0.04	3.43	
SB-11, NGRIP 950.25 m, GRIP 883.30 m	Iliinsky	74.07	0.30	14.09	1.95	0.08	0.46	2.30	4.72	1.92	0.05	0.15	3.63	35
		0.67	0.05	0.34	0.18	0.02	0.05	0.23	0.29	0.09	0.01	0.02	4.08	

FeOt = total Fe as FeO, H2Odiff is water by difference (i.e., 100-original total), n = number of analyses.

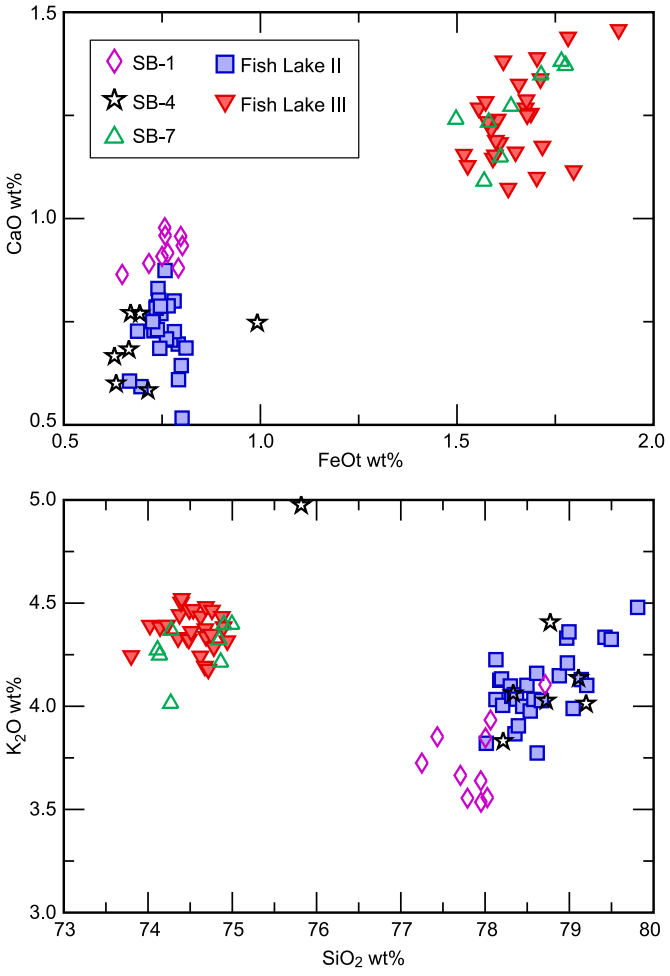

Fig. 10. Geochemical relationships between Fish Lake II and III and potential correlatives SB-4 and SB-7. SB-1 is included because it displays some on-trend behaviour with Fish Lake II (see Fig. 12 and section 4.4.1 for more details).

and high alkalis, in particular K_2O (Fig. 12; Table 6). Opala, Khangar and Ichinsky volcanos from Kamchatka, Mono-Inyo Craters, and some Mexican and Central American volcanoes (e.g., Schindlbeck et al., 2016, 2018; Portnyagin et al., 2020) produce tephra with similar geochemistry.

SB-1 was compared to published and newly collected data from several high SiO_2 and K_2O tephra, and shares similarities to a few, most notably SB-4 and Fish Lake II (Chaos Crags) (Figs. 10 and 12). Lassen Peak had a series of eruptions between 1914 and 1917. The most significant event occurred on May 22, 1915, which produced an eruption column ~9 km high and had reported ash fall as far afield as Elko, Nevada, about 500 km to the east (e.g., Eppler and Malin, 1989; Miller, 1989). However, the lack of reported geochemistry for this relatively small eruption and the poorly constrained age of SB-1, make any correlation highly speculative.

SB-2 has very low FeOt and CaO (<0.5 wt%) and relatively high Al_2O_3 (~13.4 wt%) that sets it apart from the other high silica and alkali tephra it was compared to here (e.g., Fig. 12, Table 6). Overall, the geochemical characteristics of SB-2 do not show any affiliation to tephra from any specific region.

4.4.2. ISB-5/BB-5/SB-9 (4620-4150 cal yr BP) and NDN-230-2 (2288-1830 cal yr BP)

Inter-core correlated ISB-5/BB-5/SB-5 from Irwin Smith, Bloomingdale and Sidney Bogs and NDN-230-2 from Nordan's Pond Bog are also high SiO_2 and alkali cryptotephra with relatively low FeOt (<1 wt%) and CaO (<0.5 wt%). We discriminate NDN-230-2 cryptotephra as a unique population in the resampled section of Nordan's Pond Bog that also contains Ruppert tephra. NDN-230-2 has extremely low CaO (~0.2 wt%) and is unlike anything else described here (Fig. 12, Table 6). The only published tephra geochemistry having similar composition are from the Izu Islands in Japan, such as the Izu-Kozushima-Tenjosan (Iz-Kt) eruption of 838 CE (e.g., McLean et al., 2018). At present Izu Island eruptions are not documented when NDN-230-2 was deposited.

Cryptotephra ISB-5/BB-5/SB-9 is outwardly similar to tephra from Ichinsky, Opala, and Mono Craters (Fig. 10). Ichinsky erupted during the same timeframe as this cryptotephra, and while there are reports of an older eruption with timing similar to that of Opala (OPtr; Braitseva et al., 1997), new data show that OPtr is not from Opala but from the Chasha Crater, 17.5 km northeast of Opala. There are limited glass geochemical data for the ~4.7 ka Ichinsky eruption and "OPtr", with the latter showing distinctly low K_2O and high CaO contents that exclude a correlation (Portnyagin et al., 2020). Ichinsky and the 1.4 ka Opala tephra have some geochemical similarity to the cryptotephra, suggesting it could be sourced from Kamchatka. However, the cryptotephra geochemistry plots more closely with that of North and South Mono tephra (Fig. 12).

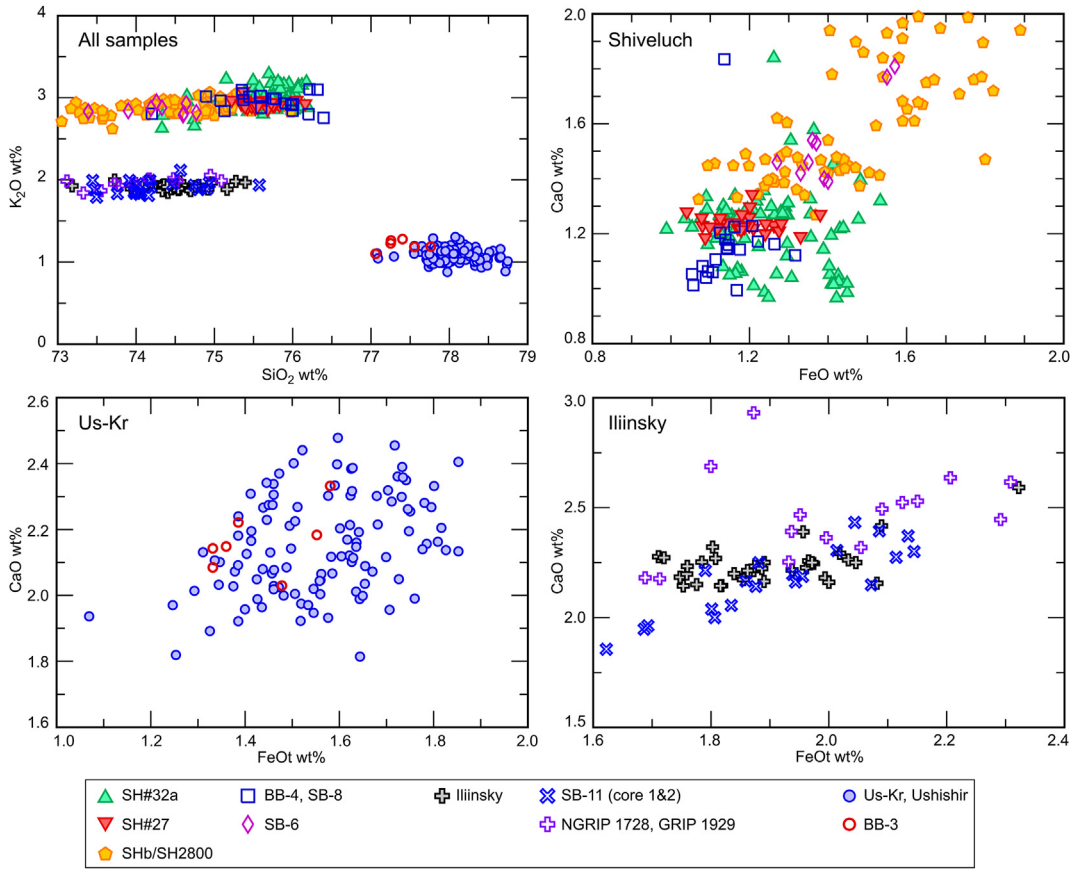

Fig. 11. Major element geochemistry illustrating possible new correlations to Kamchatkan and Kurile eruptions. Top left plot shows all potential correlatives together. Glass geochemical data for Shiveluch reference material is from Ponomareva et al. (2017) and the TephraKam database of Portnyagin et al. (2020).

Unfortunately, the exact chronology of middle Holocene eruptions from Mono Craters is not fully understood. Bursik and Sieh (2013) compiled radiocarbon dates from proximal eruptions that suggest a gap in activity at this time; between Episode 2 (~5310-5050 cal yr BP) and Episode 3 (~3700-3140 cal yr BP), recalibrated here. Conversely, Sarna-Wojcicki et al. (1988) report Mono Craters-derived tephra of similar age to the cryptotephra from Walker Lake, Nevada. However, if the interval between Episode 2 and Episode 3 is analogous to that between the North and South Mono eruptions at Walker Lake, then these may be spurious tephra that were in-washed and not primary (Bursik et al., 2014).

4.4.3. BB-6 (5210–5080 cal yr BP) and SB-10 (5550–5335 cal yr BP)

Cryptotephra SB-10 and BB-6 from Sidney Bog and Bloomingdale Bog were initially thought to correlate, but their independently derived ages do not overlap (Fig. 2F). This age offset and subtle differences in geochemical composition suggest that they are two separate events (Tables 2 and 6; Fig. 13). Geochemically, both tephra are very similar to the late Pleistocene Glacier Peak tephra (G/B; Fig. 13), indicating Glacier Peak as a possible source. Calibrated ages of BB-6 and SB-10 overlap within two standard deviations the youngest existing age for mid-Holocene activity at Glacier Peak known as set D and 'Dusty Creek' (~6800–5300 cal yr BP; Begét, 1982, 1984; Vallance et al., 2015). This period of activity is defined by a series of tephra-producing eruptions, pyroclastic flows and lahars (e.g., Begét, 1982; Vallance et al., 2015). Visible tephra from the Dusty Creek assemblage are present as far as British Columbia and geochemical averages reported from them suggest they can be differentiated from their widespread Pleistocene Glacier Peak counterparts (e.g., Hallett et al., 2001; Foit et al., 2004). New proximal geochemical data from the Dusty Creek assemblage confirm they are distinct from the Pleistocene Glacier Peak tephra and the two cryptotephra (Fig. 13, Table S8). Therefore, unless there was an eruption late in the Dusty Creek sequence that had a geochemical signature more like that of the older Pleistocene events, these new data challenge the Glacier Peak correlation. The unknown cryptotephra also fall within the geochemical variation seen in some Alaskan tephra (Fig. 13).

Higher levels of hydration indicated by lower totals also characterize BB-6 and SB-10. Careful point by point re-analyses show that these results were not caused by poor analyses on very small grains. The average hydration of these cryptotephra is greater than that of any other tephra discussed here, including potential correlatives. Greater levels of hydration could suggest that the shards are reworked from older deposits; however, this hypothesis seems extremely unlikely given that these cryptotephra have well defined peaks (e.g., no tails in shards, multiple peaks or other signs of reworking) and a distinct and homogeneous geochemistry not found in any other sample. Lower totals of these cryptotephra are likely characteristic of the tephra rather than an indication of age.

4.4.4. BB-1 (505-205 cal yr BP), BB-7 (5940-5745 cal yr BP), SB-12 (6690-6150 cal yr BP)

These three tephra from Bloomingdale and Sidney Bogs are geochemically distinct and differ in age but are grouped together because they share geochemical similarities to tephra from the Aleutian Arc-Alaska Peninsula. However, we cannot discount that

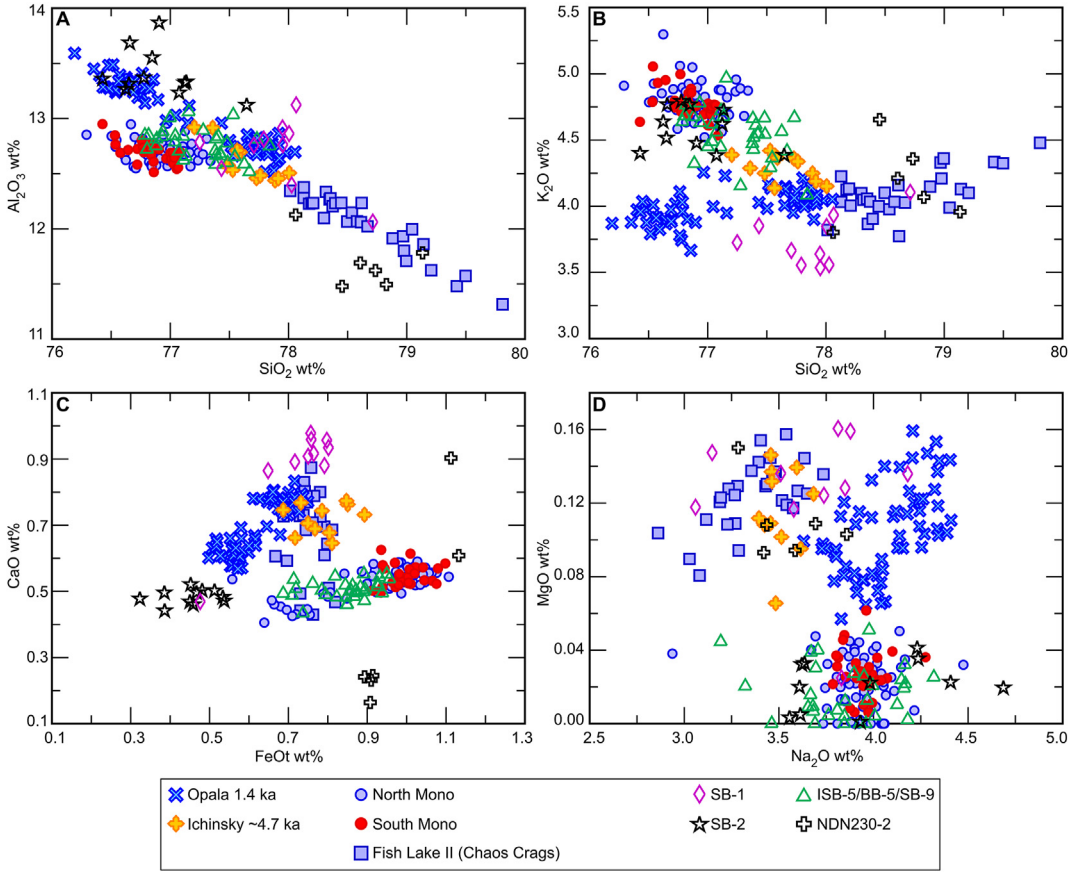

Fig. 12. High SiO_2 rhyolites with relatively high K_2O and low CaO and FeOt plotted with reference material of proximal samples of similar composition. SB-1 tends to plot with the cluster formed by Opala, Ichinsky and Fish Lake II. However, it is clearly offset from the former two in K_2O and CaO, while remains relatively on trend with Fish Lake II. SB-2 does not share a geochemical affinity to any tephra examined here, with both it and NDN-230-2 clearly separated out by FeOt and CaO (C). However, ISB-5/BB-5/SB-9 tends to plot closely with the North and South Mono tephra with only minor offsets most obvious in (B).

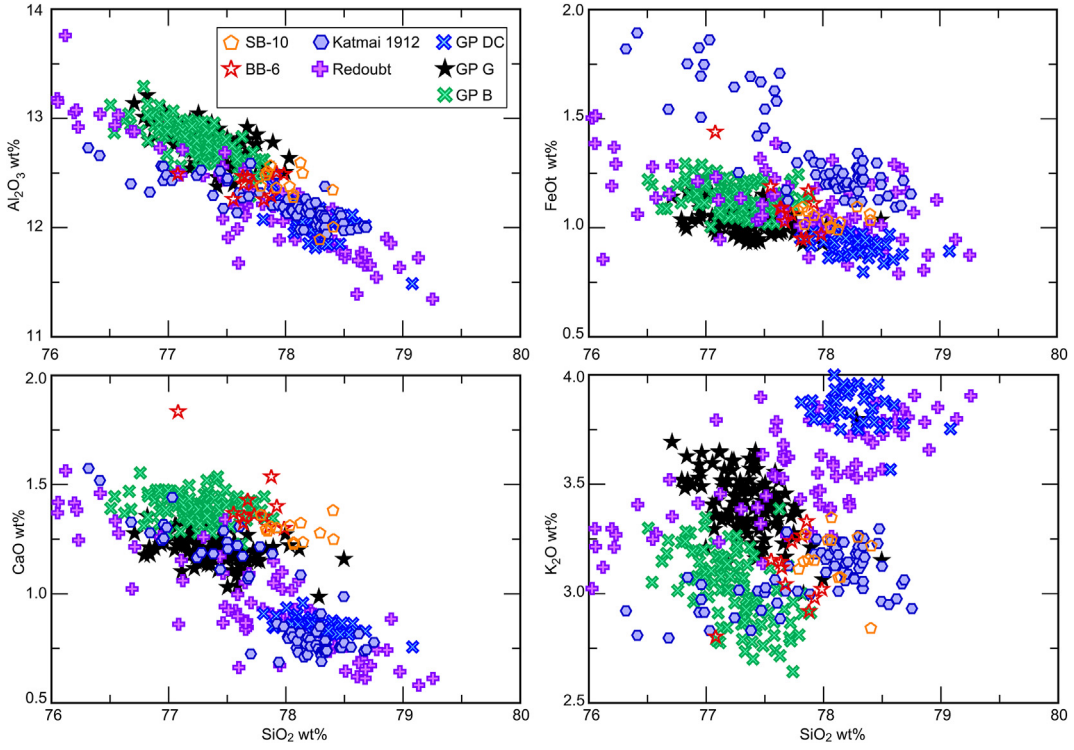

Fig. 13. SB-10 and BB-6 are most similar to Pleistocene Glacier Peak tephra B and G, but are geochemically offset from Glacier Peak's mid-Holocene eruptions (Dusty Creek; DC). Compounding the uncertainty, these tephra also plot within the fields defined by some Alaskan tephra, with Katmai 1912 and Redoubt data plotted here to illustrate this point.

they may originate from elsewhere.

BB-1 is a distinct rhyodacite with a high Cl content averaging around 0.30 wt% (Table 6). Higher Cl is a characteristic of some sources in Alaska, and BB-1 plots well with a cryptotephra first identified on the Kenai Peninsula (MP10b; Payne and Blackford, 2008), as well as a previously undescribed tephra from Alaska (UA 3467; 310-155 cal yr BP) (Fig. 14; Table S8). Chlorine was not measured for MP10b (which is also too young with an estimated age of ~1875 CE) and the Cl for BB-1 is too high for it to correlate to UA 3467. The high Cl in BB-1 does not appear to be an analytical artifact as the standards do not suggest that Cl was high during these analyses, but we were unable to reanalyse this sample to test this. Aniakchak also had a major eruption during this timeframe (e.g., Kaufman et al., 2012; Bacon et al., 2014), but Aniakchak tephra are clearly differentiated from BB-1 by TiO_2 content (Fig. 14).

BB-7 (5940–5745 cal yr BP) and SB-12 (6690–6150 cal yr BP) share some similar characteristics, but can be differentiated by CaO, FeOt and MgO (Fig. 14). Tephra with comparable geochemistry come from more recently active volcanoes in Alaska, such as Redoubt and Aniakchak (Fig. 14; e.g., Bolton et al., 2020), and samples attributed to Iliamna by Lemke (2000). BB-7 and SB-12 are most similar to Redoubt and Iliamna tephra but offset in CaO and FeOt (Fig. 14). They have no clear correlations, but their geochemistry does fall within the geochemical variability seen in Aleutian-Arc Alaska-Peninsula tephra. These two cryptotephra may also match analyses in Pyne-O'Donnell et al. (2012). In that study, several samples were comprised of mixed glass, i.e., two or more unrelated geochemical populations that had too few analyses to make any firm conclusions. Two of those samples, NDN-433 and NDN-455, contain several shards with geochemistry that overlaps BB-7 and SB-12, respectively (Fig. 15). The overlap in age estimates lends some credence to the potential linkages between these samples (Table 2), and suggest these cryptotephra, although minor, may be widely distributed.

4.4.5. SB-13 and TI-317 (combined age 7215–6065 cal yr BP)

Two tephra, one found in Thin-Ice Pond and the other in Sidney Bog, both overlie Mazama and likely correlate to each other. SB-13 (7238–6826 cal yr BP) forms a notable peak with a concentration of 56 shards/cm^3 in core 1. This peak contains both SB-13 and East Lake tephra, but SB-13 is the dominant geochemical population. TI-317 in Thin-Ice Pond forms a discrete horizon with a maximum concentration of ~80 shards/cm^3 and an average shard size of ~60 μm ($\sigma = 14$, $n = 20$). Their ages overlap, although the age range of TI-317 increases significantly (from 7087 to 6558 to 7001–5970 cal yr BP) when the age model includes the proximal age of KS_2, which closely underlies TI-317 (Fig. 2E; Table S16). Glass in both TI-317 and SB-13 is largely colourless with some brown shards, many of which contain moderate quantities of microlites. Shards have a similar blocky morphology, but pumice is more common in SB-13 (Fig. 4), although this pumice may be from East Lake, which is present in the same sample. Geochemically the two tephra are nearly identical although SB-13 has slightly higher SiO_2 than TI-317 (e.g., Figs. 14 and 15). Similar morphology, stratigraphic position, age, and high shard concentrations strongly suggest that these units are the same tephra or two closely spaced eruptions from the same source. If SB-13 and TI-317 are the same tephra, the geochemical variation could be explained by varying wind direction over the course of the eruption (e.g., Jensen et al., 2011), but not by processing methods. SB-13 was bulk mounted, while TI-317 was density separated; the lower SiO_2 average in TI-317 is the opposite as what would be expected if processing were to be implicated (i.e., density separating can cause removal of lower SiO_2 shards).

Comparisons with the University of Alberta tephra geochemical database revealed some superficial geochemical similarities to Pleistocene tephra from Alaska, but nothing with the distinctive SiO_2 to TiO_2 ratio this unit shows (Fig. 14B). However, a younger tephra from Cabin Lake in south-central Alaska (CU1152; ~1200 cal yr BP; Zander et al., 2013), which correlates to a geochemical sub-population in a sample from the interior of Alaska (UA 3465), is very similar to this cryptotephra (Fig. 14A,B,F; Table S8). They do not correlate temporally but the geochemical similarity indicates that the cryptotephra could originate from Alaska.

Alternatively, the geochemistry, age, and shard morphology of this cryptotephra are consistent with those of tephra from Mount Rainier. The cryptotephra plot well with tephra from Mount Rainier, even though these data are from units less than ~2600 cal yr BP in age (Figs. 14 and 15; Sisson and Vallance, 2008). In addition, two tephra units from Mount Rainier known as layers D and L erupted during intervals that overlap deposition of this cryptotephra (e.g., Mullineaux, 1974; Sisson and Vallance, 2008). Layers D and L are more voluminous than any other Holocene tephra units from Mount Rainier except layer C tephra (~2200 cal yr BP) and have

Table 6
Glass geochemical averages and standard deviations of unknown tephra. Data are normalized to 100%.

Tephra	SiO_2	TiO_2	Al_2O_3	FeOt	MnO	MgO	CaO	Na_2O	K_2O	P_2O_5	Cl	H_2Odiff	n
SB-1	77.80	0.10	12.77	0.75	0.06	0.14	0.92	3.64	3.70	–	0.09	5.46	9
	0.29	0.02	0.21	0.05	0.03	0.02	0.04	0.36	0.15	–	0.02	3.48	
SB-2	76.90	0.06	13.40	0.45	0.05	0.02	0.48	3.96	4.59	–	0.06	7.16	11
	0.34	0.02	0.22	0.07	0.05	0.01	0.02	0.39	0.16	–	0.02	5.09	
BB-1	68.58	0.52	15.75	3.79	0.11	0.92	3.06	4.27	2.75	–	0.31	1.89	14
	0.83	0.05	0.28	0.32	0.04	0.14	0.27	0.12	0.09	–	0.04	1.15	
NDN-230-2	78.64	0.28	11.70	0.98	0.05	0.11	0.40	3.55	4.18	–	0.17	4.09	6
	0.36	0.03	0.24	0.11	0.02	0.02	0.29	0.21	0.30	–	0.04	2.05	
ISB-5/BB-5/SB-9	77.25	0.06	12.76	0.85	0.05	0.02	0.51	3.88	4.53	–	0.11	5.74	30
	0.30	0.03	0.12	0.08	0.02	0.01	0.03	0.23	0.17	–	0.02	2.25	
BB-6	77.71	0.20	12.41	1.10	0.07	0.23	1.42	3.55	3.09	–	0.26	6.56	11
	0.25	0.06	0.10	0.14	0.03	0.04	0.15	0.14	0.16	–	0.04	1.66	
SB-10	78.06	0.19	12.35	1.04	0.08	0.23	1.29	3.39	3.16	–	0.25	6.22	13
	0.21	0.03	0.21	0.04	0.03	0.03	0.05	0.12	0.13	–	0.02	1.06	
BB-7	73.29	0.46	14.45	1.95	0.05	0.53	1.58	4.70	2.77	–	0.23	5.30	9
	1.48	0.05	0.62	0.17	0.02	0.14	0.21	0.62	0.19	–	0.04	4.88	
SB-12	73.45	0.35	13.90	2.53	0.08	0.31	1.60	4.97	2.64	–	0.20	2.69	11
	0.48	0.03	0.27	0.06	0.02	0.02	0.06	0.27	0.07	–	0.02	1.16	
T-317/SB-13	69.66	1.07	13.98	3.97	0.07	0.91	2.64	4.34	3.15	0.28	0.16	2.41	69
	0.92	0.07	0.49	0.22	0.03	0.10	0.39	0.26	0.20	0.10	0.03	1.68	

FeOt = total Fe as FeO, H_2Odiff is water by difference (i.e., 100−original total), n = number of analyses.

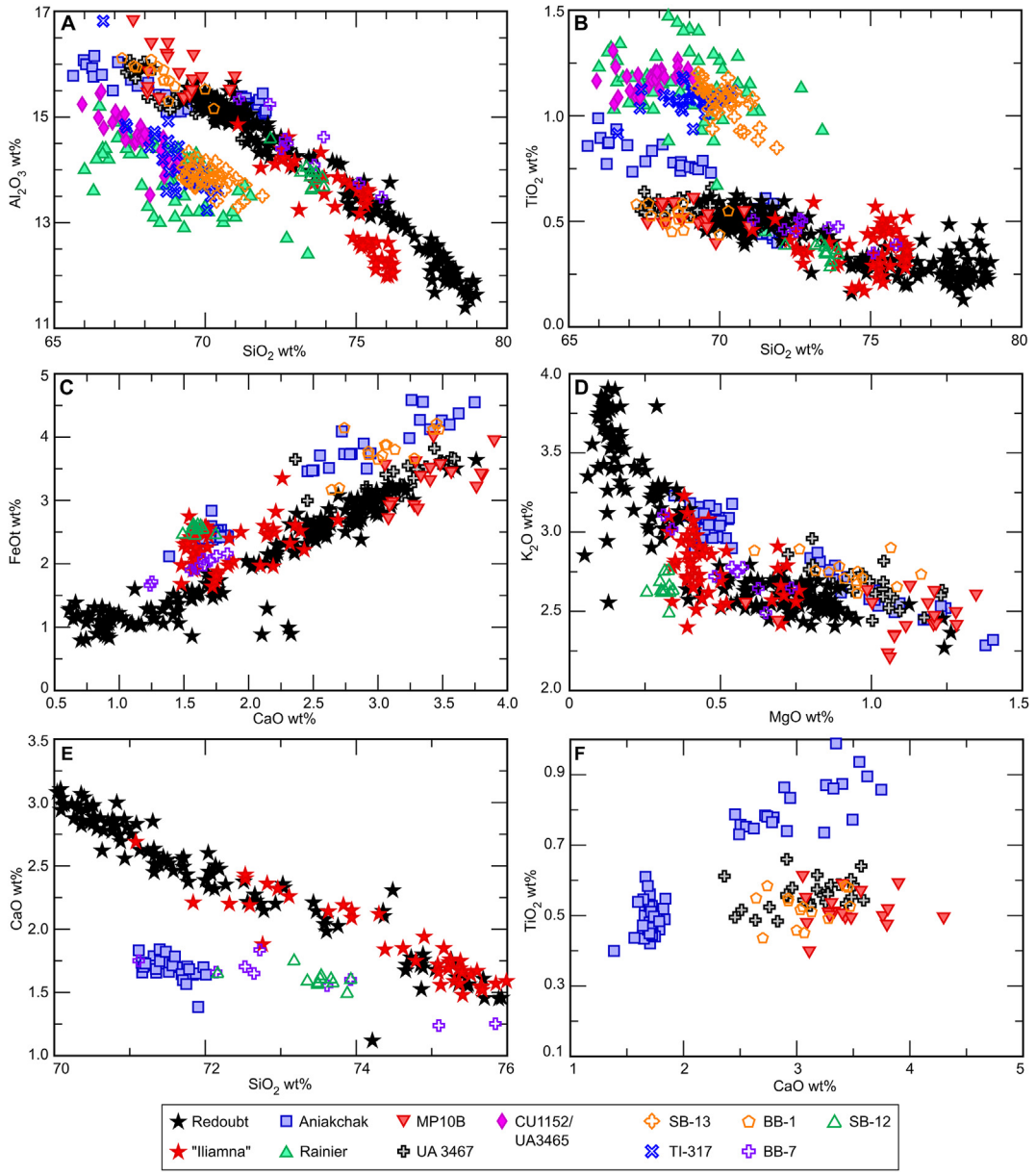

Fig. 14. Glass geochemistry of uncorrelated tephra compared with proximal samples of potential source regions. (A,B) The unknowns and the proximal material fall along two main trends with TI-317 and SB-13 clearly separated by Al_2O_3 and TiO_2. The high TiO_2:SiO_2 of these two tephra is not seen in any published records, with the exception of one Alaskan tephra CU1152 (Zander et al., 2013) and a series of mid to late Holocene tephra from Rainier (Sisson and Vallance, 2008). (C,D) BB-1, BB-7 and SB-12 are variable but generally plot on trends defined collectively by the Redoubt, "Iliamna" and Aniakchak tephra. (E) BB-7 and SB-12 are geochemically similar to these active Alaskan volcanoes but do not consistently plot with them with the greatest offset in CaO. (F) BB-1, MP10B, UA 3467 and a lower SiO_2 Aniakchak population plot together on most oxides except TiO_2, which clearly differentiates Aniakchak.

been traced as far as 40 km downwind (Vallance, unpublished data). However, both are inferred to be products of sub-Plinian eruptions and are less voluminous than the other tephra discussed here (Table 7). The only published glass geochemical data for these two units are reported as averages and standard deviations (Donoghue et al., 2007), and the comparison is inconclusive (Fig. 15C and D).

5. Summary and conclusions

Screening for cryptotephra in three ombrotrophic peat bogs from Michigan, New York and Maine, in combination with resampling at Thin-Ice Pond, Nova Scotia, and Nordan's Pond Bog Newfoundland, reveals 30 well-defined cryptotephra deposits. Of these, twelve are confidently correlated to previously described units (11 of 12 to their source volcano), while eight are tentatively correlated with a tephra or source volcano. The remaining ten tephra are of unknown origin although some do have potential source regions or volcanoes. Combining our dataset with that of previous studies, we have developed a composite tephrostratigraphy of up to 36 unique tephra spanning from ~14.0 ka to present (Fig. 16). This work presents the current state of knowledge for tephra distribution in northeastern North America, which is likely to be much more complex than presented here given the low density of sites, and the limited glass geochemical data and eruption histories from potential source regions and volcanoes.

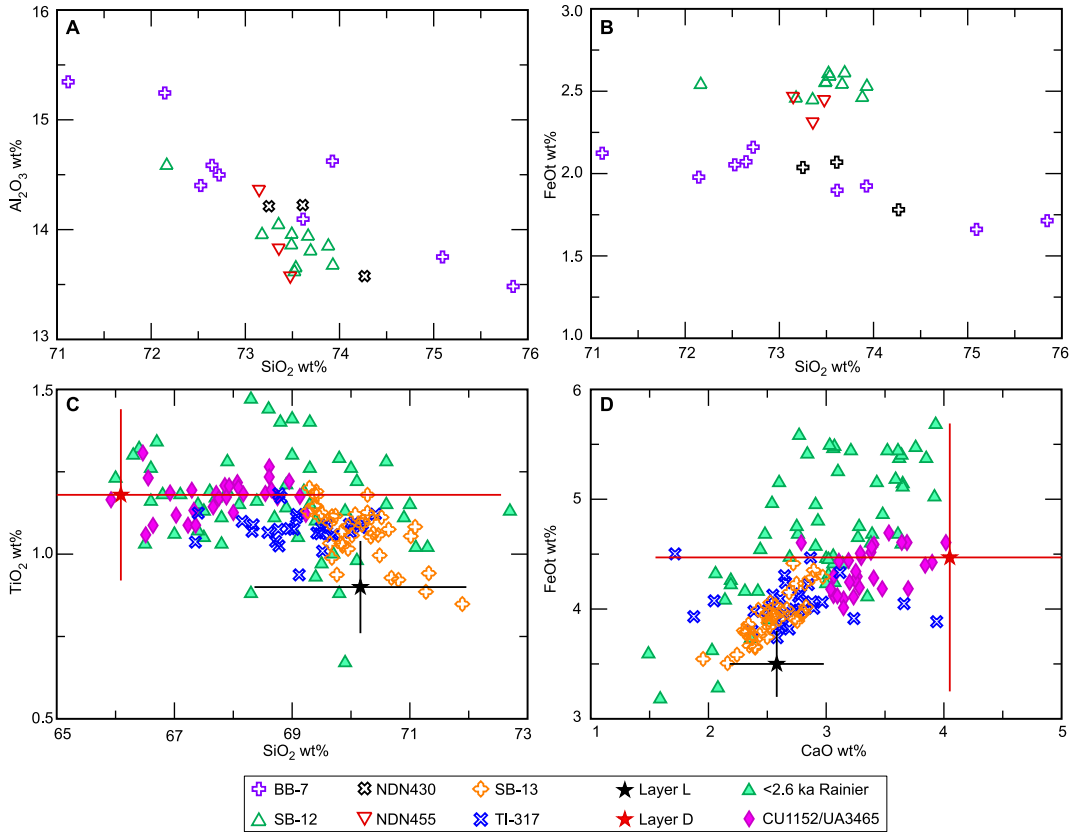

Fig. 15. Glass geochemistry of unknowns. (A,B) Comparison to glass shards in two samples from Nordan's Pond Bog to two unknowns from Bloomingdale and Sidney. (C,D) Averages and standard deviations (two sigma) of layer D and L from Mount Rainier (Donoghue et al., 2007) compared to TI-317 and SB-13, and younger Rainier and Alaskan tephra of similar composition.

Table 7
Available data on eruption characteristics of tephra discussed in this study.

Tephra	VEI	Volume (tephra, km^3)	Volume (DRE, km^3)	Column height (km)	Mass discharge (kg/s)	references
MSH layer T	4–5	1.5, 0.1–0.3	0.4, 0.031–0.089	16, 23	1, 4x10^7	Carey et al. (1995); Gardner et al. (1998); Nathenson (2017)
MSH We	4–5	1.5, 0.15–0.80	0.4, 0.039–0.21	21, 30	2.5x10^7, 1x10^8	Carey et al. (1995); Gardner et al. (1998); Nathenson (2017)
North Mono	4	0.181–0.183	0.0728	–	–	Bursik et al. (2014)
Inyo (SD,OF,GC)	3	0.01–0.1	–	~8–21	–	Nawotniak and Bursik (2010)
Jala Pumice[a]	6	10–11.4	2.9–3.7	22–30	1–8x10^7	Gardner and Tait (2000)
WRAe	6	~50	–	–	–	Lerbekmo (2008)
Newberry Pumice	4	0.4, 0.39	0.1, 0.12	21, 22	2.8x10^7	Gardner et al. (1998); Nathenson (2017)
South Mono	4	0.171–0.195	0.0732	–	–	Bursik et al. (2014)
KS_1	6	20–25	8–9	30–36	2–6x10^8	Andrews et al. (2007)
MSH Pu	3–4	0.8, 0.03–0.18	0.2, 0.008–0.047	15, 24	5x10^6, 5x10^7	Carey et al. (1995); Gardner et al. (1998); Nathenson (2017)
MSH Yn	5–6	15.3, 3–8.8	4, 0.78–2.3	31,34	1, 2x10^8	Carey et al. (1995); Gardner et al. (1998); Nathenson (2017)
Iliinsky[b]	–	2.5	0.7	–	–	recalculated from Kyle et al. (2011), isopachs and Ponomareva et al. (2017)
Rainer D	3	0.075, 0.041	0.013	–	–	Mullineaux (1974), Nathenson (2017)
Rainer L	3	0.05, 0.017	0.0054	–	–	Mullineaux (1974), Nathenson (2017)
KS_2	5	8.9–10.5	2.5–2.9	–	–	recalculated from Kyle et al. (2011), isopachs and Ponomareva et al. (2017)
Mazama	7	176		–	–	Buckland et al. (2020)
Glacier Peak G	5	6.0, 1.8–9.4	1.9, 0.57–3.0	32,37	1.4, 2x10^8	Gardner et al. (1998); Nathenson (2017)
Glacier Peak B	5	6.5, 1.9–9.4	2.1, 0.6–3.0	31, 35	1.3, 2x10^8	Gardner et al. (1998); Nathenson (2017)

Note that tephra with multiple values for volume corresponded to different estimates provided by the references cited.
[a] Values are additive or ranges for the different fall units comprising Jala (P1–P4).
[b] A minimum estimate as much of the tephra fall went into the ocean.

However, the results do show that northeastern North America is a major catchment for tephra from a variety of volcanic sources within and outside of North America. Despite the span of our sites across thousands of kilometers, there is surprising consistency in tephrostratigraphy with MSH set W, WRAe, Newberry, Ruppert, East Lake and Mazama distributed across the entire region. Mid-western records (Irwin Smith and Long Bog) were complicated by redeposited material, but there is considerable promise for the application of cryptotephra further east and north. Currently there are major gaps in the region, with no detailed studies, for example, in all of Québec. Linkages with the Pacific rim, Greenland and Europe have been established and are likely to increase as further work is done.

Key observations of our cryptotephra study include:

- A similar or greater abundance of Kamchatkan than Alaskan tephra, or at least identifiable Alaskan tephra. Poorly mapped and geochemically characterized Alaskan tephra outside the Cook Inlet area may explain this anomalous finding, and many

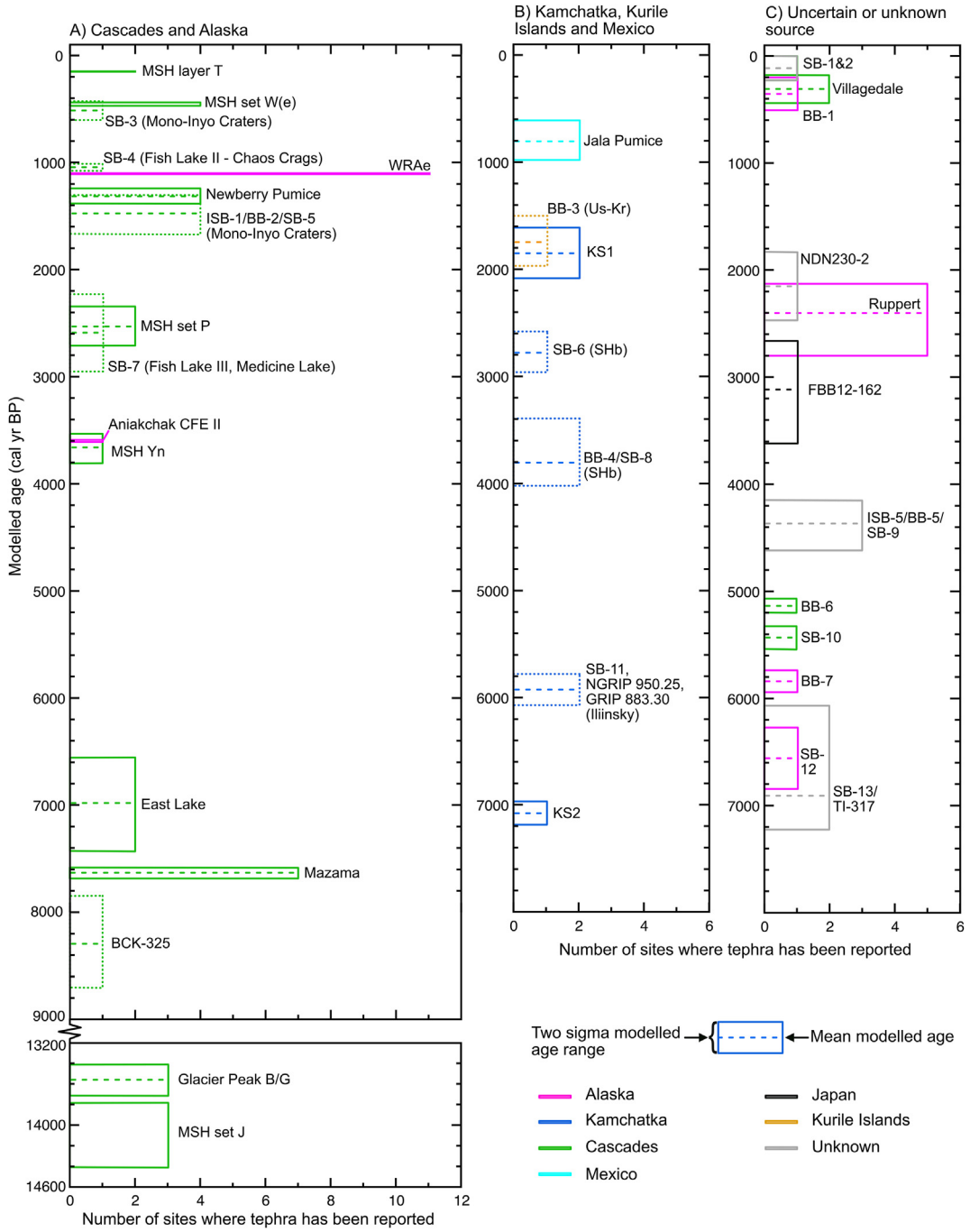

Fig. 16. All tephra found in the study region plotted by age and organized by (A,B) known or probable source region; and (C) tephra of unknown source. Probable tephra (A,B) are differentiated from confidently correlated tephra using a dotted line. Tephra of unknown origin (C) are colour coded for possible source if their data strongly suggest a specific source region. If there is more than one possible source (e.g., SB-13/TI-317) they are marked as unknown (grey).

may go unrecognized because they are deposited into the Bering Sea or Gulf of Alaska.

- Scarcity of Japanese and Kurile Island tephra. Mackay et al. (2016) identified the only potential Japanese unit in the study area, and we add one potential Kurile Island event (Us-Kr). There is also a dearth of tephra identified in Holocene sections of Greenland ice cores from these sources. Several Japanese events have been located in Pleistocene ice-core sections (Abbott and Davies, 2012; Bourne et al., 2016), while tephra from the Kuriles are completely missing from the Greenland records. However, it should be noted that tephra from the Changbaishan "Millennium eruption" (BTm; 941 ± 1 CE) of North Korea/China has been identified in Greenland (Sun et al., 2014). It is not clear why there may be a lack of tephra from sources in these regions – the results presented here are not sufficient to determine why this might be the case. We suggest the further examination of Holocene tephra records from eastern North America and Greenland could shed more light on this question.
- Growing numbers of observations that help delineate dispersal limits. For example, Aniakchak CFE II is not present at any site south of Newfoundland. South Mono, as well as MSH set P tephra, have not been found in more northerly sites and quickly tail off towards the east. Katmai 1912, which has been reported in Greenland and northern Alberta (Coulter et al., 2012; Davies et al., 2018), was not identified in any site reported here. Recent research illustrates how cryptotephra are important components of the "missing" ash volume problem (first defined by Walker, 1980 and Fierstein and Nathenson, 1992), thus improved dispersal limits and cryptotephra concentrations are key to calculating accurate total volume estimates (Cashman and Rust, 2020).
- There is a potential gap in tephra deposition between Glacier Peak tephra and Mazama. Although sites covering this full age range are limited (Table 1; Fig. 16), there is an apparent lack of tephra deposition in this region between ~14,000 and 8000 years. Currently there are too few sites covering this time range to determine if this is the result of taphonomic bias and, if not, what is causing this gap in deposition (e.g., major atmospheric shifts associated with collapse of Laurentide Ice Sheet? Quiescence in main source regions?).
- Factors other than magnitude that influence how far tephra travel. With the right synoptic or meteorological conditions (caught in jet stream? site weather during deposition and eruption?), tephra from small to moderate eruptions can be distributed great distances and deposited in high enough concentrations to be preserved in the geologic record. Table 7 lists the available data on the size of various eruptions that have, or potentially have, deposited tephra in this region. For example, the voluminous MSH Yn is high concentration cryptotephra, but is present only in Sidney Bog, while the much less voluminous potential South Mono correlative is present at all three bogs sampled for this study.
- The vagary of (crypto)tephra deposition and preservation. The absence of a tephra in one core does not preclude its presence at a site—there is value in examining more than one core per site if possible. Volcanic glass is widespread and commonly deposited in concentrations high enough to be identified and analysed. More often than not, the tephra also have a distinct geochemical signature that makes them uniquely identifiable. Uncorrelated tephra might be the result of un-analysed proximal tephra or simply previously unidentified explosive eruptions. Together these records are important in complementing other records of explosive volcanism, particularly in assessments of volcanic hazards, frequency, and potential impacts on climate.
- Dynamic tephra depositional environments that require a careful assessment of stringent criteria to confidently define and identify a primary deposit. Issues that complicate interpretations are many and include vertical reworking, a background signal of remobilised glass (e.g., detrital glass within incoming sediment), and multiple glass populations. Discriminating what comprises a primary deposit often evolves over the course of a project as a specific site's characteristics become clearer but is a necessary consideration.
- Proximal ages for Kamchatkan tephra that are often slightly younger (~100–200 years) compared to ages from distal sites. This discrepancy was noted by Cook et al. (2018b) in their discovery of Kamchatkan tephra KHG in Greenland, and Plunkett et al. (2015) for KS_2 in lake sediments. The validity of this observation will need to be tested by confirming the probable correlations, but in every single case there is an offset between the cryptotephra age and the proximal age with the cryptotephra age older. The discrepancy likely results from old bulk carbon dates and a lack of new AMS dates on proximal deposits.

Overall, our research highlights significant gaps in the present understanding of tephra dispersal and presents considerable avenues for future research. Many of these avenues go beyond the classic correlation and dating applications of tephra to the utility of cryptotephra research to the volcanological community. However, the types of data most useful for those using tephra to understand and model, for example, ash dispersal, vary from the data often reported in more typical tephra-based studies. For the past seven years there has been concerted effort by the tephrochronological and volcanological communities to establish a series of best practices that would make data collected during tephra research useful to both communities (Wallace et al., in review). A series of recommendations and template spreadsheets that outline fundamental information that should be collected and published to benefit all those interested in tephra are available at https://earthchem.org/communities/tephra/.

A major component of ensuring the future applicability of tephra research is the release of the individual geochemical analyses for the reported tephra and secondary reference materials used as quality controls. These data are fundamental in ensuring the future utility of a tephra study for all researchers. For this study we document all the geochemical data for the reference materials and cryptotephra, including data that were ultimately determined to be of limited use in the publication itself (weathered shards, populations ~<6 shards). All methods and data-processing steps are also clearly outlined to assist interlaboratory comparisons as much as possible. We have also reported all available detail on the cores collected, depths, core sections, the counts and age models to assist in reproducibility and more detailed (and potentially higher-resolution) cross-study comparisons. More specifically for the volcanological community, future cryptotephra studies should aim for more consistency in recording grain-size and morphology, if possible. The widespread adoption of these best practices will be a great service to the research community (Wallace et al., in review).

Author statement

Britta Jensen: Conceptualization, Data curation/Formal analysis, Funding acquisition, Writing – original draft, Writing – review & editing. Gill Plunkett: Conceptualization, Data curation/Formal analysis, Funding acquisition, Writing – original draft, Writing – review & editing. Sean Pyne-O'Donnell: Conceptualization, Data curation/Formal analysis, Funding acquisition, Writing – original draft, Writing – review & editing. Robert Booth: Conceptualization, Resources, Funding acquisition, Writing – review & editing. Lauren

Davies: Data curation/Formal analysis, Writing – original draft, Writing – review & editing. Connor Nolan: Data curation/Formal analysis, Writing – original draft, Writing – review & editing. Alistair Monteath: Data curation/Formal analysis, Funding acquisition, Writing – review & editing. Vera Ponomareva: Data curation/Formal analysis, Resources, Funding acquisition, Writing – original draft, Writing – review & editing. Maxim Portnyagin: Data curation/Formal analysis, Resources, Funding acquisition, Writing – review & editing. Eliza Cook: Data curation/Formal analysis, Writing – review & editing. Yan Luo: Data curation/Formal analysis, Resources, Paul Hughes: Resources. Marcus Bursik: Resources, Writing – review & editing. Les Cwynar: Resources, Funding acquisition, Writing – review & editing. James Vallance: Resources, Writing – review & editing. Graham Pearson: Resources, Writing – review & editing

Declaration of Competing Interest

The authors declare that they have no known competing financial interests or personal relationships that could have appeared to influence the work reported in this paper.

Acknowledgments

Funding for this research was provided by a Natural Sciences and Engineering Research Council of Canada (NSERC) Post-Doctoral Fellow award and NSERC Discovery Grant to B. Jensen. The collection and radiocarbon dating of the Long Bog, Sidney (core 1), Irwin Smith, and Bloomingdale cores was funded by grants for previous projects from the National Science Foundation (ATM-0625298, EAR-0902441, DEB-118676) and U.S. Geological Survey (USGS-DOI cooperative agreement 06ERAG0019) to R. Booth. Thin-Ice Pond research was supported by an NSERC Discovery Grant to L. Cwynar and by the European Community's Seventh Framework Programme (FP7/2007–2013) under grant PIEF-GA-2009-253552 to S.Pyne-O'Donnell. Dating of the Thin Ice Pond record was supported by the ^{14}CHRONO Centre for Climate, the Environment and Chronology at Queen's University Belfast. V. Ponomareva and M. Portnyagin's work on Kamchatkan tephra was supported by the Russian Science Foundation Grant # 16-17-10035. The Geologists' Association New Researchers' Scheme helped fund analyses on WRAe and Mazama from Sidney Bog core 2 (Edinburgh; A. Monteath). L. Davies would like to acknowledge support from a Leverhulme Trust Early Career Fellowship since October 2020. We would like to thank Andrew Locock of the Department of Earth and Atmospheric Sciences microprobe lab for constantly striving to improve the quality of our analyses of tiny recalcitrant cryptotephra when we first started this project in 2013, and the two anonymous reviewers, as well as Chris Harpel and Larry Mastin of the U.S. Geological Survey, for their helpful comments that led to an improved manuscript. Finally, we would also like to thank all of our colleagues who over the years have seen and commented on iterations of this project at various conferences and meetings, including INTAV— now reborn as the Commission of Tephrochronology (COT) within IAVCEI— and Volcanic Impacts on Climate and Society (VICS) working group of PAGES.

Appendix A. Supplementary data

Supplementary data to this article can be found online at https://doi.org/10.1016/j.quascirev.2021.107242.

References

Aaby, B., 1976. Cyclic climatic variations in climate over the past 5500 years reflected in raised bogs. Nature 263, 281–284.
Abbott, P.M., Davies, S.M., 2012. Volcanism and the Greenland ice-cores: the tephra record. Earth Sci. Rev. 115, 173–191.
Adolphi, F., Muscheler, R., 2016. Synchronizing the Greenland ice core and radiocarbon timescales over the Holocene e Bayesian wiggle-matching of cosmogenic radionuclide records. Clim. Past 12, 15–30. https://doi.org/10.5194/cp-12-15-2016.
Amesbury, M.J., Mallon, G., Charman, D.J., Hughes, P.D.M., Booth, R.K., Daley, T.J., Garneau, M., 2012. Statistical testing of a new testate amoeba-based transfer function for water-table depth reconstruction on ombrotrophic peatlands in north-eastern Canada and Maine, United States. J. Quat. Sci. 28, 27–39.
Andrews, B.J., Gardner, J.E., Tait, S., Ponomareva, V., Melekestsev, I.V., 2007. Dynamics of the 1800 14C yr BP caldera-forming eruption of Ksudach volcano, Kamchatka, Russia. In: Eichelberger, J., Gordeev, E., Kasahara, M., Izbekov, P., Lees, J. (Eds.), Volcanism and Subduction: the Kamchatka Region, vol. 172. American Geophysical Union Geophysical Monograph Series, pp. 325–342.
Andrews, B.J., Dufek, J., Ponomareva, V., 2018. Eruption dynamics and explosive-effusive transitions during the 1400 cal BP eruption of Opala volcano, Kamchatka, Russia. J. Volcanol. Geoth. Res. 356, 316–330.
Bacon, C.R., Neal, C.A., Miller, T.P., McGimsey, R.G., Nye, C.J., 2014. Postglacial Eruptive History, Geochemistry, and Recent Seismicity of Aniakchak Volcano, Alaska Peninsula. U.S. Geological Survey Professional Paper 1810, p. 74. https://doi.org/10.3133/pp1810.
Barber, K.E., Chambers, F.M., Maddy, D., Stoneman, R., Brew, J.S., 1994. A sensitive high-resolution record of late Holocene climatic change from a raised bog in northern England. Holocene 4, 198–205.
Begét, J.E., 1982. Postglacial volcanic deposits at Glacier Peak, Washington, and potential hazards from future eruptions; a preliminary report. U.S. Geological Survey Open-File Report 82–830, 81.
Begét, J.E., 1984. Tephrochronology of late Wisconsin deglaciation and Holocene glacier fluctuations near Glacier Peak, north cascade range, Washington. Quat. Res. 21, 304–316.
Begét, J., Mason, O., Anderson, P., 1992. Age, extent and climatic significance of the c. 3400 BP Aniakchak tephra, western Alaska, USA. Holocene 2, 51–56.
Beierle, B., Smith, D.G., 1998. Severe drought in the early Holocene (10,000–6800 BP) interpreted from lake sediment cores, southwestern Alberta, Canada. Palaeogeogr. Palaeoclimatol. Palaeoecol. 140, 75–83.
Bevilacqua, A., Bursik, M., Patra, A., Bruce Pitman, E., Yang, Q., Sangani, R., Kobs-Nawotniak, S., 2018. Late Quaternary eruption record and probability of future volcanic eruptions in the Long Valley volcanic region (CA, USA). J. Geophys. Res.: Solid Earth 123, 5466–5494.
Blockley, S.P.E., Pyne-O'Donnell, S.D.F., Lowe, J.J., Matthews, I.P., Stone, A., Pollard, A.M., Turney, C.S.M., Molyneux, E.G., 2005. A new and less destructive laboratory procedure for the physical separation of distal glass tephra shards from sediments. Quat. Sci. Rev. 24, 1952–1960.
Blockley, S.P., Ramsey, C.B., Pyle, D.M., 2008. Improved age modelling and high-precision age estimates of late Quaternary tephras for accurate palaeoclimate reconstruction. J. Volcanol. Geoth. Res. 177, 251–262.
Blockley, S.P.E., Edwards, K.J., Schofield, J.E., Pyne-O'Donnell, S.D.F., Jensen, B.J.L., Matthews, I.P., Cook, G.T., Wallace, K.L., Froese, D., 2015. First evidence of cryptotephra in palaeoenvironmental records associated with Norse occupation sites in Greenland. Quat. Geochronol. 27, 145–157.
Bolton, M.S., Jensen, B.J., Wallace, K., Praet, N., Fortin, D., Kaufman, D., De Batist, M., 2020. Machine learning classifiers for attributing tephra to source volcanoes: an evaluation of methods for Alaska tephras. J. Quat. Sci. 35, 81–92.
Booth, R.K., 2010. Testing the climate sensitivity of peat-based paleoclimate reconstructions in mid-continental North America. Quat. Sci. Rev. 29, 720–731.
Booth, R.K., Jackson, S.T., Sousa, V.A., Sullivan, M.E., Minckley, T.A., Clifford, M.J., 2012a. Multi-decadal drought and amplified moisture variability drove rapid forest community change in a humid region. Ecology 93, 219–226.
Booth, R.K., Brewer, S., Blaauw, M., Minckley, T.A., Jackson, S.T., 2012b. Decomposing the mid-Holocene Tsuga decline in eastern North America. Ecology 93, 1841–1852.
Bondarenko, V.I., Rashidov, V.A., 2018. The structure of the Ushishir volcanic massif, central kurils. J. Volcanol. Seismol. 12, 16–33.
Bourne, A.J., Cook, E., Abbott, P.M., Seierstad, I.K., Steffensen, J.P., Svensson, A., Fischer, H., Schupbach, S., Davies, S.M., 2015. A tephra lattice for Greenland and a reconstruction of volcanic events spanning 25-45 ka b2k. Quat. Sci. Rev. 118, 122–141.
Bourne, A.J., Abbott, P.M., Albert, P.G., Cook, E., Pearce, N.J., Ponomareva, V., Svensson, A., Davies, S.M., 2016. Underestimated risks of recurrent long-range ash dispersal from northern Pacific Arc volcanoes. Sci. Rep. 6, 1–8.
Braitseva, O.A., Melekestsev, I.V., Ponomareva, V.V., Kirianov, V.Y., 1996. The caldera-forming eruption of Ksudach volcano about cal. AD 240: the greatest explosive event of our era in Kamchatka, Russia. J. Volcanol. Geoth. Res. 70, 49–65.
Braitseva, O.A., Ponomareva, V.V., Sulerzhitsky, L.D., Melekestsev, I.V., Bailey, J., 1997. Holocene key-marker tephra layers in Kamchatka, Russia. Quat. Res. 47, 125–139.

Bronk Ramsey, C., 2009a. Bayesian analysis of radiocarbon dates. Radiocarbon 51, 337–360.
Bronk Ramsey, C., 2009b. Dealing with outliers and offsets in radiocarbon dating. Radiocarbon 51, 1023–1045.
Buckland, H.M., Cashman, K.V., Engwell, S.L., Rust, A.C., 2020. Sources of uncertainty in the Mazama isopachs and the implications for interpreting distal tephra deposits from large magnitude eruptions. Bull. Volcanol. 82, 23.
Bursik, M., Sieh, K., 1989. Range front faulting and volcanism in the Mono Basin, eastern California. J. Geophys. Res.: Solid Earth 94, 15587–15609.
Bursik, M., Sieh, K., 2013. Digital Database of the Holocene Tephras of the Mono-Inyo Craters, vol. 758. U.S. Geological Survey Data Series, California.
Bursik, M., 2014. South Mono Geochemical Dataset. https://vhub.org/resources/3290. U.S. Geological Survey Data Series 758.
Bursik, M., Sieh, K., Meltzner, A., 2014. Deposits of the most recent eruption in the Southern Mono Craters, California: description, interpretation and implications for regional marker tephras. J. Volcanol. Geoth. Res. 275, 114–131.
Carey, S., Gardner, J., Sigurdsson, H., 1995. The intensity and magnitude of Holocene plinian eruptions from Mount St. Helens volcano. J. Volcanol. Geoth. Res. 66, 185–202.
Cashman, K.V., Rust, A.C., 2020. Far-travelled ash in past and future eruptions: combining tephrochronology with volcanic studies. J. Quat. Sci. 35, 11–22.
Charman, D.J., Amesbury, M.J., Hinchliffe, W., Hughes, P.D., Mallon, G., Blake, W.H., Daley, T.J., Gallego-Sala, A.V., Mauquoy, D., 2015. Drivers of Holocene peatland carbon accumulation across a climate gradient in northeastern North America. Quat. Sci. Rev. 121, 110–119.
Chen, X.-Y., McLean, D., Blockley, S.P.E., Tarasov, P.E., Xu, Y.-G., Menzies, M.A., 2019. Developing a Holocene tephrostratigraphy for northern Japan using the sedimentary record from Lake kushu, rebun island. Quat. Sci. Rev. 215, 272–292.
Clifford, M.J., Booth, R.K., 2013. Increased probability of fire during late Holocene droughts in northern New England. Climatic Change 119, 693–704.
Clynne, M.A., Christiansen, R.L., Trimble, D.A., McGeehin, J.P., 2008. Radiocarbon Dates from Volcanic Deposits of the Chaos Crags and Cinder Cone Eruptive Sequences and Other Deposits, Lassen Volcanic National Park and Vicinity, California. U.S. Geological Survey Open-File Report, 02-290, 18.
Cook, E., Davies, S.M., Guðmundsdóttir, E.R., Abbott, P.M., Pearce, N.J., 2018a. First identification and characterization of Borrobol-type tephra in the Greenland ice cores: new deposits and improved age estimates. J. Quat. Sci. 33, 212–224.
Cook, E., Portnyagin, M., Ponomareva, V., Bazanova, L., Svensson, A., Garbe-Schönberg, D., 2018b. First identification of cryptotephra from the Kamchatka Peninsula in a Greenland ice core: implications of a widespread marker deposit that links Greenland to the Pacific northwest. Quat. Sci. Rev. 181, 200–206.
Coulter, S.E., Pilcher, J.R., Plunkett, G., Baillie, M., Hall, V.A., Steffensen, J.P., Vinther, B.M., Clausen, H.B., Johnsen, S.J., 2012. Holocene tephras highlight complexity of volcanic signals in Greenland ice cores. J. Geophys. Res.: Atmosphere 117 (D21).
Crocitti, M., Sulpizio, R., Insinga, D.D., De Rosa, R., Donato, P., Iorio, M., Zanchetta, G., Barca, D., Lubritto, C., 2018. On ash dispersal from moderately explosive volcanic eruptions: Examples from Holocene and Late Pleistocene eruptions of Italian volcanoes. J. Volcanol. Geoth. Res. 1–24.
Davies, L.J., Jensen, B.J.L., Froese, D.G., Wallace, K.L., 2016. Late Pleistocene and Holocene tephrostratigraphy of interior Alaska and Yukon: key beds and chronologies over the past 30,000 years. Quat. Sci. Rev. 146, 28–53.
Davies, L.J., Appleby, P., Jensen, B.J.L., Magnan, G., Mullan-Boudreau, G., Noernberg, T., Shannon, B., Shotyk, W., van Bellen, S., Zaccone, C., Froese, D.G., 2018. High-resolution age modelling of peat bogs from northern Alberta, Canada, using pre- and post-bomb 14C, 210Pb and historical cryptotephra. Quat. Geochronol. 47, 138–162.
Davies, L.J., Jensen, B.J.L., Froese, D.G., 2019. Evidence for Multiple Large Holocene Eruptions of Mt. Churchill. 20th Congress of the International Union for Quaternary Research, Dublin, Ireland. Alaska O-3118.
Davies, L.J., Jensen, B.J.L., Kaufman, D.S., 2021. Late Holocene Cryptotephra from Cascade Lake, Alaska: Supporting Data for a 21,000-year Multi-Chronometer Bayesian Age Model. https://doi.org/10.5194/gchron-2021-18. Geochronology Discussion [preprint] submitted for publication.
Davies, S.M., Abbott, P.M., Pearce, N.J.G., Wastegård, S., Blockley, S.P.E., 2012. Integrating the INTIMATE records using tephrochronology: rising to the challenge. Quat. Sci. Rev. 36, 11–27.
Davies, S.M., Abbott, P.M., Meara, R.H., Pearce, N.J., Austin, W.E., Chapman, M.R., Svensson, A., Bigler, M., Rasmussen, T.L., Rasmussen, S.O., Farmer, E.J., 2014. A North Atlantic tephrostratigraphical framework for 130–60 ka b2k: new tephra discoveries, marine-based correlations, and future challenges. Quat. Sci. Rev. 106, 101–121.
Daley, T.J., Street-Perrott, F.A., Loader, N.J., Barber, K.E., Hughes, P.D., Fisher, E.H., Marshall, J.D., 2009. Terrestrial climate signal of the "8200 yr BP cold event" in the Labrador Sea region. Geology 37, 831–834.
Donnelly-Nolan, J.M., Champion, D.E., Grove, T.L., 2016. Late Holocene Volcanism at Medicine Lake Volcano, Northern California Cascades. U.S. Geological Survey Professional Paper 1822, p. 59. https://doi.org/10.3133/pp1822.
Donoghue, S.L., Vallance, J., Smith, I.E.M., Stewart, R.B., 2007. Using geochemistry as a tool for correlating proximal andesitic tephra: case studies from Mt Rainier (USA) and Mt Ruapehu (New Zealand). J. Quat. Sci. 22, 395–410.
Donovan, J.J., Kremser, D., Fournelle, J.H., Goemann, K., 2015. Probe for EPMA: Acquisition, Automation and Analysis, Version 11: Eugene, Oregon. Probe Software. Inc.. http://www.probesoftware.com
Dugmore, A., 1989a. Icelandic volcanic ash in Scotland. Scot. Geogr. Mag. 105, 168–172.
Dugmore, A.J., 1989b. Tephrochronological studies of Holocene glacier fluctuations in south Iceland. In: Glacier Fluctuations and Climatic Change. Springer, Dordrecht, pp. 37–55.
Dugmore, A.J., Newton, A.J., Sugden, D.E., Larsen, G., 1992. Geochemical stability of fine-grained silicic Holocene tephra in Iceland and Scotland. J. Quat. Sci. 7, 173–183.
Dugmore, A.J., Larsen, G.R., Newton, A.J., 1995. Seven tephra isochrones in Scotland. Holocene 5, 257–266.
Egan, J., Staff, R., Blackford, J., 2015. A revised age estimate of the Holocene Plinian eruption of Mount Mazama, Oregon using Bayesian statistical modelling. Holocene 25, 1054–1067.
Eppler, D.B., Malin, M.C., 1989. The may 1915 eruptions of lassen peak, California, I: characteristics of events occurring on 19 may. In: Latter, J.H. (Ed.), Volcanic Hazards. IAVCEI Proceedings in Volcanology, vol. 1. Springer, Berlin, Heidelberg.
Fierstein, J., Nathenson, M., 1992. Another look at the calculation of fallout tephra volumes. Bull. Volcanol. 54, 156–167.
Foit Jr., F.F., Mehringer Jr., P.J., 2016. Holocene tephra stratigraphy in four lakes in southeastern Oregon and northwestern Nevada, USA. Quat. Res. 85, 218–226.
Foit Jr., F.F., Gavin, D.G., Hu, F.S., 2004. The tephra stratigraphy of two lakes in south-central British Columbia, Canada and its implications for mid-late Holocene volcanic activity at Glacier Peak and Mount St. Helens, Washington, USA. Can. J. Earth Sci. 41, 1401–1410.
Foo, Z.H., Jensen, B.J., Bolton, M.S., 2020. Glass geochemical compositions from widespread tephras erupted over the last 200 years from Mount St. Helens. J. Quat. Sci. 35, 102–113.
Fortin, D., Praet, N., McKay, N.P., Kaufman, D.S., Jensen, B.J., Haeussler, P.J., Buchanan, C., De Batist, M., 2019. New approach to assessing age uncertainties—The 2300-year varve chronology from Eklutna Lake, Alaska (USA). Quat. Sci. Rev. 203, 90–101.
Fricker, M.B., Kutscher, D., Aeschlimann, B., Frommer, J., Dietiker, R., Bettmer, J., Gunther, D., 2011. High spatial resolution trace element analysis by LA-ICP-MS using a novel ablation cell for multiple or large samples. Int. J. Mass Spectrom. 307, 39–45. https://doi.org/10.1016/j.ijms.2011.01.008.
Gardner, J.E., Carey, S., Sigurdsson, H., 1998. Plinian eruptions at Glacier peak and Newberry volcanoes, United States: implications for volcanic hazards in the cascade range. Geol. Soc. Am. Bull. 110, 173–187.
Gardner, J.E., Tait, S., 2000. The caldera-forming eruption of Volcan Ceboruco, Mexico. Bull. Volcanol. 62, 20–33.
Hallett, D.J., Mathewes, R.W., Foit, F.F., 2001. Mid-Holocene Glacier Peak and Mount St. Helens We tephra layers detected in lake sediments from southern British Columbia using high-resolution techniques. Quat. Res. 55, 284–292.
Hayward, C., 2012. High spatial resolution electron probe microanalysis of tephras and melt inclusions without beam-induced chemical modification. Holocene 22, 119–125.
Jarosewich, E., Nelen, J.A., Norberg, J.A., 1980. Reference samples for electron microprobe analysis. Geostand. Newsl. 4, 43–47.
Jensen, B.J.L., Froese, D.G., Preece, S.J., Westgate, J.A., Stachel, T., 2008. An extensive middle to late Pleistocene tephrochronologic record from east-central Alaska. Quat. Sci. Rev. 27, 411–427.
Jensen, B.J., Preece, S.J., Lamothe, M., Pearce, N.J., Froese, D.G., Westgate, J.A., Schaefer, J., Begét, J., 2011. The variegated (VT) tephra: a new regional marker for middle to late marine isotope stage 5 across Yukon and Alaska. Quat. Int. 246, 312–323.
Jensen, B.J.L., Reyes, A.V., Froese, D.G., Stone, D.B., 2013. The Palisades is a key reference site for the middle Pleistocene of eastern Beringia: new evidence from paleomagnetics and regional tephrostratigraphy. Quat. Sci. Rev. 63, 91–108.
Jensen, B.J.L., Pyne-O'Donnell, S., Plunkett, G., Froese, D.G., Hughes, P.D.M., Sigl, M., McConnell, J.R., Amesbury, M.J., Blackwell, P.G., van den Bogaard, C., Buck, C.E., Charman, D.J., Clague, J.J., Hall, V.A., Koch, J., Mackay, H., Mallon, G., McColl, L., Pilcher, J.R., 2014. Transatlantic distribution of the alaskan White River ash. Geology 42, 875–878.
Jensen, B.J., Beaudoin, A.B., Clynne, M.A., Harvey, J., Vallance, J.W., 2019. A re-examination of the three most prominent Holocene tephra deposits in western Canada: bridge River, Mount St. Helens Yn and Mazama. Quat. Int. 500, 83–95.
Kaufman, D.S., Jensen, B.J., Reyes, A.V., Schiff, C.J., Froese, D.G., Pearce, N.J., 2012. Late

quaternary tephrostratigraphy, ahklun Mountains, SW Alaska. J. Quat. Sci. 27 (4), 344–359.
Kelleher, P.C., Cameron, K.L., 1990. The geochemistry of the Mono craters-Mono Lake islands volcanic complex, eastern California. J. Geophys. Res.: Solid Earth 95, 17643–17659.
Kuehn, S.C., Foit Jr., F.F., 2000. Silicic Tephras of Newberry Volcano. What's New at Newberry Volcano, Oregon: Guidebook for the Friends of the Pleistocene Annual Pacific Northwest Field Trip, pp. 135–163.
Kuehn, S.C., Foit Jr., F.F., 2006. Correlation of widespread Holocene and Pleistocene tephra layers from Newberry Volcano, Oregon, USA, using glass compositions and numerical analysis. Quat. Int. 148, 113–137.
Kuehn, S.C., Froese, D.G., Carrara, P.E., Foit Jr., F.F., Pearce, N.J.G., Rotheisler, P., 2009. Major- and trace-element characterization, expanded distribution, and a new chronology for the latest Pleistocene Glacier Peak tephras in western North America. Quat. Res. 71, 201–216.
Kuehn, S.C., Froese, D.G., Shane, P.A.R., INTAV intercomparison Participants, 2011. The INTAV intercomparison of electron-beam microanalysis of glass by tephrochronology laboratories: results and recommendations. Quat. Int. 246, 19–47.
Kyle, P.R., Ponomareva, V.V., Rourke Schluep, R., 2011. Geochemical characterization of marker tephra layers from major Holocene eruptions, Kamchatka Peninsula, Russia. Int. Geol. Rev. 53, 1059–1097.
Lakeman, T.R., Clague, J.J., Menounos, B., Osborn, G.D., Jensen, B.J.L., Froese, D.G., 2008. Holocene tephras in lake cores from northern British Columbia, Canada. Can. J. Earth Sci. 45, 935–947.
Lawson, I.T., Swindles, G.T., Plunkett, G., Greenberg, D., 2012. The spatial distribution of Holocene cryptotephras in north-west Europe since 7 ka: implications for understanding ash fall events from Icelandic eruptions. Quat. Sci. Rev. 41, 57–66.
LeBoeuf, K.A., 2014. Holocene Vegetation, Hydrology, and Fire in the North-Central Adirondacks of New York. Unpublished MSc thesis. Lehigh University.
Lerbekmo, J.F., 2008. The White River ash: largest Holocene plinian tephra. Can. J. Earth Sci. 45, 693–700.
Lemke, K.J., 2000. Holocene Tephrostratigraphy, Southern Kenai Peninsula, Lower Cook Inlet, Alaska. Unpublished Master's Thesis. Utah State University. https://digitalcommons.usu.edu/etd/6718/.
Lowe, J.J., Ramsey, C.B., Housley, R.A., Lane, C.S., Tomlinson, E.L., RESET Associates, RESET Team, 2015. The RESET project: constructing a European tephra lattice for refined synchronisation of environmental and archaeological events during the last c. 100 ka. Quat. Sci. Rev. 118, 1–17.
MacInnes, B., Kravchunovskaya, E., Pinegina, T., Bourgeois, J., 2016. Paleotsunamis from the central Kuril Islands segment of the Japan-Kuril-Kamchatka subduction zone. Quat. Res. 86, 54–66.
Mackay, H., Hughes, P.D.M., Jensen, B.J.L., Langdon, P.G., Pyne-O'Donnell, S.D.F., Plunkett, G., Froese, D.G., Coulter, S., Gardner, J.E., 2016. A mid to late Holocene cryptotephra framework from eastern North America. Quat. Sci. Rev. 132, 101–113.
Mackay, H., Amesbury, M.J., Langdon, P.G., Charman, D.J., Magnan, G., van Bellen, S., Garneau, M., Bainbridge, R., Hughes, P.D., 2021. Spatial variation of hydroclimate in north-eastern North America during the last millennium. Quat. Sci. Rev. 256, 106813.
MacLeod, N.S., Sherrod, D.R., Chitwood, L.A., Jensen, R.A., 1995. Geologic Map of Newberry Volcano, Deschutes, Klamath, and Lake Counties. U.S. Geological Survey, Oregon. Miscellaneous Investigations Series. Map I-2455.
Marcaida, M., Mangan, M.T., Vazquez, J.A., Bursik, M., Lidzbarski, M.I., 2014. Geochemical fingerprinting of Wilson Creek formation tephra layers (Mono Basin, California) using titanomagnetite compositions. J. Volcanol. Geoth. Res. 273, 1–14.
McLean, D., Albert, P.G., Nakagawa, T., Suzuki, T., Staff, R.A., Yamada, K., Kitaba, I., Haraguchi, T., Kitagawa, J., Members, S.P., Smith, V.C., 2018. Integrating the Holocene tephrostratigraphy for East Asia using a high-resolution cryptotephra study from Lake Suigetsu (SG14 core), central Japan. Quat. Sci. Rev. 183, 36–58.
Millar, C.I., King, J.C., Westfall, R.D., Alden, H.A., Delany, D.L., 2006. Late Holocene forest dynamics, volcanism, and climate change at whitewing mountain and san joaquin ridge, Mono county, sierra Nevada, CA, USA. Quat. Res. 66, 273–287.
Miller, C.D., 1989. Potential hazards from future volcanic eruptions in California: U.S. Geol. Surv. Bull. 1847, 17.
Monteath, A.J., van Hardenbroek, M., Davies, L.J., Froese, D.G., Langdon, P.G., Xu, X., Edwards, M.E., 2017. Chronology and glass chemistry of tephra and cryptotephra horizons from lake sediments in northern Alaska, USA. Quat. Res. 88, 169–178.
Monteath, A.J., Teuten, A.E., Hughes, P.D., Wastegård, S., 2019. Effects of the peat acid digestion protocol on geochemically and morphologically diverse tephra deposits. J. Quat. Sci. 34, 269–274.
Mullineaux, D.R., 1974. Pumice and other pyroclastic deposits in Mount Rainier national park, Washington. U.S. Geol. Surv. Bull. 1336, 86.
Mullineaux, D.R., 1996. Pre-1980 Tephra-Fall Deposits Erupted from Mount St. Helens. Geological Survey Professional Paper 1563, Washington. U.S.
Nakagawa, M., Ishizuka, Y., Hasegawa, T., Baba, A., Kosugi, A., 2008. Preliminary Report on Volcanological Research of KBP 2007-08 Cruise by Japanese Volcanology Group. Hokkaido University, Sapporo, Japan. https://doi.org/10.6067/XCV8668F2H unpublished report (tDAR id: 391304).
Nathenson, M., 2017. Revised tephra volumes for Cascade Range volcanoes. J. Volcanol. Geoth. Res. 341, 42–52.
Nawotniak, S.E.K., Bursik, M., 2010. Subplinian fall deposits of Inyo craters, CA. J. Volcanol. Geoth. Res. 198, 433–446.
Nichols, J.E., Booth, R.K., Jackson, S.T., Pendall, E.G., Huang, Y., 2006. Paleohydrologic reconstruction based on n-alkane distributions in ombrotrophic peat. Org. Geochem. 37, 1505–1513.
Osborn, G., 1989. Glacial deposits and tephra in the Toiyabe range, Nevada, USA. Arct. Alp. Res. 21, 256–267.
Pallister, J.S., Clynne, M.A., Wright, H.M., Van Eaton, A.R., Vallance, J.W., Sherrod, D.R., Kokelaar, B.P., 2017. Field-trip Guide to Mount St. Helens, Washington—An Overview of the Eruptive History and Petrology, Tephra Deposits, 1980 Pyroclastic Density Current Deposits, and the Crater: U.S. Geological Survey Scientific Investigations Report 2017–5022–D, p. 65. https://doi.org/10.3133/sir20175022D.
Parnell, A., 2014. Bchron: radiocarbon dating, age-depth modelling, relative sea level rate estimation, and non-parametric phase modelling. R package version 4 (1).
Parnell, A.C., Buck, C.E., Doan, T.K., 2011. A review of statistical chronology models for high-resolution, proxy-based Holocene palaeoenvironmental reconstruction. Quat. Sci. Rev. 30, 2948–2960.
Paton, C., Hellstrom, J., Paul, B., Woodhead, J., Hergt, J., 2011. Iolite: freeware for the visualisation and processing of mass spectrometric data. J. Anal. At. Spectrom. 26, 2508. https://doi.org/10.1039/c1ja10172b.
Payne, R.J., Kilfeather, A.A., van der Meer, J.J., Blackford, J.J., 2005. Experiments on the taphonomy of tephra in peat. Suo 56, 147–156.
Payne, R., Blackford, J., van der Plicht, J., 2008. Using cryptotephras to extend regional tephrochronologies: an example from southeast Alaska and implications for hazard assessment. Quat. Res. 69, 42–55.
Payne, R.J., Blackford, J.J., 2008. Extending the late Holocene tephrochronology of the central Kenai peninsula, Alaska. Arctic 61, 243–254.
Payne, R., Gehrels, M., 2010. The formation of tephra layers in peatlands: an experimental approach. Catena 81, 12–23.
Pearce, N.J., Westgate, J.A., Preece, S.J., Eastwood, W.J., Perkins, W.T., 2004. Identification of Aniakchak (Alaska) tephra in Greenland ice core challenges the 1645 BC date for Minoan eruption of Santorini. G-cubed 5 (3).
Pearce, C., Varhelyi, A., Wastegård, S., Muschitiello, F., Barrientos, N., O'Regan, M., Cronin, T.M., Gemery, L., Semiletov, I., Backman, J., Jakobsson, M., 2017. The 3.6 ka Aniakchak tephra in the Arctic Ocean: a constraint on the Holocene radiocarbon reservoir age in the Chukchi Sea. Clim. Past 13, 303–316.
Persson, C., 1966. Försök till tefrokronologisk datering av några svenska torvmossar. GFF (Geol. Foren. Stockh. Forh.) 88, 361–391. https://doi.org/10.1080/11035896609448933.
Pendea, I.F., Ponomareva, V., Bourgeois, J., Zubrow, E.B., Portnyagin, M., Ponkratova, I., Harmsen, H., Korosec, G., 2017. Late glacial to Holocene paleoenvironmental change on the northwestern pacific seaboard, Kamchatka peninsula (Russia). Quat. Sci. Rev. 157, 14–28.
Pilcher, J.R., Hall, V.A., 1992. Towards a tephrochronology for the Holocene of the north of Ireland. Holocene 2, 255–259.
Pilcher, J.R., Hall, V.A., McCormac, F.G., 1995. Dates of Holocene Icelandic volcanic eruptions from tephra layers in Irish peats. Holocene 5, 103–110.
Pilcher, J., Bradley, R.S., Francus, P., Anderson, L., 2005. A Holocene tephra record from the Lofoten Islands, arctic Norway. Boreas 34, 136–156.
Plunkett, G., Coulter, S.E., Ponomareva, V.V., Blaauw, M., Klimaschewski, A., Hammarlund, D., 2015. Distal tephrochronology in volcanic regions: challenges and insights from Kamchatkan lake sediments. Global Planet. Change 134, 26–40.
Plunkett, G., Pilcher, J.R., 2018. Defining the potential source region of volcanic ash in northwest Europe during the Mid- to Late Holocene. Earth Sci. Rev. 179, 20–37.
Ponomareva, V.V., Sulerzhitsky, L.D., Dirksen, O.V., Zaretskaia, N.E., 2001. Holocene paleosols as records of intervals of volcanic quiescence in the Kurile Lake region, South Kamchatka. In: Juvigné, E., Raynal, J.P. (Eds.), Tephras, chronology, archaeology". Les dossiers de l'Archéo-Logie n° 1. CDERAD ed., pp. 91–100
Ponomareva, V.V., Kyle, P.R., Melekestsev, I.V., Rinkleff, P.G., Dirksen, O.V., Sulerzhitsky, L.D., Zaretskaia, N.E., Rourke, R., 2004. The 7600 (^{14}C) year BP Kurile Lake caldera-forming eruption, Kamchatka, Russia: stratigraphy and field relationships. J. Volcanol. Geoth. Res. 136, 199–222.
Ponomareva, V., Kyle, P., Pevzner, M., Sulerzhitsky, L., Hartman, M., 2007. Holocene eruptive history of Shiveluch volcano, Kamchatka peninsula, Russia. In: Eichelberger, J., Gordeev, E., Izbekov, P., Kasahara, M., Lees, J. (Eds.), Volcanism and Subduction: the Kamchatka Region, vol. 172. Geophysical Monograph Series, pp. 263–282.
Ponomareva, V., Portnyagin, M., Derkachev, A., Juschus, O., Garbe-Schönberg, D., Nürnberg, D., 2013. Identification of a widespread Kamchatkan tephra: a middle

Pleistocene tie-point between Arctic and Pacific paleoclimatic records. Geophys. Res. Lett. 40, 3538–3543.
Ponomareva, V., Portnyagin, M., Pevzner, M., Blaauw, M., Kyle, P., Derkachev, A., 2015. Tephra from andesitic Shiveluch volcano, Kamchatka, NW Pacific: chronology of explosive eruptions and geochemical fingerprinting of volcanic glass. Int. J. Earth Sci. 104, 1459–1482.
Ponomareva, V., Portnyagin, M., Pendea, I.F., Zelenin, E., Bourgeois, J., Pinegina, T., Kozhurin, A., 2017. A full Holocene tephrochronology for the kamchatsky peninsula region: applications from Kamchatka to north America. Quat. Sci. Rev. 168, 101–122.
Portnyagin, M.V., Ponomareva, V.V., Zelenin, E.A., Bazanova, L.I., Pevzner, M.M., Plechova, A.A., Rogozin, A.N., Garbe-Schönberg, D., 2020. TephraKam: geochemical database of glass compositions in tephra and welded tuffs from the Kamchatka volcanic arc (northwestern Pacific). Earth Syst. Sci. Data 12 (1).
Porter, S.C., 1978. Glacier Peak tephra in the north cascade range, Washington: stratigraphy, distribution, and relationship to late-glacial events. Quat. Res. 10, 30–41.
Powers, H.A., Wilcox, R.E., 1964. Volcanic ash from Mount Mazama (crater lake) and from Glacier peak. Science 144, 1334–1336.
Preece, S.J., Westgate, J.A., Stemper, B.A., Péwé, T.L., 1999. Tephrochronology of late Cenozoic loess at Fairbanks, central Alaska. Geol. Soc. Am. Bull. 111, 71–90.
Pyne-O'Donnell, S.D., Jensen, B.J., 2020. Glacier Peak and mid-Lateglacial Katla cryptotephras in Scotland: potential new intercontinental and marine-terrestrial correlations. J. Quat. Sci. 35, 155–162.
Pyne-O'Donnell, S., Hughes, P.D.M., Froese, D.G., Jensen, B.J.L., Kuehn, S.C., Mallon, G., Amesbury, M.J., Charman, D.J., Daley, T.J., Loader, N.J., Mauquoy, D., Street-Perrott, F.A., Woodman-Ralph, J., 2012. High-precision ultra-distal Holocene tephrochronology in north America. Quat. Sci. Rev. 52, 6–11.
Pyne-O'Donnell, S.D.F., Cwynar, L.C., Jensen, B.J.L., Vincent, J.H., Kuehn, S.C., Spear, R., Froese, D.G., 2016. West Coast volcanic ashes provide a new continental-scale Lateglacial isochron. Quat. Sci. Rev. 142, 16–25.
Rabett, R.J., Pryor, A.J., Simpson, D.J., Farr, L.R., Pyne-O'Donnell, S., Blaauw, M., Crowhurst, S., Mulligan, R.P., Hunt, C.O., Stevens, R., Fiacconi, M., 2019. A multi-proxy reconstruction of environmental change in the vicinity of the north Bay outlet of pro-glacial lake algonquin. Open Quat. 5 (1).
Razzhigaeva, N.G., Ganzei, L.A., Grebennikova, T.A., Mokhova, L.M., Arslanov, K.A., Kopoteva, T.A., Rybin, A.V., 2012. Development of lacustrine-boggy sedimentary environments in the ancient rasshua island caldera (central Kuril islands) in the Holocene. Russian Journal of Pacific Geology 6, 326–338.
Razzhigaeva, N.G., Matsumoto, A., Nakagawa, M., 2016. Age, source, and distribution of Holocene tephra in the southern Kurile Islands: evaluation of Holocene eruptive activities in the southern Kurile arc. Quat. Int. 397, 63–78.
Riehle, J.R., 1985. A reconnaissance of the major Holocene tephra deposits in the upper Cook Inlet region, Alaska. J. Volcanol. Geoth. Res. 26, 37–74.
Reimer, P.J., Austin, W.E., Bard, E., Bayliss, A., Blackwell, P.G., Ramsey, C.B., Butzin, M., Cheng, H., Edwards, R.L., Friedrich, M., Grootes, P.M., 2020. The IntCal20 Northern Hemisphere radiocarbon age calibration curve (0–55 cal kBP). Radiocarbon 62, 725–757.
Roland, T.P., Mackay, H., Hughes, P.D.M., 2015. Tephra analysis in ombrotrophic peatlands: a geochemical comparison of acid digestion and density separation techniques. J. Quat. Sci. 30, 3–8.
Sampson, D.E., Cameron, K.L., 1987. The geochemistry of the Inyo volcanic chain: multiple magma systems in the Long Valley region, eastern California. J. Geophys. Res.: Solid Earth 92, 10403–10421.
Sarna-Wojcicki, A.M., Morrison, S.D., Meyer, C.E., Hillhouse, J.W., 1987. Correlation of upper Cenozoic tephra layers between sediments of the western United States and eastern Pacific Ocean and comparison with biostratigraphic and magnetostratigraphic age data. Geol. Soc. Am. Bull. 98, 207–223.
Sarna-Wojcicki, A.M., Lajoie, K.R., Meyer, C.E., Adams, D.P., Robinson, S.W., Anderson, R.S., 1988. Tephrochronologic Studies of Sediment Cores from Walker Lake, Nevada. U.S. Geological Survey Open-File Report, pp. 88–548.
Schachtman, N.S., MacGregor, K.R., Myrbo, A., Hencir, N.R., Riihimaki, C.A., Thole, J.T., Bradtmiller, L.I., 2015. Lake core record of grinnell glacier dynamics during the latest Pleistocene deglaciation and the younger dryas, glacier national park, Montana, USA. Quat. Res. 84, 1–11.
Schindlbeck, J.C., Kutterolf, S., Freundt, A., Alvarado, G.E., Wang, K.L., Straub, S.M., Hemming, S.R., Frische, M., Woodhead, J.D., 2016. Late Cenozoic tephrostratigraphy offshore the southern Central American Volcanic Arc: 1. Tephra ages and provenance. G-cubed 17, 4641–4668.
Schindlbeck, J.C., Kutterolf, S., Freundt, A., Eisele, S., Wang, K.L., Frische, M., 2018. Miocene to Holocene marine tephrostratigraphy offshore northern Central America and southern Mexico: pulsed activity of known volcanic complexes. G-cubed 19, 4143–4173.
Sieh, K., Bursik, M., 1986. Most recent eruption of the Mono Craters, eastern central California. J. Geophys. Res.: Solid Earth 91, 12539–12571.
Sieron, K., Siebe, C., 2008. Revised stratigraphy and eruption rates of Ceboruco stratovolcano and surrounding monogenetic vents (Nayarit, Mexico) from historical documents and new radiocarbon dates. J. Volcanol. Geoth. Res. 176, 241–264.
Sisson, T.W., Vallance, J.W., 2008. Frequent eruptions of Mount Rainier over the last ~2,600 years. Bull. Volcanol. 71, 595–618.
Smith, D.G.W., Westgate, J.A., 1968. Electron probe technique for characterising pyroclastic deposits. Earth Planet Sci. Lett. 5, 313–319.
Spano, N.G., Lane, C.S., Francis, S.W., Johnson, T.C., 2017. Discovery of mount Mazama cryptotephra in lake superior (north America): implications and potential applications. Geology 45, 1071–1074.
Stuiver, M., Borns, H.W., Denton, G.H., 1964. Age of a widespread layer of volcanic ash in the southwestern Yukon Territory. Arctic 17, 259–261.
Sun, C., Plunkett, G., Liu, J., Zhao, H., Sigl, M., McConnell, J.R., Pilcher, J.R., Vinther, B., Steffensen, J.P., Hall, V., 2014. Ash from Changbaishan Millennium eruption recorded in Greenland ice: implications for determining the eruption's timing and impact. Geophys. Res. Lett. 41, 694–701.
Theisen, A.A., Borchardt, G.A., Harward, M.E., Schmitt, R.A., 1968. Neutron activation for distinguishing Cascade Range pyroclastics. Science 161, 1009–1011.
Tomlinson, E.L., Thordarson, T., Müller, W., Thirlwall, M., Menzies, M.A., 2010. Microanalysis of tephra by LA-ICP-MS — strategies, advantages and limitations assessed using the Thorsmörk ignimbrite (Southern Iceland). Chem. Geol. 279, 73–89.
Toohey, M., Sigl, M., 2017. Volcanic stratospheric sulfur injections and aerosol optical depth from 500 BCE to 1900 CE. Earth Syst. Sci. Data 9, 809–831.
Turney, C.S., 1998. Extraction of rhyolitic component of Vedde microtephra from minerogenic lake sediments. J. Paleolimnol. 19, 199–206.
Turney, C.S., Lowe, J.J., Davies, S.M., Hall, V., Lowe, D.J., Wastegård, S., Hoek, W.Z., Alloway, B., 2004. Tephrochronology of Last Termination sequences in Europe: a protocol for improved analytical precision and robust correlation procedures (a joint SCOTAV–INTIMATE proposal). J. Quat. Sci. 19, 111–120.
Vallance, J.W., Van Eaton, A.R., Ramsey, D.W., 2015. Late Pleistocene and Holocene Geology and Hazards at Glacier Peak Volcano. AGUFM, Washington vols. 33B-3088.
van der Bilt, W.G., Lane, C.S., Bakke, J., 2017. Ultra-distal Kamchatkan ash on Arctic Svalbard: towards hemispheric cryptotephra correlation. Quat. Sci. Rev. 164, 230–235.
Vinther, B.M., Clausen, H.B., Johnsen, S.J., Rasmussen, S.O., Andersen, K.K., Buchardt, S.L., Dahl-Jensen, D., Seierstad, I.K., Siggaard-Andersen, M.-L., Steffensen, J.P., Svensson, A., Olsen, J., Heinemeier, J., 2006. A synchronised dating of three Greenland ice cores throughout the Holocene. J. Geophys. Res. 111, D13102. https://doi.org/10.1029/2005JD006921.
Volynets, O.N., Ponomareva, V.V., Braitseva, O.A., Melekestsev, I.V., Chen, C.H., 1999. Holocene eruptive history of Ksudach volcanic massif, South Kamchatka: evolution of a large magmatic chamber. J. Volcanol. Geoth. Res. 91, 23–42.
Waitt, R.B., Begét, J.E., 2009. Volcanic Processes and Geology of Augustine Volcano, Alaska, vol. 1762. U.S. Geological Survey Professional Paper, p. 78.
Walker, G.P., 1980. The Taupo pumice: product of the most powerful known (ultraplinian) eruption? J. Volcanol. Geoth. Res. 8, 69–94.
Wallace, K., Bursik, M. Kuehn, S., Kurbatov, A., Abbott, P., Bonadonna, C., Cashman, K., Davies, S., Jensen, B., Lane, C., Plunkett, G., Smith, V. Tomlinson, E., Thordarsson, T., and Walker, D. Community established best practice recommendations for tephra studies-from collection through analysis. Nature Scientific Data: SDATA-20-01163, in review.
Wastegård, S., Davies, S.M., 2009. An overview of distal tephrochronology in northern Europe during the last 1000 years. J. Quat. Sci. 24, 500–512.
Westgate, J.A., 1977. Identification and significance of late Holocene tephra from Otter Creek, southern British Columbia, and localities in west-central Alberta. Can. J. Earth Sci. 14, 2593–2600.
Westgate, J.A., Dreimanis, A., 1967. Volcanic ash layers of recent age at banff national park, Alberta, Canada. Can. J. Earth Sci. 4, 155–161.
Wilcox, R.E., 1965. Volcanic ash chronology. In: Wright Jr., H.E., Frey, D.G. (Eds.), Quaternary of the United States. Princeton Univ. Press, Princeton, N.J., pp. 807–816
Wood, S.H., 1977. Distribution, correlation, and radiocarbon dating of late Holocene tephra, Mono and Inyo craters, eastern California. Geol. Soc. Am. Bull. 88, 89–95.
Yamaguchi, D.K., Hoblitt, R.P., 1995. Tree-ring Dating of Pre-1980 Volcanic Flowage Deposits at Mount St. Helens, Washington, vol. 107. Geological Society of America Bulletin, pp. 1077–1093.
Yamaguchi, D.K., Hoblitt, R.P., Lawrence, D.B., 1990. A new tree-ring date for the "floating island" lava flow, Mount St. Helens, Washington. Bull. Volcanol. 52, 545–550.
Zander, P.D., Kaufman, D.S., Kuehn, S.C., Wallace, K.L., Anderson, R.S., 2013. Early and late Holocene glacial fluctuations and tephrostratigraphy, Cabin Lake, Alaska. J. Quat. Sci. 28, 761–771.
Zander, P.D., Kaufman, D.S., McKay, N.P., Kuehn, S.C., Henderson, A.C., 2018. Using correlated tephras to refine radiocarbon-based age models, upper and lower Whitshed Lakes, south-central Alaska. Quat. Geochronol. 45, 9–22.

Zaretskaya, N.E., Ponomareva, V.V., Sulerzhitsky, L.D., 2007. Radiocarbon dating of large Holocene volcanic events within south Kamchatka (Russian Far East). Radiocarbon 49, 1065–1078.
Zdanowicz, C.M., Zielinski, G.A., Germani, M.S., 1999. Mount Mazama eruption: calendrical age verified and atmospheric impact assessed. Geology 27, 621–624.
Zelenin, E., Kozhurin, A., Ponomareva, V., Portnyagin, M., 2020. Tephrochronological dating of paleoearthquakes in active volcanic arcs: a case of the Eastern Volcanic Front on the Kamchatka Peninsula (northwest Pacific). J. Quat. Sci. 35, 349–361.
Zoltai, S.C., 1989. Late Quaternary volcanic ash in the peatlands of central Alberta. Can. J. Earth Sci. 26, 207–214.
Zoltai, S.C., Vitt, D.H., 1990. Holocene climatic change and the distribution of peatlands in western interior Canada. Quat. Res. 33, 231–240.